LBL-32657
UC-404

Lawrence Berkeley Laboratory
UNIVERSITY OF CALIFORNIA

Materials Sciences Division

Development of Low Dielectric Constant Alumina-Based Ceramics for Microelectronic Substrate

S.J. Wu
(Ph.D. Thesis)

May 1993

REFERENCE COPY
Does Not
Circulate
Bldg. 50 Library.
LBL-32657
Copy 1

Prepared for the U.S. Department of Energy under Contract Number DE-AC03-76SF00098

DISCLAIMER

This document was prepared as an account of work sponsored by the United States Government. While this document is believed to contain correct information, neither the United States Government nor any agency thereof, nor the Regents of the University of California, nor any of their employees, makes any warranty, express or implied, or assumes any legal responsibility for the accuracy, completeness, or usefulness of any information, apparatus, product, or process disclosed, or represents that its use would not infringe privately owned rights. Reference herein to any specific commercial product, process, or service by its trade name, trademark, manufacturer, or otherwise, does not necessarily constitute or imply its endorsement, recommendation, or favoring by the United States Government or any agency thereof, or the Regents of the University of California. The views and opinions of authors expressed herein do not necessarily state or reflect those of the United States Government or any agency thereof or the Regents of the University of California.

LBL-32657

Development of Low Dielectric Constant Alumina-Based Ceramics for Microelectronic Substrate

Shun Jackson Wu

Ph.D. Thesis

Department of Materials Science
and Mineral Engineering
University of California, Berkeley

and

Materials Science Division
Lawrence Berkeley Laboratory
University of California
Berkeley, CA 94720

May, 1993

This work was supported by the Director, Office of Energy Research, Officer of Basic Energy Sciences, Materials Sciences Division, of the U.S. Department of Energy under Contract No. DE-AC03-76SF00098.

Abstract

Development of Low Dielectric Constant Alumina-Based Ceramics for Microelectronic Substrates

by

Shun Jackson Wu

Doctor of Philosophy in Engineering-Materials Science and Mineral Engineering

University of California at Berkeley

Professor Lutgard C. De Jonghe, Chair

The performance of high speed computers depends not only on IC chips, but also on the signal propagation speed between these chips. The signal propagation delay in a computer is determined by the dielectric constant of the substrate material to which the IC chips are attached. In this study, a ceramic substrate with a low dielectric constant ($k \approx 5.0$) has been developed. When compared with the traditional alumina substrate ($k \approx 10.0$), the new material corresponds to a 37% decrease in the signal propagation delay.

Glass hollow spheres are used to introduce porosity ($k = 1.0$) to the alumina matrix in a controlled manner. A surface coating technique via heterogeneous nucleation in aqueous solution has been used to improve the high temperature stability of these spheres. After sintering at 1400°C, isolated spherical pores are uniformly distributed in the almost

fully dense alumina matrix; negligible amounts of matrix defects can be seen. All pores are isolated from each other. Detailed analyses of the chemical composition find that the sintered sample consists of α-alumina, mullite and residual glass. Mullite is the chemical reaction product of alumina and the glass spheres. Residual glass exists because current firing conditions do not complete the mullitization reaction.

The dielectric constant of the sintered sample is measured and then compared with the predicted value using Maxwell's model. Mechanical strength is evaluated by a four-point bending test. Although the flexural strength decreases exponentially with porosity, samples with 34% porosity ($k \approx 5.0$) still maintain adequate mechanical strength for the proper operation of an microelectronic substrate.

Development of Low Dielectric Constant Alumina-Based Ceramics for Microelectronic Substrates

Table of Contents

1. Introduction and Research Purpose.....1

1.1 Introduction.....1

1.2 Importance of the Dielectric Constant.....2

1.3 Research Purpose.....4

References for Chapter 1.....5

2. Technical Background.....7

2.1 Mixing Rules.....7

2.2 Microstructure Design.....9

2.2.1 Mechanical Strength of Porous Substrates.....10

2.2.2 Hermeticity of Porous Substrates.....11

2.2.3 Thermal Conductivity of Porous Substrates.....12

2.2.4 Designed Microstructure of Porous Substrates.....14

2.3. Review of Current Development.....15

Reference for Chapter 2.....17

3. Experimental Procedures.....20

3.1 Starting Materials.....20

3.1.1 Alumina (Al_2O_3) Matrix.....20

3.1.2 Glass Hollow Spheres.....22

3.2 Sample Preparation.....23

3.2.1 The Importance of Surface Coating....23

3.2.2 Coating Procedures....26

3.2.3 Slip Casting....29

3.3 Characterization and Evaluation....31

Reference for Chapter 3....33

4. Results and Discussions....37

4.1 Aumina Coating on Glass Hollow Spheres....37

4.1.1 Surface Coating by Heterogeneous Nucleation....37

4.1.2 Optimization of Coating Parameters. 41

4.1.3 Calcination....42

4.2 Densification of Green Compacts....46

4.3 Microstructure....50

4.4 Porosity....53

4.5 Chemical Composition of Sintered Samples....56

4.6 Dielectric Constant and Maxwell's Mixing Model....59

4.7 Flexural Strength of Sintered Samples....62

Reference for Chapter 4....65

5. Conclusions....70

Tables....72

Figures....75

Acknowledgments

I wish to express my acknowledgment to Professor Lutgard C. De Jonghe for guiding my research throughout the period of my study in U.C. Berkeley. I also thank my other group members for their assistance and friendship. Special gratitude goes to Shari Yokota for her proofreading of the manuscript. In addition, I would like to thank Professor Alan W. Search and Professor Iain Finnie for their reviewing this thesis and valuable comments.

Finally, I would like to give my special thanks to my wife, Chia-Chu, my children, Rosemary and Daniel and my parents, for their continuous love and support. Without their inspiration and encouragement, this work would never be finished.

Chapter 1

Introduction and Research Purpose

1.1 Introduction

The microelectronic substrate is an integral part of the computer circuitry. In general, it performs several key functions for the normal operation of a computer system. Both active and passive IC devices are mechanically supported by the substrate. Power is supplied through metal traces in the substrate. Devices are also interconnected by internal wires for signal distribution. The heat generated during operation of a computer system is, traditionally, dissipated by thermal conduction through the substrate. In fact IC packaging has been identified to be one of the ten most critical technologies for the advancement of mankind in the 1990s [1].

Based on their functions, a satisfactory microelectronic substrate should satisfy the following requirements:

* High electrical resistivity (i.e. $>10^{12}$ ohm-m at room temperature).
* Low dielectric Constant (i.e. < 10 at 1 MHz and room temperature).
* High thermal conductivity (i.e. > 100 W/m-K at room temperature).
* Fair mechanical strength.
* Thermal expansion coefficient matching IC chips (i.e. 3.0×10^{-6}/°C for Si chips).
* Atmospheric, chemical and thermal stability during processing and operation.
* Low material cost.
* Easy manufacturability.

Ceramics have played an important role in the development of microelectronic substrates. They provide excellent dielectric properties to support fine conductive metal traces. When compared to other materials, such as plastics, ceramics offer superior mechanical and thermal properties, as well as chemical stability against environmental attack (e.g. solvents, temperature and humidity). Various conventional ceramics are currently being used as substrate materials (Al_2O_3, BeO, AlN, Si_3N_4, etc.). New ceramic materials (glass-ceramics, mullite and cordierite) are also under investigation for specific applications. The choice of material is mainly based on the application's requirements as well as the user's preference. Among these materials, however, alumina (Al_2O_3) has been the primary choice and it is believed that alumina will be used for the majority of such application in the future [2-4]. This is mainly because it provides a good combination of material properties, as well as low material and manufacturing costs.

1.2 Importance of the Dielectric Constant

In general, the speed of a computer system is determined by the following three factors:

1) IC transistor speed.
2) Propagation speed through interconnection within IC chips.
3) Propagation speed through interconnection between IC chips in the substrate.

In the 1970s, when the integration of IC devices was not so dense, the computer speed was mainly determined by the chip performance (items 1 and 2) rather than the substrate (item 3). However, currently the IC devices (VLSI) are so powerful that the computer speed is often limited by the signal propagation speed in the substrate. The

speed of future large computer systems is expected to double or triple from the current 40 to 50 Mips (millions of instructions per second) during the 1990s [2]. To improve the performance of such high speed computer systems, therefore, not only must high-speed IC devices be exploited, but also the signal propagation delay in the substrate (T_d) has to be reduced. Due to recent progresses in fine patterning deposition, new transistor structures and semiconductor process techniques, the IC chip has been able to keep up with the high-speed demand. In the past ten years, therefore, there has been a significant shift from chip performance to substrate performance as the dominant factor in total system delay. The semiconductor industry is now looking at new substrates which can provide higher signal propagation speed (lower signal propagation delay) than the current alumina substrate.

The propagation delay (T_d) of a signal wave in a metal trace is directly related to the dielectric constant of the surrounding substrate material according to the equation:

$$T_d = (k)^{1/2} \cdot l/c \qquad (1\text{-}1)$$

where k : relative dielectric permittivity (dielectric constant) of the substrate material

l : distance that the signal travels

c : speed of light in the conductive metal trace($\approx 3 \times 10^8$ m/sec)

As shown in Figure 1-1, signal propagation delay can be reduced by decreasing the dielectric constant of the surrounding substrate material. For propagation of a signal over a distance of 1 meter in the alumina substrate ($k \approx 10$), the propagation delay is close to 10 nanoseconds. Although this value appears to be small, the total delay time for many megabits of information which travel through large computer systems can be significant. In fact, in current applications of the alumina substrate, the delay caused by the substrate

already exceeds the chip delay. It is urgent, therefore, to have the dielectric constant of the substrate as low as possible. The immediate industrial goal is $k \approx 5$ [3,5] which, according to equation 1-1, results in a propagation delay of 7.5 nanoseconds. This value, when compared with that of an alumina substrate, corresponds to an almost 35% increase of propagation speed in the computer system. Besides reducing the signal propagation delay, low values of k can also reduce the crosstalk between conductive lines in the substrate, thereby allowing high trace density as well as thinner layers for the multilayer substrate [6,7].

In a microelectronic substrate there are two types of configurations of metal traces: stripline and microstrip, as shown in Figure 1-2. For multilayer substrates where signal traces are buried inside substrate materials (stripline), equation 1-1 can be used. In the configuration of a single layer substrate, signal traces are on the surface of the substrate (microstrip). In this case, portions of metal traces are surrounded by free space and therefore a "reduced" propagation delay should be considered [6].

1.3 Research Purpose

There are two approaches which lower the signal propagation delay in microelectronic substrates. The first is to focus on new materials. In searching for possible substrate materials with low k value, organic materials (e.g. polyimide) with dielectric constant less than 3 have been investigated. However, as mentioned previously, concerns remain about some of their properties, with moisture absorption being the most serious problem. Organic materials are therefore inherently less reliable in high-performance applications. Some ceramics with lower dielectric constants than that of alumina, such as glass-ceramics [7-9], mullite ($3Al_2O_3 \cdot 2SiO_2$) [10-12] and cordierite

($2Al_2O_3 \cdot 2MgO \cdot 5SiO_2$) [13-15] have been of interest lately. However ,when compared with the current well-developed alumina substrate, there are drawbacks to these new materials, such as new and complicated manufacturing processes, potential reliability problems and relatively expensive material. Their acceptance by the microelectronic industry, therefore, need to be further explored [2].

A promising alternative is to improve the alumina (Al_2O_3) substrate material so that its dielectric properties meet current requirements. The benefits of this approach over others are fast adoption of modified material, reliable performance and low overall manufacturing cost. The purpose of this study is, therefore, to develop a new alumina-based substrate material with a low dielectric constant, so that the signal propagation delay in the substrate can be reduced. The goal is to lower the *k* value from the current 10 to about 5, without sacrificing other properties necessary to advanced substrate applications.

References for Chapter 1

1. A.Police, "Transforming the Decade: 10 Critical Technologies," *N Y Times, Sci. Times,* [Jan. 1] 35-38 (1991).
2. R.R. Tummala, "Ceramic and Glass-Ceramic Packaging in the 1990s," *J. Am. Ceram. Soc.,* 74 [5], 859-908 (1991).
3. L.M. Sheppard, "Surge in Electronic Materials Continues," *Am. Ceram. Soc. Bull.*, 70 [9], 1467-1477 (1991).
4. J.L. Sprague, "Multilayer Ceramic Packaging Alternatives," *IEEE Trans. Comp. Hybrids Manuf. Technol.*, 13 [2], 390-396 (1990).
5. R.R. Tummala and E.J. Rymaszewski, *Microelectronics Packaging Handbook,*

Van Nostrand-Reinhold, New York, 1989.

6. W.A. Yarbrough, T.R. Gururaja and L.E. Cross, "Materials for IC packaging with Very Low Permittivity via Colloidal Sol-Gel Processing," *Am. Ceram. Soc. Bull.*, 66 [4], 692-698 (1987).

7. Y. Shimada, Y. Yamashita and H. Takamizawa, "Low Dielectric Constant Multilayer Glass-Ceramic Substrate with Ag-Pd Wiring for VLSI Package," *IEEE Trans. Comp. Hybrids Manuf. Technol.*, 11 [1], 163-170 (1988).

8. Y. Shimada, K. Utsumi, M. Suzuki, H. Takamizawa, M. Nitta and T. Watari, "Low Firing Temperature Multilayer Glass-Ceramic Substrate," *IEEE Trans. Comp. Hybrids Manuf. Technol.*, 6 [4], 382-388 (1983).

9. S. Kanzaki, M. Ohashi and H. Tabata, "Mullite-Silica Ceramics for Insulating Substrate Material," in *Ceramic Transactions, Vol. 6 : Mullite and Mullite Matrix Composites*, 389-399 (1990).

10. J. Tanaka, S. Kajita and M. Treason, "Mullite Ceramics for the Application to Advanced Packaging Technology," *Mat. Res. Soc. Symp. Proc.*, vol. 154, 369-378 (1989).

11. T. Kurihara, M. Horiuchi, U. Takeuchi and S. Wakabayashi, "Mullite Ceramic Substrate for Thin-Film Application," in *Proc. 40th Electronic Components Conf.*, 68-75 (1990).

12. M. Horiuchi, K. Mizushima, Y. Takeuchi and S. Wakabayashi, "New Mullite Ceramic Packages and Substrates," *IEEE Trans. Comp. Hybrids Manuf. Technol.*, 11 [4], 439-446 (1983).

13. R.W. Dupon, R.L. McConville and M.S. Thompson, "Low Temperature Route to Cordierite Ceramics Using a Reactive Liquid Phase Sintering Aid," *Mat. Res. Soc. Symp. Proc.*, Vol. 154, 351-356 (1989).

14. B. Mussler and M. Shafer, "Preparation and Properties of Mullite-Cordierite

Composites," *Am. Ceram. Soc. Bull.*, 63 [5] 705-714 (1984).

15. R. Anderson, R. Gerhardt and J. Wachtman, Jr., " Thermal, Mechanical and Dielectric Properties of Mullite-Cordierite Composites," in *Advances in Ceramics, Vol. 26 : Ceramic Substrates and Packages for Electronic Applications*, 265-277 (1987).

Chapter 2

Technical Background

2.1 Mixing Rules

It is well known that the dielectric constant of a material can be reduced by the addition of a second phase with a low k value. Based on the spatial distribution of the second phase in the matrix, several mixing models have been proposed to predict dielectric constant of composites [1-3]. Before describing these equations, which relate the dielectric constant to the volume fraction of second phase, the assumptions inherent in the application of these models should be examined. The first assumption is simple addivity, which means that the existence of one phase does not affect the dielectric properties of others. All phases in the composites behave like pure phases. The second assumption is that the "third phase" in composites, such as phase boundaries and grain boundaries, can be neglected. For composites made by mixing ceramic powders, the final microstructure is on the scale of a micrometer or larger, so these assumptions are usually valid. In cases of nanoscale powders or systems where chemical reactions are likely to occur, the volume fraction of interfacial phase may be substantial and can no longer be ignored. In this case the dielectric property of the "third phase" has to be considered and the mixing model should, therefore, be modified.

Figure 2-1 illustrates three basic configurations for two-phase composites. The parallel model (a) predicts the behavior of composites with two phases stacked parallel to the electric field. This model also applies to longitudinal fiber composites and open pore structures. The dielectric constant, k, is given as:

$$k = \sum_i v_i k_i \qquad (2\text{-}1)$$

where k_i and v_i are dielectric constant and volume fraction of phase i in the composite, respectively. The series model (b), on the other hand, fits composites with phases stacked perpendicular to the direction of the applied electric field. This model also applies to transverse fiber composites. In this case the dielectric constant of the composite, k, is given as:

$$\frac{1}{k} = \sum_i \frac{v_i}{k_i} \qquad (2\text{-}2)$$

These two mixing models can be generalized as:

$$k^n = \sum_i v_i k_i^n \qquad (2\text{-}3)$$

where $n = 1$ for the parallel mixing model and $n = -1$ for the series mixing model. Parallel and series mixing models provide upper and lower bounds for the dielectric constant of composites. Any other type of mixing should give an average k between values predicted by these two extremes. In an intermediate case ($n = 0$) with random connected second phase or irregularly shaped inclusions, Lichtenecker's logarithmic mixing rule is often applied. Since $k^n \rightarrow 1 + n \log k$ when $n \rightarrow 0$, equation 2-3 can be simplified as:

$$\log k = \sum_i v_i \log k_i \qquad (2\text{-}4)$$

In the special case where spherical second phase particles are dispersed in a continuous matrix phase (0-3 connectivity), the dielectric constant can be predicted by the well-known Maxwell's model:

$$k = \frac{v_m k_m (\frac{2}{3} + \frac{k_d}{3k_m}) + v_d k_d}{v_m (\frac{2}{3} + \frac{k_d}{3k_m}) + v_d} \qquad (2\text{-}5)$$

where phase d is the dispersed second phase and phase m is the continuous matrix phase. This type of mixing includes closed pore structures and particulate composites. Since Maxwell's model best describes the microstructure of products in the current study, it will be used as a mathematical base to predict the dielectric constant of composites throughout this research.

2.2 Microstructure Design

Since air has the lowest possible dielectric constant of all materials with $k \approx 1$, it was chosen as the second phase in this investigation. The focus here is to develop an alumina-based porous ceramic for application to microelectronic substrates. The effect of porosity on the dielectric constant of alumina for three models is shown in Figure 2-2. As discussed above, parallel and series model form the upper and lower bounds for the predictions of the composite dielectric constant. Figure 2-2 demonstrates that the addition of pores to the alumina matrix is an effective method to reduce the effective dielectric constant of composite materials. According to Maxwell's mixing model, at least 45% porosity will be needed to achieve the goal of $k \approx 5$. From Figure 2-1, the series model predicts the lowest k value for all types of mixing. Such type of mixing should, therefore, be the most effective method for the current research. However, an inhomogeneous structure such as the series configuration, with alternating layers of alumina and pores, will have very low mechanical strength. Delamination between layers will occur easily. Local concentrations of pores may also cause reliability problems, such as moisture penetration

and metal traces shorting to each other. Therefore the series mixing method is not practical and will not be attempted in this study.

The utilization of porosity has been investigated widely in the substrate industry and proven to be an effective method to lower the dielectric constant of ceramic substrates. Unfortunately, due to the nature of free space, the introduction of pores into the dense matrix will deteriorate some bulk properties. Among them hermeticity, mechanical strength and thermal conductivity are most relevant to the normal operation of the substrate and will be discussed in detail.

2.2.1 Mechanical Strength of Porous Substrates

The mechanical strength of ceramics is critically dependent on microstructure [4-6]. The most important variables that control the strength of ceramic materials are grain size and porosity, as well as pore characteristics. The effect of porosity on the mechanical properties of ceramics has been reviewed in detail by Rice [5] and other workers. Although there has been less development of strength-porosity relations than of elasticity-porosity relations, it is now concluded that, similar to elasticity, the relationship between strength and porosity can be described by a exponential equation:

$$\sigma = \sigma_0 \exp(-bp) \qquad (2\text{-}6)$$

where σ is the strength of a ceramic with volume fraction porosity p, σ_0 is the strength of the dense ceramic and b is a constant which depends on the pore characteristics, including pore size, pore shape and spatial distribution of pores. The values of b range from 4 to 7 [7]. Such broad variations are believed to be caused by inhomogeneities in the pore characteristics of testing samples. According to equation 2-6, the mechanical strength of porous ceramics strongly depends not only on the average porosity (p) but also on the

homogeneity of pores (b). For ceramics with fixed volume fraction of porosity, careful control of pore parameters is, therefore, critical to minimize the degradation of mechanical strength in the materials.

The dependence of strength on grain size of a brittle polycrystalline material can be expressed as [4,7]:

$$\sigma = c \cdot G^{-a} \qquad (2\text{-}7)$$

where G is the grain size and c and a are empirical constants. The value of a is found to be 1/2 for grain sizes ranging from 1 to 300 μm. Therefore for polycrystalline ceramics, if the grain size increases from 1 to 10 μm, the mechanical strength will be reduced to ≈ 1/3 of the original value. In cases when b in equation 2-6 is independent of the grain size, equations 2-6 and 2-7 can be combined to give the relation of strength with porosity and grain size simultaneously:

$$\sigma = c \cdot G^{-a} \exp(-bp) \qquad (2\text{-}8)$$

From the above discussions, it is concluded that controlled porosity as well as a fine-grain matrix are the two most critical factors to obtain strong porous ceramics.

2.2.2 Hermeticity of Porous Substrates

Hermeticity of microelectronic substrates is important to assure the environment-related reliability. A broad range of failure mechanisms can be initiated by exposure to the ambient environment, with metal trace corrosion being the most severe. Corrosion can occur chemically or electrochemically in a computer system. Chemical corrosion occurs, for instance, when metal traces are attacked by corrosive materials used during substrate manufacturing. For electrochemical corrosion to occur, several conditions are necessary. First, a humid environment must be present. Second, a suitable electrolyte must be

available. Third, depending on the electrolyte present, an external applied voltage may be necessary for the corrosion to occur. Ceramic materials, such as alumina or other substrate materials, are an effective moisture barrier. The conductive metal traces buried inside the substrate are protected from moisture and other contaminants (Cl^-, F^- and Na^+). Therefore, no electrochemical corrosion should occur in a dense substrate.

There is a tendency for continuous porosity to occur in very porous materials. Percolation theory [8] states that inclusions of uniform size will form a continuous network when their volume fraction ≈ 0.16. Furthermore, a nondensified matrix may also help to link pores which are otherwise separated from each other. The interconnected pores provide a quick pathway for moisture and other contaminants to migrate through the matrix to metal traces. Electrochemical corrosion may then occur at these locations and cause failures of the computer system. Another problem with porous substrates is that, during the screen printing of conductive metal for multilayer substrates, viscous metal may flow into these interconnected pores and produce a short circuit.

Continuous porosity may also degrade the insulating property of substrates [9,10]. Adsorbed moisture containing conductive contaminants will reduce the electrical resistivity of the substrate material, and cause reliability problems. Furthermore, H_2O is a strong dipolar molecular material with $k \approx 80$, and, therefore, the adsorbed moisture will increase the dielectric constant of the substrate substantially. The retention of hermeticity is therefore important for the proper operation of porous ceramic substrates.

2.2.3 Thermal Conductivity of Porous Substrates

During operation of a computer system, heat will be generated which has to be dissipated for the normal function of IC chips. In general, the semiconductor device junction temperature (the location of the heat source) has to be lower than 85°C. Excessive temperature rise during operation can lead to system reliability problems. This is because that various failure mechanisms in IC chips are thermally activated, such as corrosion and metal interdiffusion. Higher device temperatures mean higher diffusion rates of reactant ions which accelerate the occurrence of those failures. It has been found that the failure rate increases by a factor of ≈ 2 for every 10°C increase in the device temperature [11].

The traditional way to remove heat from IC devices is through solder pad interconnections to the substrate. The substrate is then cooled by either natural or forced air convection. Therefore thermal conductivity is a critical material property for good substrate materials. Conventional circuits are air cooled for power densities of up to 1 W/cm^2. More heat will be generated in high-speed computers and, therefore, substrate materials with higher thermal conductivity should be considered. Generally speaking, ceramic materials with the following properties will have high thermal conductivity:

* Low molecular weight.
* Strong interatomic bonding.
* Simple crystal structure.
* Low anharmonicity.

Based on these criteria, several ceramics, such as AlN, SiC and BeO, are expected to have high thermal conductivity. In fact, these materials have been investigated for applications where heat dissipation is the major concern [11-14]. They can provide power

dissipation up to about 15 W/cm^2 in the air-cooling mode. However, in recent high-performance computer systems, the growing number of circuits per chip and of chips per module are continually increasing the power density requirements and, therefore, the cooling requirements. The expected power requirement for a top-of-the-line computer system in the early 1990s will be in the range of 20 W/cm^2 [15], which is beyond the level that these high-thermal conductivity ceramics can provide. In this case it would be difficult to dissipate the heat effectively by the substrate alone and, therefore, an external cooling method would be necessary.

The thermal conductivity of porous materials follows the mixing rules similar to those for the dielectric constant. Due to the extremely low thermal conductivity of free space, the composite thermal conductivity will be reduced significantly by the existence of pores. However, thermal dissipation in present high-performance computer systems is less troublesome than before. This is because a completely new cooling technique in the thermal management has been developed, which is shown in Figure 2-3. In this method each chip is directly contacted by a high thermal conductivity heat sink. By such configuration, the heat can be dissipated from the back of IC chips without going through the substrate itself. The heat sink is then cooled using either helium gas or cold running water. Cooling the chip directly allows a much wider choice of ceramics. Now materials selection can be based solely on other desired properties.

2.2.4 Designed Microstructure of Porous Substrates

It is now clear that the main concerns for porous ceramic substrates are non-hermeticity and low mechanical strength. Low thermal conductivity problems can be

solved by using the external heat sink cooling method and, therefore, will not be addressed further in this investigation.

Based on the above discussions, several microstructural characteristics are essential for the proper operation of porous ceramic substrates:

* Isolated (closed) pores.
* Small pore size, spherical shape and uniform spatial distribution of pores in the matrix.
* Dense and strong matrix.

These characteristics are meant to ensure the hermeticity of the porous ceramic as well as to minimize the degradation of mechanical strength by pores. Figure 2-4 shows a schematic diagram of the desired microstructure based on these considerations. The goal of this study is to produce ceramics with such a designed microstructure, so that the critical substrate properties, i.e., low dielectric constant, good hermeticity and fair mechanical strength, can be obtained.

2.3 Review of Current Development

There are several methods available for the addition of porosity to ceramic materials. The simplest way is underfiring green compacts such that full density is not achieved at the designated firing conditions [16]. However, it was found that pore characteristics cannot be controlled. The pores are often of irregular shape and interconnected. Therefore, although it is a very simple process, such "partial densification" techniques are considered unsuitable for substrate applications. Another method is the volatilization of polymer spheres to create free spaces which were originally occupied by these spheres [9, 17-18].

This method has good control of pore size and shape. However, there are also several drawbacks for such a technique. First, the burnout process is carried out at temperatures less than 500°C, which is well below the densification temperature of the ceramic matrix. A significant amount of pore shrinkage occurred during densification (i.e. pores shrank at the same rate as the ceramic matrix), which reduced the final porosity after sintering. Second, at high loading of polymer spheres there was a high probability for spheres to touch each other, which might then form connected porosity after burnout. Third, thermal decomposition of polymer spheres would introduce some contaminants to the ceramic matrix. Carbon, being electrically conductive, is the most dangerous residue among them. Studies show that even small amounts of residual carbon increase the electrical conductivity and degrade insulating property of the ceramic. The dielectric constant of the substrate is also increased significantly by the existence of residual carbon [15,19-21].

Pores generated by foaming agent have been investigated by some workers [22-25]. In this method, a low boiling point component (e.g. Freon or other gas generating ingredient) is first dispersed in the gel as liquid droplets and later heated above its boiling temperature to induce foam by vaporization. However, this is a relatively complicated process. In order to obtain a highly porous microstructure with isolated pores, careful control of gel viscosity, foaming agent concentration and firing conditions is needed. Also, although pores with a spherical shape can be achieved, there is generally a very large size distribution of pores in the final product. Another problem is that, although the pores were isolated, the wall thickness between neighboring pores is very difficult to control and can be very thin. In subsequent manufacturing processes or usage, these thin walls might break and cause interconnected pores. In other work, Cross, *et al.* [3] developed an ultra low dielectric constant silica-based porous substrate via the colloidal sol-gel method ($k <$

2). However this material has extremely low mechanical strength and, therefore, require further study.

Glass hollow spheres have been used widely in the fields of thermal-insulation, acoustic-isolation, buoyancy, weight-reduction and compression-resistance. However, their potential as a source of added porosity to ceramic substrates has only recently been recognized and investigated [26-28]. Compared with other porosity-adding methods, the application of glass hollow spheres has several advantages: clean and easy processing, good control of pore characteristics and excellent reproducibility. Previous studies used either glass [26,27] or calcium aluminate cement [28] as the matrix material. In this study, a similar approach, which has not yet been investigated by other workers, is used to introduce controlled porosity to the alumina matrix.

References for Chapter 2

1. W.D. Kingery, H.K. Bowen and D.R. Uhlmann, in *Introduction to Ceramics,* 2nd edition, Chap. 18, John Wiley & Sons, Inc., New York, 1976.
2. R. Gerhardt, "Composites for Electronic Substrate Applications," *Mat. Res. Soc. Symp. Proc.*, Vol. 108 101-107 (1988).
3. U. Mohideen, T.Gururaja, L.E. Cross and R. Roy, "Ultra-Low Dielectric Constant Porous Silica Thick Films for High-Speed IC Packaging," *IEEE Trans. Comp. Hybrids Manuf. Technol.*, 11 [1], 159-162 (1988).
4. F.P. Knudsen, "Dependence of Mechanical Strength of Brittle Polycrystalline Specimens on Porosity and Grain Size," *J. Am. Ceram. Soc.*, 42 [8] 376-387 (1959).
5. R.W. Rice, "Microstructure Dependence of Mechanical Behavior of Ceramics," in *Treatise on Materials Science and Technology, Vol. 11: Properties*

and Microstructure, 199-381 (1977).

6. A.G. Evans and G. Tappin, "Effect of Microstructure on the Stress to Propagate Inherent Flaws," *Proc. Brit. Ceram. Soc.*, 20, 275-297 (1972).
7. W.D. Kingery, H.K. Bowen and D.R. Uhlmann, in *Introduction to Ceramics*, 2nd edition, Chap. 15, John Wiley & Sons, Inc., New York, 1976.
8. R. Zallen, *The Physics of Amorphous Solids*, John Wiley & Sons, Inc., New York, 1983, pp. 183-186.
9. K. Kata, A. Sasaki, Y. Shimada and K. Utsumi, "New Fabrication Technology of Low Dielectric Permittivity Multilayer Ceramic Substrate," *ISHM Proceedings* 308-315 (1990).
10. S. Stein, R. Wahlers and D. Dychala, "Low K Multilayer Dielectric Systems," *Proc. 5th IMC*, 120-127 (1988).
11. R.R. Tummala and E.J. Rymaszewski, *Microelectronics Packaging Handbook*, Van Nostrand-Reinhold, New York, 1989.
12. J.W. Balde, "Multichip Packaging and the Need for New Materials," *J. Electron. Mater.*, 8 [2] 221-227 (1989).
13. D. Suryanarayana, "Thermally Conductive Ceramics for Electronic Packaging," *J. Electron. Packaging*, 111 192-198 (1989).
14. E.M. Rabinovich, "Ceramic Materials for Electronic Packaging," *J. Electron. Packaging*, 111 183-191 (1989).
15. R.R. Tummala, "Ceramic and Glass-Ceramic Packaging in the 1990s," *J. Am. Ceram. Soc.*, 74 [5], 859-908 (1991).
16. R.L. Wahlers, S.J. Stein and G.P. Sykora, "Tapes and Thick Films for High Frequency Packaging," *ECC 40th Proceedings*, 116-121 (1990).
17. K. Tsukamoto, Y. Yoneda and Y. Sakabe, "Fabrication and Properties of Low Dielectric Constant Ceramic Substrate," *IMC 1990 Proceedings*, 299-303 (1990).

18. J.K. Yamamoto, K. Kata and Y. Shimada, "Fabrication of Controlled Porosity in a Tape Cast Glass Ceramic Substrate Material," *Mat. Let.*, 8 [8], 278-282 (1989).

19. D.W. Kellerman, " The Development and Characterization of a Low Dielectric Constant Thick Film Material," in *Proc. 37th Electronic Components Conf.*, 316-327 (1987).

20. G.V. Chandrashekhar and M. W. Shafer, "Dielectric Properties of Sol-Gel Silica Glasses," *Mat. Res. Soc. Symp. Proc.* Vol. 73, 309-315 (1983).

21. K. Niwa, N. Kamehara, H. Yokoyama, K. Yokouchi and K. Kurihara, "Multilayer Ceramic Circuit Board with Copper Conductor," in *Advances in Ceramics, Vol. 19: Multilayer Ceramic Devices*, 41-47 (1985).

22. T. Fujiu, G.L. Messing and W. Huebner, "Processing and Properties of Cellular Silica Synthesized by Foaming Sol-Gels," *J. Am. Ceram. Soc.*, 73 [1], 85-90 (1990).

23. S.J. Stein, R. Wahlers, C. Huang, T. Grunstein and G. Sykora,"VLSI Packaging Materials Using Fireable Metallic and Dielectric Films," *IMC 1990 Proceedings*, 155-161 (1990).

24. R.L. Wahlers, S.J. Stein and G.P. Sykora, "Tapes and Thick Films for High Frequency Packaging," *ECC 40th Proceedings*, 116-121 (1990).

25. J. F. MacDowell, G.H. Beall, "Low K Glass-Ceramics for Microelectronic Packaging," in *Ceramic Transactions, Vol. 15: Materials and Processes for Microelectronic Systems*, 259-277 (1990).

26. D.W. Kellerman and R. Peluso, "The Application of Low Dielectric Constant Thick Film Materials on Low Temperature Cofired Glass/Ceramic Material," *ISHM Proceedings*, 345-351 (1990).

27. M.J. Leap, W. Huebner and I. Eicher, "Low-Permittivity, Silica, Hollow-Glass-Microsphere 0-3 Composites," in "Ceramic Substrates and Packaging for

Electronic Application," *Advances in Ceramics*, Vol. 26, 399-407 (1987).

28. P. Sliva, L.E. Cross, T.R. Gururaja and B.E. Scheetz, "Relative Dielectric Permittivity of Calcium Aluminate Cement-Glass Microsphere Composites," *Mat. Let.*, 4 [11,12], 475-480 (1986).

Chapter 3

Experimental Procedures

This chapter discusses experimental procedures for powder processing, forming techniques (slip casting), densification of the green compact, microstructural characterization, and evaluation of the dielectric constant and flexural strength. The surface coating technique for glass hollow spheres, to improve their high temperature processibility, will also be described in detail. A flowchart of experimental procedures is shown in Figure 3-1.

3.1 Starting Materials

3.1.1 Alumina (Al_2O_3) Matrix

As discussed previously (Section 2-2), porous ceramics with a fine-grained and fully dense matrix are desired. To achieve this goal, high quality alumina powders with fine grains, high purity, no agglomerates and narrow size distribution should be used. It has been shown that a more uniform microstructure is produced by use of high purity powders and narrow particle size distribution [1,2]. This was mainly because during solid-state sintering, both the thermodynamic driving force (reduction of excess surface energy) and the kinetic mechanism (short diffusion distance) were favored by using high-purity, fine particles. In this study, commercial high purity α-Al_2O_3 powder (AKP53) from Sumitomo Chemical America, Inc. was chosen as the matrix material. The purity is $\geq$ 99.995% with major impurities of Si $\leq$ 25 ppm, Na $\leq$ 10 ppm, Mg $\leq$ 10 ppm and Cu $\leq$ 10 ppm. The as-received powder was specified to have an average particle size of 0.3 μm with small size distribution. These powders, according to their specifications, were

deagglomerated to provide high sinterability. However, in a preliminary sintering test of compacts made from as-received powers, the theoretical density (3.98 g/cm^3) was difficult to obtain. SEM (Scanning Electron Microscopy) examination revealed a small amount of agglomerates which were believed to cause the low final density.

It is well known that submicrometer powders agglomerate easily [3]. Agglomerates, if not broken down during the forming process, result in compacts with a non-uniform green density. The agglomerates themselves, being of high packing density, sinter quickly to nearly theoretical density and create large voids between densified agglomerates [4-7]. Thus, it is critical to minimize the amount of agglomerates in green compacts before densification starts. Bowen, *et al.* [8-9] reported that ultrasonication and sedimentation of a well-dispersed slurry were effective techniques to remove agglomerates. These two methods were also used in the current study to eliminate agglomerates in the as-received alumina powders.

Previous electrophoresis analysis found that the isoelectric point (IEP) of Al_2O_3 powders in water solution is pH = 9 [10]. If the pH value is away from this value, surface charge of the same sign builds up on the dispersed Al_2O_3 particles. At optimal range (pH = 3 - 4 for alumina powders in aqueous suspension [11-13]), the surface charge is strong enough to overcome the van der Waals attraction force so that, under the effect of electrostatic forces, these dispersed particles repel each other and form a stable suspension. In this experiment, as-received Al_2O_3 powders were first dispersed in distilled water to form a dilute aqueous dispersion of $\approx$ 5 vol% solid concentration. Nitric acid was used to adjust the pH value to $\approx$ 3.5. An ultrasonic probe (Model W-375 from Heat System-Ultrasonics, Inc.) was then applied to the suspension for about 15 minutes to break down soft agglomerates. The remaining suspension was then allowed to stand still

for the settling of hard agglomerates. After 48 hours of sedimentation, the slurry was decanted and air dried in a fume hood under an infrared lamp while being stirred with a magnetic stirring bar. The dried powder cake was then ground with mortar and pestle and passed through a 100 mesh (126 μm) nylon sieve. SEM examination found fine particles in the range of 0.2 - 0.4 μm without any agglomerates. The processed powders were stored in a desicator for later use.

3.1.2 Glass Hollow Spheres

Commercial glass hollow spheres are available in the micron size range and are reasonably priced (per unit volume). In this study, electronic-graded Eccospheres SDT 60 microspheres from Grace Syntactics was used. Table 3-1 lists some of their important properties. Basically, these spheres were mainly used for applications requiring one or more of the following properties:

* virtually no alkali and therefore little detrimental alkali migration.
* temperature stability to 900°C.
* size range as low as 5 μm.
* good strength while maintaining low density.
* excellent dielectric properties.

These spheres are basically borosilicate glass with low alkali levels. They were chosen as the porosity-adding material in this study because of their small size, spherical shape, low density and good handling strength. X-ray diffraction analysis (XRD) of as-received spheres showed no obvious diffraction peaks, indicating that they are amorphous.

A preliminary SEM examination of the as-received spheres showed that they were predominently intact powders with perfect spherical shape. See Figure 3-2 for a micrograph of the material. However, a small amount of broken pieces as well as a few very large spheres (40-60 μm) were also observed. In order to narrow the size distribution and to remove the unwanted debris, the spheres were first sieved through a 37 μm mesh on a mechanical vibrator. Spheres with sizes larger than this value were thereby removed. The sieved spheres they were suspended in distilled water overnight. Because the density of intact glass hollow spheres (0.51 g/cm^3) was lower than that of water, they rose to the top of the aqueous solution. On the other hand, broken pieces as well as solid particles settled to the bottom of the beaker. The floating portion was then carefully removed from the solution and dried in the fume hood. The yield after these processes is ≈ 90 wt% of starting materials. SEM examination of processed powders found intact spheres ranging from 5 μm to 37 μm. No broken pieces or large spheres could be observed. The average diameter of spheres after processing was 21 μm with a standard deviation of 10 μm. The size distribution of spheres was determined from SEM micrographs by measuring 500 individual particles and was a good fit to a truncated normal distribution.

Glass wall thicknesses were determined by crushing some spheres and examining the broken pieces under SEM. The thicknesses were in the range of 0.8 μm ~ 1.2 μm. However, a small amount of spheres with very thin wall (≤ 0.5 μm) was also seen. Based on the observed average diameter and wall thickness, the average void size inside the hollow spheres (inside radius) was calculated to be ≈ 9.5 μm. Since glass walls were found to be fully dense, the average porosity of glass hollow spheres, from geometric calculation, was determined to be ≈ 0.74.

3.2 Sample preparation

3.2.1 The Importance of Surface Coating

One main drawback of glass hollow spheres is their softening point, which is ≈ 900°C for SDT 60 spheres. This temperature is relatively low when compared with the processing temperature of the Al_2O_3 matrix, which is normally in the range of 1450°C~ 1650°C. Low softening temperature implies that, during densification of the alumina matrix, the glass walls would soften, deform and lose their integrity. Furthermore, in high loading composites these spheres have a tendency to touch each other, as illustrated by the schematic drawing shown in Figure 3-3. According to percolation theory [14], equal-sized inclusions start to form a continuous network in the matrix with volume fraction ≥ 0.16. At a volume fraction ≥ 0.22, nearly all inclusions would be part of the same percolative cluster [15]. At temperatures below the softening point of the glass spheres, adjacent pores were isolated from each other by rigid glass walls. However, it was expected that during densification of the alumina matrix, the glass walls would soften and flow viscously. Under the effect of surface tension viscous walls between the two touching spheres could pull away and, therefore, cause an opening between neighboring pores. In this way, isolated pores would link together and connected porosity was formed in the matrix.

To verify such a hazard, a simple test was conducted as follows: a composite sample was prepared by mixing as-received glass hollow spheres (20 vol%) and alumina powders (80 vol%), according to the flowchart shown in Figure 3-1 (except for omission of the alumina coating process). The green compact was then sintered at 1450°C in air. Figure 3-4 shows the SEM micrograph of a polished sample after sintering. The matrix was found to be fully dense. However, a significant amount of connected porosity occurred at

locations where glass spheres touched each other before sintering. The arrow indicates small opening between two neighboring pores, indicating an early stage of pore linkage. A small degree of pore deformation was also observed. This micrograph confirmed the concern that as-received glass hollow spheres could not satisfy the research requirement, i. e. closed porosity. Interconnected pores in the alumina matrix cause both hermeticity and mechanical strength of the substrate to deteriorate seriously, which defeats the purpose of this study.

Hollow spheres made from high temperature ceramics, such as alumina or mullite, are commercially available. These materials should avoid the pore connecting problem because they are stable at the high densification temperature of the alumina matrix. However, they are all in the millimeter range, which is considered too large for application in microelectronic substrate and, therefore, cannot be used in this study.

To ensure pore isolation during sintering, the high temperature stability of glass hollow spheres has to be improved and direct contact between the glass shells must be prevented. In the present research, a surface coating method was used and proved to be an effective way to accomplish these purposes. The surface of each glass sphere was coated with a layer of refractory material, as illustrated in Figure 3-5 , so that the integrity of the glass spheres could be preserved during subsequent high temperature processes. For its applications in this study, a good coating layer should have following properties:

* The coating layer should be thermally stable at high temperature ($\geq 1450^{o}C$).
* The coating layer should be compatible with the alumina matrix.
* The coating layer itself, or its reaction product with other components in the sample, should also be a good substrate material.

* The coating process should be easy to implement and the total cost should be low.

Considering these requirements, alumina was chosen as an ideal coating material. In the current coating experiment, a thin layer of alumina precursor was first coated onto the surface of the glass spheres and then thermally converted into α-alumina. Detailed coating procedures are discussed in the next section.

3.2.2 Coating Procedures

A variety of techniques have been investigated to form coatings on different core particles. Generally speaking, they can be of either a physical heterocoagulation method or a chemical precipitation method. For the colloidal heterocoagulation method [10, 16-17], an electrostatically stabilized suspension of large core particles and small coating particles are mixed together under conditions such that the two types of particles have opposite surface charges. However, this technique has some drawbacks: first, it can only be used in a system where two types of particles have opposite surface charge at the same pH value of the solution. This occurs only when the IEPs of the two types of particles are significantly different from each other. Second, it has been shown that the adsorption of colloidal particles on the surface of oppositely charged core particles is limited to essentially a monoparticle layer. Coating thicknesses are therefore difficult to control. Third, fine coating particles may form bridges between larger core particles and then flocculation occurs.

Several heterogeneous precipitation techniques have been investigated to produce thin coating layers of ceramics or ceramic precursor on various matrix particles [18-23]. Kapolnek and DeJonghe [19, 23] first developed a controlled heterogeneous precipitation

method by which a thin layer of alumina precursor was successfully coated onto the surface of SiC whiskers in aqueous solution. The coating layer was then thermally converted into alumina. In the present study, a similar technique was used to coat a thin layer of alumina onto the surface of glass hollow spheres. However, due to the special nature of hollow spheres, such as light weight and low crushing strength, certain processing conditions have been modified.

Figure 3-6 shows a flowchart of the coating procedures. The coating experiments were accomplished in a flat-bottomed flask on a hot bath. The flask was partially immersed in an oil bath for stable temperature control during the heating period. Analytic reagent-grade chemicals and distilled water were used throughout the coating experiment to minimize any contamination caused by the starting materials. 0.01M aluminum sulfate hydrate ($Al_2(SO_4)_3 \cdot 18H_2O$) from Fisher Scientific and 0.02M urea ($CO(NH_2)_2$) from J. T. Baker were first dissolved completely in distilled water. Urea was used to provide a stable supply of hydroxide ions which were necessary for the precipitation reaction [24]. The solution was then passed through a 0.22 μm filter to remove any undissolved materials. The processed glass hollow spheres (after sieving and sedimentation) were then added to the solution and dispersed thoroughly. The correct amounts of hollow spheres were difficult to determine analytically. This is because the composition of the coating product (before calcination) could not be determined exactly. Instead, the optimal amounts of hollow spheres were determined by a series of coating experiments until an acceptable coating layer had been obtained.

The mixture in the beaker was slowly heated to the final temperature of 95 ± 1°C and was held at this temperature for 12 hours. Violent stirring of the solution is needed for a good mixing of hollow spheres and reactants. For good control of the precipitation

process, a condenser was connected to the flask to prevent excessive water loss during the coating process. Due to the weak crushing strength of glass hollow spheres, a spinning propeller was used to replace the usual magnetic stirring bar to avoid breakage of the spheres. Upon heating, urea decomposed slowly and released ammonium ions and hydroxide ions uniformly throughout the aqueous solution. The decomposition reaction is given as: $CO(NH_2)_2 + 3H_2O = CO_2 + 2NH_4^+ + 2OH^-$. The introduction of hydroxide ions gradually increased the pH value of the solution and caused the solubility of aluminum sulfate to decrease [25,26]. Once the solubility limit of aluminum sulfate was exceeded, aluminum sulfate precipitated onto the surface of the glass spheres.

Upon completion of the heating period, the flask was removed from the oil bath and allowed to stand still. The glass hollow spheres after being coated with a layer of alumina precursor were of higher density than water and, therefore, they settled to the bottom of the flask. The supernatant was then separated from the coated spheres and discarded. Any uncoated spheres would float on the surface of the solution and be removed together with the supernatant. The remaining coated spheres were then rinsed repeatedly with distilled water using a pressure filtration unit and air dried under the fume hood. Dried spheres were heated at constant rate of 1°C/min. and were calcined in a static air furnace at 1150°C for 2 hours convert the alumina precursor into α-alumina. Coated spheres before and after calcination were characterized using SEM and XRD. Powder x-ray diffraction patterns were obtained with a diffractometer (Siemens, model D500) using Cu Kα radiation with a range of $2\theta = 5$ to 65 degrees. The chemical composition of the coating layer after calcination was determined by energy dispersive spectroscopy (EDS) on the SEM. Wet chemical analysis (by Metallurgical Laboratories, Inc. in San Francisco, CA) with a detection limit of 0.01 wt% was also used to verify the results obtained from EDS analysis. Rutherford Backscattering Spectrometry (RBS) was used to analyze trace

amounts of sulfur (S) which might be left over after calcination. The true particle density of coated spheres after calcination was measured using a helium gas pycnometer by Corning Laboratory Services. In this measurement, samples were outgassed 4 hours in a vacuum oven at 150°C and then measured by the Micromeritics helium autopycnometer.

3.2.3 Slip Casting

A non-densified matrix is mainly caused by inhomogeneous particle packing during consolidation of green powders. High green density with uniform packing in a green body is essential for even shrinkage and elimination of matrix voids during the densification period. An uniform green microstructure will prevent local sintering rate variations and allow more homogeneous densification across the specimen. The final microstructure of the matrix after sintering will be dense, thereby resulting better mechanical and hermetic properties.

Fine particles, because of their poor flowability, often results in uneven die filling after dry pressing. This condition causes non-uniform green density. Rotation milling of fine powders can convert them into loosely bonded granules. These free-flowing granules will tend to fill the die homogeneously. However, high pressure will be needed to compact these granules for high green density. This can be achieved by either uniaxial die pressing or cold isostatic pressing at high pressure. Previous studies [27] reported that the green density obtained by die pressing alumina granules at 350 MPa was only 50% of theoretical density, which is considered too low for fine ceramic processing. The cold isostatic technique can improve the packing density and uniformity significantly. The green density reached ≈ 61% of the theoretical density with cold isostatic pressing at 1380

MPa [28]. The resulting green microstructure was found to be much more uniform than that of compacts formed by die pressing.

According to the flowchart shown in Figure 3-1, composite samples with AKP 53 fine alumina powders as the matrix phase, and coated glass hollow spheres as the dispersed phase were formed. Glass hollow spheres, due to their brittle nature, are very weak in compression. Table 3-1 lists the wt% of collapsed spheres under increasing pressures. It is obvious that high pressure forming methods, either die pressing or cold isostatic pressing, cannot be used as a compacting method with the current system. Uniaxial die pressing of mixed powders with low pressure ($\leq$ 10 MPa) provided adequate handling strength. However, the green density was very low and, therefore, resulted in unsatisfactory densification of the alumina matrix.

One pressureless method to achieve both high green density and homogeneous packing of green samples, without breaking weak spheres, is the slip casting technique. Slip casting is a wet forming method that consolidates powders in a mold directly from a well-dispersed slurry [29,30] and, therefore, avoids the sphere crushing problem during high pressure forming. It has been reported [31-33] that the green microstructure formed by slip casting is much more dense and uniform than that produced by dry pressing.

However when slip casting composite materials, there is always a tendency for the different phases to segregate if they are different in size or density. The phase with larger size and/or higher density will settle first and accumulate at the bottom of the mold, while the phase with smaller size or lower density will remain at the top. In the current system, since the coated spheres are much larger than the fine alumina powders (21 μm vs. 0.3 μ m), they will settle at a much faster rate than that of the fine alumina powders, thereby

causes phase segregation of the two materials in the final product. In an investigation of the suspension of Al_2O_3-SiC whisker composites, Sacks, *et al.* [11] proposed several methods to overcome such phase segregation problems: (1) using suspensions with a high solid content to hinder settling; (2) consolidating the suspension rapidly to minimize the time available for segregation; (3) using suspensions with high viscosity to retard the settling of all phases; and (4) adjusting solution pH so that different phases bear opposite surface charges and, therefore, heterocoagulation occurs. In the present study methods (1) and (2) were used to produce a homogeneous green structure after consolidation of the composite samples. High viscosity should not be considered for good slip casting processes because it causes several problems: low final green density, trapped air in the slurry, and difficulty in filling the mold completely. The heterocoagulation method is not applicable to the current system. This is because, after calcination, both the matrix and the dispersed phase have the same surface material (alumina coated spheres in the alumina matrix) and, therefore, an electrostatic attraction force cannot exist between these two phases.

In this study, a well-dispersed aqueous suspension of fine alumina powders was first prepared by adjusting the pH to ≈ 3.5. Ultrasonication was used to improve dispersion of the alumina powders in the solution. Calculated amounts of coated spheres were then added slowly to this solution. The overall solid content was high, ≈ 50 vol%. Slip casting was carried out using a plastic mold placed on top of a water-absorbing block made from plaster of Paris. To minimize the consolidation time, shallow cavities (6 mm in diameter $\times$ 6 mm in height) in the plastic mold were used. The plaster of Paris block was also optimized to provide a fast water absorption rate. The suspension was poured continuously into the cavities until solid samples were formed. Green samples were dried overnight at room temperature in the fume hood and then removed from the mold. Green

compacts of pure alumina were also prepared simultaneously and used as a reference. The green density of pure alumina samples was ≈ 60% of theoretical density. For composite samples, green densities were in the range of 65% ~ 68% of their respective theoretical density.

3.3 Characterization and Evaluation

Densification studies were performed on a high temperature Orton dilatometer at a constant heating rate of 5°C/min. in air. To determine the effect of slip casting on the phase segregation during consolidation of composite compacts, sintered samples were cross-sectioned parallel to the slurry casting direction. Samples were ground with successively finer diamond wheels and then finally polished with diamond pastes down to 0.25 μm. After polishing, they were thermally etched in air at 1300°C for 1 hour to reveal grain boundaries and other features. SEM was used to examine the microstructure of the polished surface. Samples were sputter coated with a thin layer of Au/Pd to avoid the charging effect during SEM examination. Volume fraction of porosity was determined by the liner fraction method on five randomly chosen areas of a polished surface. For a random sample, it has been shown [34] that the volume fraction of a phase is equal to the linear fraction of the same phase. Imaging analysis was also tried; however, due to the poor contrast between some shallow pores and the matrix, this technique was found to be unsuitable for the current study. The density of pure alumina samples after sintering was determined by Archimede's water displacement method. XRD was used to determine the chemical composition after reaction sintering the present Al_2O_3-SiO_2 system.

The dielectric constant of sintered samples was measured at room temperature at 1 MHz typical frequency, using a HP 4194A Impedance/Gain-Phase Analyzer and 16034

electrode fixture. To assure good electrical contact between sample surfaces and electrodes, the opposing surfaces of sintered cylindrical samples were first polished and then coated with Au/Pd by sputter deposition. Figure 3-7 illustrates the testing sample with electrode plating and the sample set-up on the test fixture which was used in this measurement. The dielectric constant was determined according to the following equation:

$$k = \frac{t \times C}{\pi \times r^2 \times \varepsilon_o} \qquad (3\text{-}1)$$

where k : relative dielectric permittivity (dielectric constant)

t : thickness of test sample (m)

C : capacitance of test sample (F)

r : radius of test sample (m)

ε_o: permittivity of vacuum (8.854×10^{-2} coul^2/nt-m^2)

The mechanical strength of sintered samples was evaluated in four-point flexural mode. This method was chosen due to its convenience and accuracy over other testing methods. Rectangular test bars with dimensions: 30 mm long × 4 mm width × 4 mm thick were prepared by slip casting method. Specimens were polished with SiC grinding papers to 12 μm, and sharp edges were also ground to avoid experimental error. The four-point bending test was performed on an Instron universal testing machine (model 1122) at a crosshead speed of 0.5 mm/min. Flexural strength was determined by the following equation:

$$\sigma_{b4} = \frac{3P(L-l)}{2wt^2} \qquad (3\text{-}2)$$

where σ_{b4} : four-point flexural strength

P : maximum load at fracture of testing bar

L : distance between lower supporting point (19.5 mm)

l : distance between upper supporting point (6 mm)

w : width of testing bar

t : thickness of testing bar

References for Chapter 3

1. E.A. Barringer and H.K. Bowen, "Ceramic Powder Processing," *Ceramic Engineering and Science Proceedings*, 285-297, May-June (1984).
2. K. Yamada, "Present Situation and Future Technology of Alumina Chemical in Japan," *Alumina Chemical: Science and Technology Handbook*, 561-567. Edited by L. D. Hart, The American Ceramic Society, Inc. (1990).
3. M.F. Yan, "Effects of Physical, Chemical, and Kinetic Factors on Ceramic Sintering," in *Advances in Ceramics, Vol. 21: Ceramic Powder Science*, 635-670 (1987).
4. F.F. Lange, "Sinterability of Agglomerated Powders," *J. Am. Ceram. Soc.*, 67 [2] 83-89 (1984).
5. F.W. Dynys and J.W. Halloran, "Influence of Aggregates on Sintering," *J. Am. Ceram. Soc.*, 67 [9] 596-601 (1984).
6. K. Kendall, "Microstructure of Submicron Powders and Green Compacts," in *British Ceramic Proceedings, No. 42: Complex Microstructure*, 81-90 (1989).
7. F.F. Lange and B.M. Metcalf, "Processing-Related Fracture Origins: II, Agglomerate Motion and Cracklike Internal Surfaces Caused by Differential Sintering," *J. Am. Ceram. Soc.*, 66[6] 398-406 (1983).
8. M. Parish and H.K. Bowen, "Narrow size Distribution Powders from Commercial

Ceramic Powders," *Ceramics International*, 10 [2] 75-77 (1984).

9. T.R. Gattuso and H.K. Bowen, "Processing of Narrow size Distribution Alumina," in *Advances in Ceramics, Vol. 10: Structure and Properties of MgO and Al_2O_3 Ceramics*, 644-655 (1984).
10. P.E. Debely, E.A. Barringer and H.K. Bowen, "Preparation and Sintering Behavior of Fine-Grained Al_2O_3-SiO_2 Composite," *J. Am. Ceram. Soc.*, 68 [3] C76-C78 (1985).
11. M.D. Sacks, H.W. Lee and O.E. Rojas, "Suspension Processing of Al_2O_3/SiO_2 Whisker Composites," *J. Am. Ceram. Soc.*, 71 [5] 370-379 (1988).
12. T. Kimura, Y. Matsuda, M. Oda and T. Yamaguchi, "Effects of Agglomerates on the Sintering of Alpha-Al_2O_3," *Ceramics International*, 13 [1] 27-34 (1987).
13. J.S. Moya, J. Rubio and J.A. Pask, "Electrophoretic Behavior of Silica-Bearing Alumina Surfaces," *Ceram. Bull.* 50 [12], 1198-1200 (1980).
14. R. Zallen, in *The Physics of Amorphous Solids*, pp. 183-186, John Wiley & Sons, Inc., New York, 1983.
15. F.F. Lange, L. Atteraas and F. Zok, "Deformation Consolidation of Metal Powders Containing Steel Inclusions," *Acta Metall. Mater.*, 39 [2], 22209-291 (1991).
16. R.K. Iler, "Adsorption of Colloidal Silica on Alumina and of Colloidal Alumina on Silica," *J. Am. Ceram. Soc.*, 47 [4] 194-198 (1964).
17. T. Garino, "Heterocoagulation as an Inclusion Coating Technique for Ceramic Composite Processing," *J. Am. Ceram. Soc.*, 75 [3] 514-18 (1992).
18. A.K. Garg and L.C. De Jonghe, "Microencapsulation of Silicon Nitride Particles with Yttria and Yttria-Alumina Precursors," *J. Mater. Res.*, 5 [1] 136-141 (1990).
19. D. Kapolnek and L.C. De Jonghe, "Particulate Composites from Coated Powders," *J. Euro. Ceram. Soc.*, 7, 345-351 (1991).
20. S. Kratohvil and E. Matijevic, "Preparation and Properties of Coated, Uniform,

Inorganic Colloidal Particles: I, Aluminum (Hydrous) Oxide on Hematite, Chromia and Titania," *Advances Ceramic Mat.*, 2 [4] 798-803 (1987).

21. B. Fegley Jr., P. White and H.K. Bowen, "Preparation of Zirconia-Alumina Powders by Zirconium Alkoxide Hydrolysis," *J. Am. Ceram. Soc.*, 68 [2] C60-C62 (1985).
22. H. Okamura, E. . Barringer and H.K. Bowen, "Preparation and Sintering of Monosized Al_2O_3-TiO_2 Composite Powder," *J. Am. Ceram. Soc.*, 68 [3] C22-C24 (1986).
23. D. Kapolnek, "Synthesis of Alumina-Coated SiC Whiskers for Production of SiC Whisker-Reinforced Alumina Composite Materials," M.S. Thesis, University of California, Berkeley, May 1989.
24. L. Gordon, M.L. Salutsky and H. H. Willard, *Precipitation from Homogeneous Solution Chap. 2: Precipitation of Hydroxides and Basic Salts*, Wiley, New York (1959).
25. J.E. Blendell, H.K. Bowen and R.L. Coble, "High Purity Alumina by Controlled Precipitation from Aluminum Sulfate Solutions," *Am. Ceram. Soc. Bull.*, 63 [6], 797-801 (1984).
26. B.C. Cornilsen and J.S. Reed, "Homogeneous Precipitation of Basic Aluminum Salts as Precursors for Alumina," *Am. Ceram. Soc. Bull.*, 58 [12], 1199 (1979).
27. R.G. Frey and J.W. Halloran, "Compaction Behavior of Spray-Dried Alumina," *J. Am. Ceram. Soc.*, 67 [3] 199-203 (1984).
28. J.T. Lin, "Temperature History and Microstructure of Alumina," Ph.D. Thesis, University of California at Berkeley, May 1992.
29. A.O. Boschi and E. Gilbart, "Wet Forming Processes as a Potential Solution to Agglomeration Problems," in *Advanced Ceramic Processing and Technology, Vol. 1*, 73-93, (1990).
30. R.E. Cowan, "Slip Casting," in *Treatise on Materials Science and Technology, Vol.*

9: Ceramic Fabrication Process, 153-171 (1976).

31. E.F. Adams, "Slip-Cast Ceramics," in *Refractory Materials, A Series of Monographs, Vol. 5 - IV,* 145-184 (1971).
32. T.S. Yeh and M.D. Sacks, "Effect of Green Microstructure on sintering of Alumina," in *Ceramic Transaction, Vol. 7: Sintering of Advanced Ceramics,* 309-331 (1990).
33. H.H. Lee, "Influence of Slip-Casting and Dry-Pressing on Structure Evolution of Alumina Compacts," J. Mat. Sci., 27, 6673-6678 (1992).
34. W. D. Kingery, H.K. Bowen and D.R. Uhlmann, in *Introduction to Ceramics,* 2nd edition, Chap. 11, John Wiley & Sons, Inc., New York, 1976.

Chapter 4

Results and Discussions

4.1 Alumina Coating on Glass Hollow Spheres

4.1.1 Surface Coating by Heterogeneous Nucleation

The heterogeneous coating principle can be explained with the help of a modified LaMer diagram, as shown in Figure 4-1. First, a quantity of coating precursor (alumina sulfate hydrate) and pH adjusting material (urea) are completely dissolved in the liquid. Then, dispersed hollow spheres used as nucleation sites are added to this solution. Initially the pH value in the solution is low and the solubility limit of the dissolved precursor is higher than the concentration of this material in the solution. No precipitation reaction will occur. As the pH value is increased by the decomposition of urea at elevated temperature, the solubility limit of alumina sulfate hydrate decreases accordingly [1,2]. Once the concentration of dissolved precursor exceeds its solubility by a critical amount, before excess material precipitates homogeneously, it will precipitate heterogeneously on the surface of the dispersed hollow spheres. If the pH value increases slowly enough, heterogeneous nucleation will deplete excess material from the solution until the precursor concentration drops to the solubility limit. A further increase in the pH value results in further precipitation, causing the continuous growth of the precipitated grains. At the same time, the concentration of precursor keeps on decreasing and follows the solubility limit. Since the concentration of reactants is now well below the nucleation limit, no further heterogeneous nucleation occurs. Therefore, after reaction, the coating layer will be composed of small grains with a narrow size distribution.

In the coating study, the following criteria should be satisfied so that the coated spheres can fully fulfill their purposes as the porosity adding agent in the alumina matrix.

* Thin coating layer with small grains.
* Good adherence of coating layer to the surface of glass hollow spheres.
* No uncoated or partially-coated spheres.
* Minimum amount of homogeneous precipitation.

A thin coating layer is needed because a thick layer will take too much volume fraction of glass hollow spheres, thus defeats the porosity-adding purpose of such material. For example, the porosity of a hollow sphere with a wall thickness of 1.0 μm and inner radius of 9.5 μm is 0.74. If the thickness of the coating layer is also 1.0 μm, then the wall thickness will be doubled, which reduces the porosity to 0.56. This corresponds to ≈ 24% decrease of the available free space for the same amount of hollow spheres. Figure 2-2 indicates that at least 0.45 porosity is needed to reduce the dielectric constant of the alumina substrate to 5. Assuming that all coated spheres are close packed in the matrix, then the maximum volume fraction of these spheres is estimated to be ≈ 0.64 [3]. For the designed microstructure the matrix should be dense, i.e., porosity should be exclusively caused by hollow spheres. Under these assumptions the volume fraction of free space in a hollow sphere should be at least 0.45 ÷ 0.64 = 0.70 of coated spheres. This value requires that hollow spheres, with 9.5 μm inner radius, should have a total wall thickness ≈ 1.2 μm after coating.

As will be discussed later (section 4-5), the final product in this study consists of several components with different dielectric constants. These components are alumina ($k \approx 10.0$), mullite ($k \approx 6.5$), and glass ($k \approx 5.0$). The effective dielectric constant of the

multiphase matrix will, therefore, be lower than that of the monolithic alumina phase. Also, during calcination, the glass wall softened and mixed with the coating layer (to be discussed in section 4.1.3), thus reducing the total wall thickness of the coated hollow spheres. These considerations allow the coating layer to be thicker than the value predicted in the last paragraph. Furthermore, a coating layer that is too thin may not be strong enough to provide high temperature stability for the hollow spheres. The optimal coating thickness should, therefore, be determined experimentally.

Good adherence of the coating layer to the surface of hollow spheres is required to facilitate subsequent experimental processes. After coating, the adhesion force is believed to be mainly caused by the hydrogen bond between hydrated coating layer and the glass surface which was saturated with silanol groups (SiOH). Mechanical interlock between precipitated grains can also provide additional mechanical stability. Therefore small precipitated grains promote adhesion of the coating layer to the hollow spheres.

Homogeneously precipitated grains, although they can also be converted into α-alumina by calcination, should be minimized for two reasons: first, the quantity of these grains cannot be well controlled, thus it will be difficult to determine precisely the relative amounts of phases in preparing the composite samples. Second, the morphology and size of these free alumina grains are significantly different from that of the fine-grained alumina matrix powders. Such microstructural inhomogeneity in the matrix causes differential shrinkage, which retards the densification rate as well as results in sintering defects [4-6]. Homogeneous precipitation should, therefore, be avoided during the coating process.

Figure 4-2 shows a micrograph of coated glass hollow spheres after drying. Under optimal coating conditions there were no uncoated or partially coated spheres and the

amount of free alumina precursor grains (indicated by the arrow) was negligible. All spheres were coated with a thin, uniform layer of small cube-shaped alumina precursor grains with edge lengths close to 1 μm ~ 1.5 μm. Figure 4-3 shows a high magnification image of a coated sphere after drying. The coating thickness was determined by crushing some coated spheres and examining the fragments of the coating layer under SEM. Average coating thickness was in the range of 1 μm ~ 1.5 μm with small variations.

After drying in the fume hood, the coated spheres behaved like free-flowing powders. Large cracks were observed in the coating layer, as shown in Figure 4-3. These cracks were believed to be caused by the volume shrinkage accompanying water loss during drying. The coating layer adhered well to the hollow spheres which could be handled in the next calcination step without causing any coating detachment. The adhesion force between precipitated grains and the surface of the spheres was evaluated by a simple test in an ultrasonic bath. After ultrasonication for 30 seconds, most of the coating materials had detached from the glass spheres. This result supported the hypothesis that the bonding force was caused by the weak hydrogen bond between precipitated grains and the glass surface. However, weak bonding at this stage was not a problem because during the subsequent calcination step, portions of the coating layer (now α-alumina grains) would mix with the viscous glass wall, which acted as a strong binding medium that firmly attached the alumina grains to the hollow spheres.

Researchers using a similar coating process concluded that the precursor grains consisted of a mixture of several aluminum sulfate hydrate compounds [7], which included $Al_6O_9SO_3 \cdot xH_2O$ and $3Al_2O_3 \cdot 4SO_3 \cdot 8H_2O$. In the current coating experiments the aluminum precursor layer was also crystalline, as indicated by sharp X-ray diffraction peaks. However, the spectra did not have a perfect match to any of the patterns in the

available literature. Complex crystal structures of hydrated alumina sulfates with varying water content might cause such ill-defined diffraction peaks. Since the alumina precursor was only an intermediate phase in the coating experiment, further investigation of the exact chemical compositions of the sulfates was not attempted in this study.

4.1.2 Optimization of Coating Parameters

Coating is a complicated process that involves many parameters. Among them, however, the following factors are found to have the most significant effect on the outcome of the coating process: concentration of nucleation sites, stirring speed, and coating temperature. In this study a series of experiments were carried out to optimize the coating conditions. One of the parameters was varied for each test until a satisfactory coating result was obtained.

In developing an optimal coating process, it was found that adjusting the available surface area for nucleation, i. e., the concentration of glass hollow spheres, was more effective than varying the reactant concentrations (alumina sulfate hydrate and urea). When the concentration of glass spheres was too high, the available surface area for heterogeneous nucleation was large, which resulted in many uncoated or partially coated spheres. On the other hand, if an insufficient number of spheres were added to the suspension, less surface area was available and, therefore, there were no uncoated or partially coated spheres and the coating thickness increased. However, the amount of free alumina precursor from homogeneous precipitation, which was very difficult to be removed from the solution, also increased. Thus, proper control of the concentration of glass spheres is critical to achieve a good coating.

With proper control of the propeller stirring speed, hydroxide ions released from the urea could be evenly distributed in the solution, which resulted in uniform nucleation throughout the solution. Otherwise local variations of pH values caused nonuniform heterogeneous precipitation which created a wide size distribution of precursor grains. Also, at locations with a high concentration of hydroxide ions, the supersaturation of reactants (alumina sulfate) might cause homogeneous precipitation. Vigorous stirring must be maintained throughout the entire coating period to ensure good dispersion of glass spheres in the aqueous solution. Otherwise these light-weight spheres would float on top of the solution and remained uncoated even after a long reaction time. The requirements of an uniform distribution of hydroxide and a good dispersion of spheres in the solution make the stirring speed an important factor in the coating experiment.

Decomposition rate of urea mainly depended on the solution temperature. Too low a temperature did not release enough hydroxide ions to initiate the precipitation reaction. On the other hand, if the coating temperature was too high, then the increased hydroxide release rate quickly raised the pH value of the solution, i.e., the supersaturation level of the reactants. Therefore, before excess reactants could be removed by the heterogeneous precipitation reaction, the homogeneous nucleation limit would be reached which caused homogeneous precipitation to occur. Careful control of the solution temperature was, therefore, one of the most critical parameters to achieve an optimal coating results.

4.1.3 Calcination

Calcination of the alumina precursor coating prior to sintering is necessary so that the gaseous products (mainly SO_2, O_2 and H_2O) can be removed before they are trapped inside the densified matrix. Residual SO_2 and H_2O gases greatly deteriorate the dielectric

properties of the alumina matrix as well as cause reliability problems in future use. X-ray diffraction analysis was used to study the phase evolution to optimize the firing schedule. It was found that during calcination γ-alumina formed first via decomposition of the alumina precursor at a temperature of 700°C ~ 900°C, and then converted into α-alumina at ≈ 1150°C which was similar to previous reports. [1,8]. At temperatures lower than 1150°C, complete conversion to α-alumina was difficult to achieve. Converting γ-alumina into α-alumina was critical to the densification of the alumina matrix. This was because previous studies had shown that densification was impeded if the starting powders were not in the stable form and underwent some kind of phase transformation during heating [9-12].

Figure 4-4 shows an X-ray diffraction pattern of coated spheres after calcination at 1150°C for 2 hours. All of the alumina precursor had been converted into α-alumina. No γ-alumina peaks could be found. The majority of the glass spheres were still in the amorphous phase, as indicated by a large hump in the diffraction pattern. However, a small amount of α-cristobalite peaks was also detected. Thermodynamically, heating silica glass at 1150°C can transform it into β-cristobalite, β-quartz or β-tridymite. However, the kinetics of each transformation determine which phase will form. Since β-cristobalite is structurally the most similar to silica glass, the transformation rate into such a phase will be faster than into the other two phases. Therefore, during calcination, SiO_2 crystallized into β-cristobalite. Upon cooling, α-cristobalite, which is the low temperature polymorph of β-cristobalite, formed.

The decomposition reaction of the alumina precursor was found to be topotactic, meaning that the crystal structure transformed without a change in the original crystal morphology. Figure 4-5 is a morphological comparison of coating grains before and after

calcination, which clearly shows that the α-alumina grains obtained from the decomposition reaction still retained original precursor shapes. Although there was no obvious morphological change, a large weight loss (≈ 40 wt%) was observed accompanying the decomposition reaction. The large weight loss is believed to be caused by dehydration and desulfurization reactions at elevated temperatures. This implies that the α-alumina coating layer had become very porous after calcination. As shown in Figure 4-5(b), the microstructure of the α-alumina now consists of a vermicular network in which both the solid phase and pore were continuous.

Figure 4-6 (a) shows a micrograph of coated spheres after calcination. The alumina coating layer was seen to be partially mixed with the glass wall. It is believed that during calcination, since the firing temperature was higher than the softening point of the glass wall (1150°C vs. 900°C), the viscous glass flowed outward under the effect of capillary forces caused by fine porosity in the α-alumina coating layer. This effect, combined with gas expansion inside the hollow spheres, contributed to the mixing of the coating layer with the glass wall. The walls of the coated spheres after calcination could be treated as a mixture of α-alumina and silica glass. This mixing phenomenon firmly bound the coating layer to the glass wall and greatly facilitated later handling and manufacturing processes.

Under the microscope, the calcined spheres had good spherical shapes; no deformation could be observed. Most of the spheres were intact; however, a very small amount of coated spheres (< 1%) were broken. See Fig. 4-6 (b). Judging from their appearance, it is believed that such burst-type fracture was caused by the internal gas pressure that exceeded the mechanical strength of the glass wall. The wall thickness of the broken spheres was found to be less than 0.5 μm. There were no other anomalies in

the calcined spheres. The calcined spheres were free-flowing powders and could be processed as normal ceramic powders.

The mechanical response of the hollow spheres under the effect of internal pressure is analyzed as follows: since the inside radius of the hollow spheres ($\approx$ 9.5 μm) is an order of magnitude greater than the wall thickness of the broken spheres ($\leq$ 0.5 μm), the variation in stress across the wall can be neglected and the stresses on the spheres can be determined from the consideration of static equilibrium only. Thin-walled theory is therefore used in this analysis. According to this theory, the tangential stress (or hoop stress), σ_t, in the wall under the internal pressure, p, can be expressed by the equation:

$$\sigma_t = \frac{p \times r}{2t} \qquad (4\text{-}1)$$

where p : internal pressure at elevated temperature

r : sphere inner radius

t : wall thickness

According to the manufacturer's data, the gas pressure inside the hollow spheres at room temperature is close to one atmosphere pressure (14.7 psi). Therefore, by using the ideal gas equation ($pv = nRT$), the internal pressure at the softening temperature (900°C) will be $\approx$ 57 psi. Fitting all available data into Equation 4-1, the tangential stress in the glass wall is $\approx$ 570 psi at this temperature. According to Table 3-1, this pressure would cause approximately 1 % of the glass hollow spheres to break, a value which agrees well with the SEM observation. A careful examination of the broken spheres found no evidence of viscous flow of the glass wall. This observation indicates that all fractures occurred at temperatures below the softening point of the glass. At temperatures above

the softening point, viscous flow of glass released the internal pressure and, therefore, no more spheres should fracture.

Both EDS and wet chemical techniques were performed on calcined samples for chemical composition analysis. They all showed similar results. The weight ratio of Al_2O_3 : SiO_2 was found to be 50.6 % : 49.4 %. The yield of the coating process is low; only ≈ 18 wt% of the concentration of the original aluminum ions were precipitated from the solution to form the alumina coating. This was because only those aluminum ions which exceeded the solubility limit could be depleted from the solution to form the precursor coating. The rest of the material remained in solution and could not be precipitated out.

During calcination, complete removal of the sulfur is needed. This is because small amounts of sulfur in the substrate reacts with moisture to form sulfuric acid, which corrodes the nearby metal traces and IC chips. The trace amount of sulfur was measured by the RBS technique with a detection limit of 100 ppm. As shown in Figure 4-7 no sulfur could be detected by this method. Which means that the amount of residual sulfur, if it exists, is less than 100 ppm. This result indicates that the current calcination schedule fully convert the alumina precursor into α-alumina. True particle density was determined to be 1.3 gm/cm^3 using helium gas pycnometry. The theoretical density of the solid phase was calculated to be 2.87 gm/cm^3 from the weight fraction of each component in the calcined spheres. From these data the average porosity of the coated spheres after calcination was calculated to be 0.55. Compared with the porosity of uncoated hollow spheres (0.74), the coating process reduced the volume fraction of porosity significantly. However, subsequent experimental results demonstrates that the coating layer still provides adequate porosity to lower the dielectric constant and meet the research goal.

4.2 Densification of Green Compacts

Since the mixture of Al_2O_3 and SiO_2 is not thermodynamically stable at the sintering temperature, their chemical reaction during densification should be discussed first. According to the Al_2O_3-SiO_2 phase diagram (Figure 4-8) [13], mullite is the only stable compound under normal atmospheric pressure. The mullite formation temperature in the Al_2O_3-SiO_2 system varies significantly, ranging from 1000°C to more than 1500°C. For the same chemical composition and firing conditions, the exact mullitization temperature depends on the powder preparation method, which includes conventional mixing of oxides, colloidal mixing (sol-gel method) and solution-precipitation techniques.

For conventional mixing of oxides [14-18], since the powders used in the process are relatively coarse, the scale of mixing for the reaction is on the order of one micrometer. Thus, high processing temperatures are often required to achieve fast enough diffusion rate for reactions to be accomplished in a reasonable period of time. Although mixing of submicron powders resulted in some mullite formation at temperature as low as 1300°C, complete mullitization generally require much higher temperatures, ranging from 1600°C –1750°C.

Colloidal mixing methods [19-25] refers to mullite prepared from a suspension of very fine particles (sols). In fact, this technique is similar to the conventional mixing of oxide powders, except that the size of the reacting particles is much smaller (typically in the range of 5–50 nm). Since the distance for chemical diffusion is very short in this case, lower reaction temperatures for mullite formation are expected. Mullite formation could be observed at temperatures as low as 1200°C. However, complete reaction could not be achieved unless the sample was held at 1400°C for an extended time.

Since the temperature for mullitization decreases as the mixing of the reacting particles become more intimate, homogeneous mixing at the molecular level is expected to have the lowest reaction temperature. Molecular mixing could be achieved by using a solution-precipitation technique [26-28], such as dissolving appropriate aluminum- and silicon-bearing salts in a suitable solvent. By using this method, mullite formation was observed at temperatures as low as 1000°C, although the reaction was not complete until 1200°C.

To understand the evolution of mullite in the current system, composite samples consisting of alumina/coated spheres mixtures were prepared with the overall composition of Al_2O_3 : SiO_2 = 72 wt% : 28 wt%, which corresponded to the 3:2 stoichiometric mullite composition. Such a chemical composition would facilitate the mullite formation and, therefore, the precise mullitization temperature could be detected. These samples were fired at progressively higher temperatures and then analyzed by x-ray diffraction (XRD). It was found that under current experimental conditions, mullite started to form at ≈ 1300°C, corresponding to the mullitization temperature of mixtures prepared by conventional mixing of oxides. Above this temperature, mullite continued to develop at the expense of Al_2O_3 and SiO_2.

The densification behaviors of green compacts both with and without coated spheres were evaluated using a high temperature dilatometer. Figure 4-9 shows the shrinkage curves of pure alumina sample and of composite samples with various loading of spheres. The pure alumina sample started to densify at 1100°C and continued to shrink until ≈ 1500°C. At this temperature, the final density was close to 98% of the alumina theoretical density (3.98 g/cm^3). The densification of the samples loaded with coated spheres were

less than that of the pure sample. Figure 4-9 clearly shows that the addition of coated spheres to the alumina matrix significantly reduced the shrinkage rate of the composite samples over the entire densification period. At temperatures lower than the mullite formation temperature of the current system (≈1300°C), the low shrinkage rates of composite samples were caused by the poor sinterability of glass hollow spheres. This phenomenon could be attributed to two factors. First, the internal pressure at elevated temperature exerted an expansion force which opposed the shrinkage of hollow spheres. Second, during calcination, viscous flow of silica glass caused an early densification at the periphery of the coated spheres; a process similar to the viscous sintering of ceramic-filled composites [29-31]. Therefore, further densification in these areas was difficult. As the firing temperature increased, mullite started to form and further reduced the densification rate of the composite sample. Above 1400°C, significant amounts of mullite formed and the dilation caused by the mullite formation exceeded the shrinkage effect of the Al_2O_3/SiO_2 matrix and, therefore, an overall expansion was observed, as evidenced by curve (a) in Fig. 4-9. Based on these observations, the processing temperature of composite samples in this study was determined to be 1400°C. Sintering at higher temperatures would cause the de-densification of the composite samples and, therefore, were not attempted.

Several mechanisms during the mullite formation contribute to the expansion. First, since the density of mullite ($3Al_2O_3 \cdot 2SiO_2$, $\rho = 3.16$ g/cm^3) is lower than the density of the original $3Al_2O_3 + 2SiO_2$ mixture ($\rho = 3.32$g/cm^3), the chemical reaction, $3Al_2O_3 + 2SiO_2 \rightarrow 3Al_2O_3 \cdot 2SiO_2$ results in an overall volume expansion (≈ 4.6 %). During sintering, the amount of mullite formed increases with the firing temperature. If a sufficient amount of mullite is formed, the expansion effect may overcome the shrinkage effect of the matrix, and, therefore, a net expansion of the sample will occur. Second,

mullite powders are not as sinterable as the original Al_2O_3/SiO_2 matrix. This is mainly due to the slow diffusion rate of components in the complex mullite structure [34]. Therefore, high temperature is required to provide enough thermal energy to densify the mullite powders. As the firing temperature increases, more mullite forms and, as a result, a stable framework of less-sinterable mullite forms which prevents further densification of the matrix. Earlier studies [16-17, 35] on the reaction-sintering of Al_2O_3/SiO_2 mixtures also found that the formation of mullite retarded the shrinkage rate of the mixture.

In the study of reaction sintering of powder mixtures, it is often desirable to have densification prior to reaction. This can be achieved by varying one or more parameters, such as the crystalline form of reactants, particle size and firing temperature. Among these, however, particle size seems to be the most effective parameter [18,35]. According to the work done by Yangyun and Brook on the reaction-sintering of powder compacts [36], the densification rate depended on D^{-2} or D^{-3} (D being the particle size), whereas the reaction kinetics depended on D^{-1} or D^{-2}. This means that the densification mechanism is favored with respect to the reaction mechanism by decreasing the reactant particle sizes. In this study, since the particle sizes of the alumina matrix powders were very fine (0.2 μ m-0.4 μm), the densification rate was favored over the mullitization reaction rate in the current Al_2O_3-SiO_2 system.

4.3 Microstructure

To help discuss the nature of porosity in this study, pores are categorized into two types: inclusion pores and matrix voids. Inclusion-type pores are defined to be exclusively caused by intact hollow spheres. They are added to the system in a controlled manner to reduce its dielectric constant and, therefore, a high volume fraction of inclusion pores is

always desired. Any other types of pores in the matrix are classified as matrix voids. This type of void includes small intergranular and intragranular pores as well as large voids originated from particle agglomerations and packing imperfections. Matrix voids can not be controlled easily and will, therefore, degrade the system's mechanical and hermetic properties. Hence, although their presence also contribute to the reduction of the dielectric constant, the amount of such matrix voids should be minimized. When examining a polished surface under the microscope, inclusion pores are spherical in shape, which makes them easily differentiated from the irregularly shaped matrix voids.

Figure 4-10 predicts the final porosity of sintered samples as a function of weight % of coated spheres in green compacts, using 0.55 as the effective porosity of coated spheres after calcination. The curve was based on two assumptions. First, after sintering, the matrix itself was fully dense and all pores came from the free space in hollow spheres, i.e., they were all inclusion-type pores. Second, there was no shrinkage of hollow spheres, i.e., inclusion pores remained the same size throughout the sintering process. Figure 4-10 was used to determine the relative amount of starting materials for the preparation of green compacts, so that desired porosity in the final products could be obtained. Six groups of samples with predicted final porosity of 0.10, 0.15, 0.20, 0.23, 0.33 and 0.36 were analyzed. The last two groups were chosen because they corresponded to samples containing 60 vol% and 66 vol% of coated spheres, respectively, which were close to the maximum random packing density of monosized spheres (≈ 64 vol %) [37-39].

Figure 4-11 shows micrographs of polished samples with increasing porosity after sintering at 1400°C (no soaking) in air. In all three samples pores were found to be uniformly distributed. Neither phase segregation nor pore clusters could be observed. Since the cross-section was parallel to the direction of slip casting, this observation proved

that the slip casting process was an effective method to produce composite samples with a homogeneous distribution of second phase (coated spheres) in the matrix.

Figure 4-12 shows a typical high magnification micrograph of a sintered sample. In this picture, the alumina matrix was found to be fairly dense. All pores were spherical in shape without deformation; however, different morphologies on the inside surface of pores were observed. In pore (a), typical of the majority of pores, many well developed crystals in elongated shapes were seen. In pore (b) elongated grains were less obvious than in pore (a); whereas in pore (c), no such elongated grains could be seen, only a smooth surface covering the internal area of the pore. The needle-like crystals in pores (a) and (b) were mullite grains formed from the chemical reaction of Al_2O_3 and SiO_2. In current system it is believed that the low softening point glass behaved like a viscous liquid at elevated temperature, which enhanced the chemical interdiffusion rate of reactants and, therefore, facilitated the grain growth of mullite in the preferred direction. Different morphologies of pore (a), (b) and (c) were believed to be caused by the variation in thickness of the glass walls (refer to section 3.1.2). Spheres with thin walls had less glass to react with the α-alumina and, therefore, less glass would be left over after sintering. Figure 4-13 illustrates an internal surface of a pore with significant amounts of elongated mullite grains. A small amount of unreacted glass was seen amid these grains. On the other hand, if spheres had thick walls then the amount of unreacted glass also increased. A large amount of residual glass would then cover the internal surface of the pores, making the newly formed mullite grains less obvious. Figure 4-12 (d) indicates a shallow-cut pore which, because its deep pocket trapped secondary electrons during SEM examination, appeared much darker than other pores in the picture.

A few crescent-like voids (e), less than 1 vol. % of total porosity, were observed in all samples. They were believed to be caused by the debris of thin-walled spheres which broke under high internal pressure during calcination (refer to section 4.1.3). The debris melted at the high sintering temperature, penetrated into the surrounding matrix, and left voids behind which were originally occupied by these debris. Such voids in the matrix still retained the original shapes of the broken pieces. A detailed examination on the inside area of these voids found elongated mullite grains, similar to the grains observed in pore (a) and (b). A small amount of isolated sintering defects (f), due to nondensification of the matrix, were also observed, especially for samples with high loading of coated spheres (Figure 4-11 (c)). As mentioned above, the existence of any type of matrix voids, such as (e) and (f), should be avoided. However, due to their relatively small numbers and sizes when compared with inclusion pores, their existence was insignificant and could be ignored in the current investigation. No other obvious defects in the sintered samples was observed.

In Figure 4-11 some pores were very close, especially at a high volume fraction of spheres. Detailed examination found that they were always isolated from each other by a solid wall. There were no voids at the interstitial area, proving that the slip casting technique can be used to prepare dense and homogeneous microstructures for composite samples. The neighboring pores were separated by a dense matrix which prevented the formation of interconnected pores. The shortest pore-to-pore distance in the sample was found to be ≈ 3 μm. Such a small distance implied that the glass spheres touched each other after green compact formation. In this case, if there was no coating layer between the glass spheres, connected porosity would form at the contacting area during sintering. It demonstrated, therefore, that the surface coating technique was an effective method to preserve the integrity of pores during high temperature process.

4.4 Porosity

In the current study, the matrix voids should be minimized. This could be achieved by improving the slip casting process as well as optimizing the sintering schedule. On the other hand, the inclusion pores should be maximized. To make full use of the glass hollow spheres which supplied inclusion pores in the final product, these spheres should be stable and not shrink during densification of the matrix. Otherwise, the purpose of such porosity-adding material would be defeated. In general, in the final stage of densification, large pores are always more stable than small pores for two basic reasons [40-42]. First, the thermodynamic stability of a pore depends on its critical coordination number, n_c, which is a function of the relative sizes of pore and surrounding grains (i.e., dihedral angle) [42]. If the number of grains surrounding the pore, n, is larger than n_c, the pore will have a negatively curved surface and stay stable during sintering. Only when n was smaller than n_c will a pore shrink. Second, in terms of kinetic consideration, it will simply take a much longer time to fill a large void by diffusion. Zhao and Harmer [43] demonstrated that there was a very severe kinetic limitation for the removal of large pores in alumina. For example, they predicted that it would take several months to completely remove pores in the 6 - 8 μm range in alumina at 1600°C. The same work also found that pores (≈ 3 - 4 μm) remained at approximately the same size in alumina even after firing at 1800°C for 5 hours. In this study, the pore sizes were much larger than the grain sizes of alumina matrix (20 μm vs. 0.3 μm). The coordinating number, n, would be very large ($n >> n_c$) and, therefore, such large pores should be stable thermodynamically throughout the sintering process. Furthermore, kinetics limitations would also prevent any obvious shrinkage of such large pores during densification of the matrix.

In the current study, it is believed that in the early stage of sintering (before mullite formation), inclusion pores were stable and did not shrink, as discussed in section 4.2. At higher temperatures, less sinterable mullite grains started to form on the pore surface, which further stabilized these pores. Considering these factors, together with the thermodynamic and kinetic limitations discussed above, inclusion pores were expected to be stable and retain their sizes throughout the sintering process. Figure 4-14 compares the measured porosity after sintering with the predicated porosity as a function of volume fraction of coated spheres. If pore shrinkage occurred during densification, then the measured porosity should be less than the predicated value. Figure 4-14 shows that at low volume fraction, where the alumina matrix was fully dense, the measured porosity agreed very well with the predicted values. This experimental result clearly indicates that the postulate of pore stability is valid in this study.

High porosity is always desired for the reduction of the dielectric constant. This can be achieved by increasing the amount of coated hollow spheres in the green compacts. However, the volume fraction (X) of coated spheres is not without limit. In order to obtain a final microstructure with a dense matrix, a sufficient amount of alumina (AKP53) has to be supplied to fill all open spaces between coated spheres. At low volume fractions of coated spheres, this is not a problem since there are relatively large amounts of alumina available. As the volume fraction of coated spheres increases, the relative amount of alumina (1-X) will decrease correspondingly. When the volume fraction of coated spheres reaches its maximum random packing density ($X_m \approx 0.64$), there will be just enough alumina powders to fill all open spaces which are left over by the densely packed spheres. With higher loading of coated spheres, i.e., when $X > X_m$, the amount of matrix alumina will not be sufficient to fill all the interstices between the coated spheres and, therefore, some voids will form in the matrix. The volume ratio of coated spheres to alumina,

$(X_m/1-X_m) \approx 1.78$, is, therefore, a theoretical loading limit when preparing green samples. Any volume ratio higher than this critical value in the original mixture will result in matrix voids, which are not desired in this study and should be avoided.

Due to the existence of matrix voids, the actual porosity of sintered samples with high volume fractions of coated spheres is expected to be higher than predicted values. Figure 4-14 shows at low loading of spheres the measured values has a good match with the predicted data. However, the measured porosity starts to exceed the predicted porosity at volume fraction ≈ 0.60. This value is lower than the maximum density of random packing of spheres. Imperfect packing of coated spheres during slip casting of green compacts might be the reason for this lower value. Figure 4-15(a) illustrates the polished surface of a sample with spheres loading higher than the critical value (0.64 volume fraction). In this case, the sintered sample contained 0.66 volume fraction of coated spheres. At first glance there is no obvious difference between this picture and Figure 4-11, except for higher porosity shown by Figure 4-15(a). However, a detailed examination of this sample reveals that, besides inclusion-type spherical pores, some irregularly shaped matrix voids also exist. An example of such a void is indicated by the arrow sign in this figure and is shown in detail in Figure 4-15(b).

Further evidence of matrix voids caused by the lack of matrix alumina is illustrated in Fig. 4-16, which shows a polished sample with an even higher loading of spheres (80 vol%). It is obvious that due to the limited supply of matrix powder, continuous porosity was formed. In such cases, although the volume fraction of porosity is very high, the mechanical strength and hermetic property of the sintered samples will be severely degraded and, therefore, the material is not suitable for microelectronic applications. From the above discussion, it was concluded that at low loading of spheres, porosity could

be introduced to the matrix in a controlled manner to produce a good porous substrate material. When the volume fraction of coated spheres is close to their maximum random packing density, matrix voids start to form and the porosity can no longer be controlled.

4.5 Chemical Composition of Sintered Samples

Quantitative analysis of the chemical composition of crystalline phases in the final products was carried out by X-ray diffraction (XRD). To determine the relative amounts of alumina and mullite in the sintered sample, a calibration curve was first made by the following procedures: mixtures containing α-alumina and 5, 10, 20,·····,80 wt% mullite were mechanically mixed and analyzed by X-ray diffractometer. Peak ratios of the two phases were then calculated using $I_M / (I_A + I_M)$, where I_A and I_M were areas under the α-alumina (113) peak and mullite (121, 211) peaks, respectively. They were chosen because of their strong intensities as well as their lower overlapping effect from the background when compared with other peaks. A calibration curve was drawn using $I_M / (I_A + I_M)$ as a function of wt% alumina, as shown in Figure 4-17.

The diffraction pattern of a polished sample after sintering is shown in Figure 4-18. Alpha-alumina and mullite were the only phases which could be detected under current testing conditions. However, as discussed in section 4-3, the chemical reaction between Al_2O_3 and SiO_2 was not complete and some SiO_2 was left over. The reason why residual SiO_2 peaks were not seen in the XRD pattern could be due to the small amount of crystalline SiO_2 phase (cristobalite), which was below the detection limit of the diffractometer (≤ 3 %). However, in the current system, it was more likely that the majority of residual SiO_2 was an amorphous phase and, therefore, could not be detected. According to previous investigations of the reaction-sintering of the Al_2O_3-$2SiO_2$ system

[35], cristobalite was more reactive with α-alumina to form mullite than amorphous SiO_2. It was therefore less likely for the cristobalite to be left over after mullitization.

To verify this statement experimentally, a simple test was performed. Pure coated spheres were subjected to the normal sintering process, i.e. 1400°C in air, and then analyzed by XRD. The diffraction pattern is shown in Figure 4-19 with reference peak positions of cristobalite superimposed on the patterns. Since the Al_2O_3 : SiO_2 ratio in pure coated spheres was close to 1, there should be a significant amount of SiO_2 left after firing. If the residual SiO_2 was in the crystalline form (cristobalite), then the peaks should be detected easily. However, as shown in Figure 4-19, only α-alumina and mullite peaks were found in the diffraction pattern. No peaks corresponding to cristobalite or other crystalline phases of SiO_2, such as quartz or tridymite, could be detected. Instead a diffuse hump with a center close to the cristobalite peak was observed. This indicated that the residual SiO_2 phase after the designated firing schedule was amorphous. All amorphous glass which had been crystallized to cristobalite at elevated temperature reacted quickly with α-alumina and, therefore, could not be detected by XRD analysis.

Based on the above discussion, it was concluded that the final compositions of sintered samples contained α-alumina, mullite and residual amorphous glass. The relative amounts of these phases depends on the initial composition of green samples. Since amorphous SiO_2 could not be analyzed by XRD, its relative amount (x wt%) in the final product can be calculated using the following equation:

$$F_{\alpha,t} = (1 - x) \times F_{\alpha} + (1 - x) \times (1 - F_{\alpha}) \times 0.718 \qquad (4\text{-}2)$$

where $F_{\alpha,t}$ is the initial wt% of α-alumina before sintering and can be determined from the initial compositions of the green compacts. x is the wt% of residual SiO_2 in the sintered

sample which is to be determined, and (1-x) is the wt% of alumina/mullite mixture in the sintered sample (excluding the SiO_2 phase). F_α is the wt% of alumina in the alumina/mullite mixture and can be determined from Figure 4-17 and 4-18. The first term, $(1 - x) \times F_\alpha$, is therefore the amount of "free" alumina in the alumina/mullite mixture. $(1 - F_\alpha)$ is the wt% of mullite in the alumina/mullite mixture and 0.718 is the wt% of alumina in mullite (assuming a $3Al_2O_3 \cdot 2SiO_2$ mullite composition). The second term, $(1 - x) \times (1 - F_\alpha) \times 0.718$, is, therefore, the amount of alumina in the mullite structure.

Figure 4-20 shows vol% of phases in sintered samples as a function of wt% coated spheres. Samples containing more than 33 wt% (60 vol%) coated spheres were not analyzed. This was because such samples contained matrix voids and should be avoided. As shown in Figure 4-20, with increasing amounts of hollow spheres, both mullite and porosity in the sintered samples increased, while alumina decreased due to its chemical reaction with SiO_2. According to the Al_2O_3-SiO_2 phase diagram (Figure 4-8), the final microstructure of the samples being analyzed should be a mixture of α-alumina and mullite only. However, previous studies of mullite formation indicated that complete mullitization of oxide powder mixtures required a reaction temperature of at least 1600°C for long times [14-18]. Compared with the sintering schedule in this study, i.e., 1400°C with no soaking time, it is clear that current firing conditions are not high enough to achieve a complete chemical reaction of Al_2O_3 and SiO_2. Although complete mullitization could be obtained by either increasing the firing temperature or prolonging the sintering time, it was not attempted in this study. This was mainly because that, as shown in Figure 4-9, further development of mullite caused the de-densification of samples which, in turn, induced microstructural defects in the final products. The final microstructure of the sintered sample can, therefore, be envisaged as a composite consisting of uniformly dispersed pores

in a dense multiphase matrix. Each pore is surrounded by a mullite/glass mixture, with α-alumina acting as the continuous phase.

4.6 Dielectric Constant and Modified Maxwell's Equation

It has been demonstrated that the microstructure of sintered samples can be best described by Maxwell's mixing model, i.e., spherical pores uniformly distributed in a continuous solid matrix. Maxwell's equation (equation 2-5) is used to investigate the effect of coated glass hollow spheres on the dielectric constant of the sintered samples. According to the previous discussion (section 2.1), however, Maxwell's mixing model applies only to composites with a single-phase matrix. In the current system, since the matrix contains more than one phase, it is, therefore, necessary to modify Maxwell's mixing equation. In this study, two approaches are used and both show quite similar results.

(1) Spherical pores uniformly distributed in an multicomponent matrix

In the first approach, the final microstructure is considered to consist of spherical pores ($k \approx 1$) uniformly distributed in a dense solid matrix. Before using Maxwell's equation to predict the dielectric constant of the sintered samples, the k value of the matrix should be determined first. Since in such a multicomponent matrix, alumina is the continuous phase and mullite/glass mixture is the dispersed phase, it is reasonable to also use the Maxwell's equation to determine the effective dielectric constant of the solid matrix (k') :

$$k' = \frac{v_m k_m (\frac{2}{3} + \frac{k_d}{3k_m}) + v_d k_d}{v_m (\frac{2}{3} + \frac{k_d}{3k_m}) + v_d}$$

where phase d is for mullite/glass mixture phase and phase m is for continuous alumina phase.

In the mullite/glass mixture the amount of glass is small (≤ 5 vol%, as shown in Figure 4-20) and the k values of mullite and glass are close to each other (k = 6.5 and 5.0 for mullite and glass, respectively). It is, therefore, appropriate to use the simple rule of mixing to predict the dielectric constant of the mullite/glass mixture.

$$k_d = v_m k_m + v_g k_g$$

where phase m is for mullite and phase g is for glass. After obtaining the k' value of the solid phase, the dielectric constant of the sintered sample can then be calculated according to Maxwell's equation, using multicomponent solid as the continuous phase and air as the dispersed phase.

(2) Glass/mullite hollow spheres uniformly distributed in the alumina matrix

The second approach assumes that the final microstructure contains spherical hollow spheres with a mullite/glass shell uniformly distributed in the continuous α-alumina matrix. In calculating the effective dielectric constant of hollow spheres, k', since none of the

constitutive phases (free space, mullite and glass) is continuous, simple rule of mixing should be used:

$$k' = v_{fs}k_{fs} + v_m k_m + v_g k_g$$

where phase fs is for free space, phase m is for mullite, and phase g is for glass.

After obtaining the effective dielectric constant of the hollow spheres as a whole, the Maxwell's equation is used by assuming alumina as the continuous phase and hollow spheres with a mullite/glass shell as the dispersed phase.

$$k = \frac{v_m k_m (\frac{2}{3} + \frac{k_d}{3k_m}) + v_d k_d}{v_m (\frac{2}{3} + \frac{k_d}{3k_m}) + v_d}$$

where phase d is for dispersed mullite/glass hollow spheres ($k_d = k', v_d = v'$) and phase m is for continuous alumina phase.

Table 4-1 lists calculated k values of sintered samples following the procedures discussed above. Relative amounts of each phases were obtained from Figure 4-20. Two sets of calculated values are found to have an excellent match with each other, indicating that both approaches are valid methods to predict the dielectric constant of sintered samples in the present system.

Figure 4-21 shows the modified Maxwell's mixing curve using data from Table 4-1. Also shown in this figure, for comparison, are curves of the simple mixing rule and

Maxwell's mixing rule before modification (assuming alumina only matrix). It clearly demonstrate that the modified Maxwell's mixing curve is significantly lower than the curve without modification, which is beneficial for the purpose of this study. Obviously the presence of mullite and glass, which has a much lower dielectric constant than the α-alumina matrix, decreases the effective k value of the solid phase and, therefore, the total dielectric constant of the composite materials. The measured k values of samples are also drawn in this figure and are found to be in fair agreement with the modified Maxwell's mixing curve. With 33 wt% spheres (60 vol% spheres and 0.34 final porosity) the dielectric constant of the composites was as low as 5.1, which met the research goal of this study.

4.7 Flexural Strength of Sintered Samples

Substrates are subjected to mechanical stress during manufacturing operations which convert a blank substrate into an electronic part ready to be attached to a circuit board. Some of these operations, such as pinning and soldering, apply mechanical stress to the substrate. Transportation and handling processes also induce stresses high enough to cause failure. These failures are costly because they occur in the final stage of manufacturing operations of a computer system. The mechanical strength requirement of microelectronic substrates need not be very high; however, a minimum value should be satisfied [44,45].

The effect of pores on the mechanical strength of bulk ceramics has been studied extensively. In general, pores may have any or all of the following effects on the mechanical behavior of ceramics:

1. Pores reduce the loading bearing area and therefore increase effective stress.
2. Pores act as stress concentration factors and increase local stress near pores [46,47].
3. Pores act as an integral part of flaws and increase the critical flaw length [48,49]
4. Pores may connect to each other to form large cracks [46].

Typical serological relations of average porosity and mechanical strength are usually not applicable to porous ceramics. This is because fracture will generally follow the path of maximum free space and minimum solid phase. Therefore, in a discussion of the effect of porosity on the mechanical strength of ceramics, the homogeneity of porosity is important. In evaluating the mechanical behavior of porous ceramics the extremes of pores, rather than average porosity, must be considered. Since fracture is a weak-link type process, failure will occur from the largest or most extremely shaped pore, or pore clusters, or interconnected pores. All of these features are often observed in samples with non-controlled porosity. On the other hand, a well controlled porosity, i.e., spherical pores with narrow size range and uniform spatial distribution, will minimize such extremes. Therefore, based on the degree of pore inhomogeneity; a considerable range of mechanical strength can be observed for different testing samples with the same porosity.

Full densification of the matrix is also an important factor to determine the mechanical strength of porous ceramics. As discussed before, matrix voids are often of irregular shape and difficult to control. Such voids will link neighboring pores and increase the effective pore size. Large voids may also act as critical flaws. Both effects greatly reduce the mechanical strength of testing samples.

As discussed in section 2.2.1, the existence of pores reduces the mechanical strength of bulk ceramics according to the equation: $\sigma = \sigma_0 \exp(-bp)$, with b in the range of 4-7.

Inhomogeneity of pore characteristics, i.e., variations in pore size, shape and location are probably the most important factors causing such wide range of b values. A lower b value indicates that the porosity in the testing specimen is well controlled, which also means that the mechanical strength of such a sample is higher than samples with non-controlled porosity.

As shown in Figure 4-12, the matrix of sintered samples was found to be well densified. A minimum amount of matrix defects was observed. The pores were uniformly distributed in the sample. There were no connected porosity and all pores were spherical without any obvious deformation. Sharp cusps inside the pore, caused by the interpenetrating long mullite grains, may introduce a high stress concentration and cause a significant reduction of mechanical strength. However, in the current system, residual amorphous SiO_2 from unreacted glass walls will fill these cusps and, therefore, greatly reduce the potential danger of such a stress concentration effect. Since samples being tested showed the desired microstructure with controlled porosity, the mechanical strength should be less degraded by the existence of pores, i.e., b values in equation 2-6 should be in the lower range.

Mechanical strength was evaluated in the four-point flexure mode and the results are shown in Fig. 4-22. Each point in this figure is the average value of 5 samples. The flexural strength of dense pure alumina is high (470 MPa). However, as expected, the flexural strength decreases rapidly with increasing porosity. By fitting σ_o, σ and p into equation 2-6, b values are calculated to be in the range of 4.0-4.4, as shown in Table 4-2. Data show trend of higher b values in samples with higher porosity. This might be caused by the existence of a small amount of matrix voids in these samples. Considering the larger pore sizes (≈20μm) in testing samples when compared with other work [46-49],

such low b values are believed to be a good indication that the current fabrication technology is effective to prevent a large degradation in the mechanical strength of porous ceramics. At 0.34 porosity the flexural strength is reduced to 105 MPa. This value, although it is relatively low, can still meet the industrial requirements for current microelectronic applications [44,45].

References for Chapter 4

1. J.E. Blendell, H.K. Bowen and R.L. Coble, "High Purity Alumina by Controlled Precipitation from Aluminum Sulfate Solutions," *Am. Ceram. Soc. Bull.*, 63 [6], 797-801 (1984).
2. B.C. Cornilsen and J.S. Reed, "Homogeneous Precipitation of Basic Aluminum Salts as Precursors for Alumina," *Am. Ceram. Soc. Bull.*, 58 [12], 1199 (1979).
3. H.J. Frost and R.Raj, "Limiting Densities for Dense Random Packing of Spheres," *J. Am. Ceram. Soc.*, 65[2], C19-C21 (1982).
4. M.J. O'Hara and I.B. Cutler, "Sintering Kinetics of Binary Mixtures of Alumina Powders," *Proc. Brit. Ceram. Soc.*, 12 145-154 (1969).
5. J.P. Smith and G.L. Messing, "Sintering of Bimodelly Distributed Alumina Powders," *J. Am. Ceram. Soc.*, 67 [4] 238-242 (1984).
6. W.H. Tuan, E.Gillbart and R.J. Brook, "Sintering of Heterogeneous Ceramic Compacts, Part 1 Al_2O_3-Al_2O_3," *J. Mater. Sci.*, 24 1062-1068 (1989).
7. D. Kapolnek, "Synthesis of Alumina-Coated SiC Whiskers for Production of SiC Whisker-Reinforced Alumina Composite Materials," M.S. thesis, U. C. Berkeley (1989).
8. M.D. Sacks, T.Y. Tseng and S. Y. Lee, "Thermal Decomposition of Spherical Hydrated Basic Aluminum Sulfate," *J. Am. Ceram. Soc.*, 63 [2] 301-310 (1984).

9. C.J.P. Steiner, R.M. Spriggs and D.P.H. Hasselman, "Synergetic Pressure Sintering of Al_2O_3," *J. Am. Ceram. Soc.*, 55[2], 115-116 (1972).

10. D.I. Matkin, W. Munro and T.M. Valentine, "Some Factors Affecting the Reactive Hot Pressing Behavior of Alumina," *J. Mater. Sci.*, 6, 974-980 (1971).

11. A.C.D. Chaklader and L. G. McKenzie, "Reactive Hot-Pressing of Clays and Alumina," *J. Am. Ceram. Soc.*, 49[9], 477-483 (1966).

12. P.A. Badkar and J.E. Bailey, "The Mechanism of Simultaneous Sintering and Phase Transformation in Alumina," *J. Mater. Sci.*, 11, 1794-1806 (1976).

13. J.A. Pask, "Critical Review of Phase Equilibrium in the Al_2O_3-SiO_2 System," in *Ceramic Transactions, Vol. 6: Mullite and Mullite Matrix Composites*, 1-13 (1990).

14. M.D. Sacks and J.A. Pask, "Sintering of Mullite," in *Materials Science Research, Vol. II: Processing of Crystalline Ceramics*, 193-203 (1978).

15. M.D. Sacks and J.A. Pask, "Sintering of Mullite-Containing Materials: I, Effect of Composition," *J. Am. Ceram. Soc.*, 65 [2], 65-70 (1982).

16. A.P.S. Rana, O. Aiko and J.A. Pask, "Sintering of α-Al_2O_3 /Quartz and α-Al_2O_3 /Cristobalite Related to Mullite Formation." *Ceram. Int.*, 8, 151-153 (1982).

17. Y. Nurishi and J.A. Pask, "Sintering of α-Al_2O_3-Amorphous Silica Compacts," *Ceram. Int.*, 8, 57-59 (1982).

18. P.D.D. Rodrigo and P.Boch, "High Purity Mullite Ceramics by Reaction Sintering," *Int. J. High. Technol. Ceram.*, 1, 3-30 (1985).

19. B.B. Ghate, D.P.H. Hasselman and R.M. Spriggs, "Synthesis and Characterization of High Purity, Fine Grained Mullite," *Bull. Am. Ceram. Soc.*, 52 [9], 670-672 (1973).

20. M.D. Sacks and J.A. Pask, "Sintering of Mullite-Containing Materials: II, Effect of Agglomeration," *J. Am. Ceram. Soc.*, 65 [2] 70-77 (1982).

21. M.G.M.U. Ismail, Z. Nakai and S. Somiya, "Microstructure and Mechanical Properties of Mullite Prepared by the Sol-Gel Method," *J. Am. Ceram. Soc.*, 70 [1],

C7-C8 (1987).

22. R. Roy, S. Komarneni and D.M. Roy, "Multi-Phasic Ceramic Composites Made by Sol-Gel Technique," in *Mat. Res. Soc. Symp. Proc., Vol. 32: Better Ceramics Through Chemistry,* 347-359 (1984).

23. S. Komarneni, Y. Suwa and R. Roy, "Application of Compositionally Diphasic Xerogels for Enhanced Densification: The System Al_2O_3-SiO_2," *J. Am. Ceram. Soc.*, 69 [7], C155-C156 (1986).

24. B. Sonuparlak, "Sol-Gel Processing of Infrared Transparent Mullite," *Adv. Ceram. Mater.*, 3 [3] 263-267 (1988).

25. W.C. Wei and J.. Halloran, "Phase Transformation of Diphasic Aluminosilicate Gels," *J. Am. Ceram. Soc.*, 71 [3], 166-172 (1988).

26. G.Y. Meng and R.A. Huggins, "A New Chemical Method for Preparation of Both Pure and Doped Mullite," *Mat. Res. Bull.*, 18, 581-588 (1983).

27. Y. Hirata and K. Shimada, "Preparation and Sinterability of Fine Mullite Powder from Mixed Alkoxides," in *Mullite*, 89-122, 1985.

28. L.A. Paulick, Y.F. Yu and I.I. Mah, "Ceramic Powders from Metal Alkoxide Precursors," in *Advances in Ceramics, Vol. 21: Ceramic Powder Science,* 121-129 (1987).

29. K.G. Ewsuk, "Ceramic-Filled-Glass Composite Sintering, " in *Ceramic Transaction, Vol. 15: Materials and Processes for Microelectronic Systems,* 279-295 (1990).

30. K.G. Ewsuk and L.W. Harrison, "Densification of Glass-Filled Alumina Composites," in *Ceramic Transactions, Vol. 7: Sintering of Advanced Ceramics,* 436-451 (1990).

31. G.W. Scherer, "Viscous Sintering of Particle-Filled Composites," *Ceram. Bull.*, 70 [6], 1059-1063 (1991).

32. D.B. Ghate, D.P.H. Hasselman and R.M. Spriggs, "Kinetics of Pressure-Sintering

and Grain Growth of Ultra Fine Mullite Powder," *Ceram. Inter.*, 1, 105-110 (1975).

33. P.C. Dokko, J.A. Pask and K.S. Mazdiyzsni, "High Temperature Mechanical Properties of Mullite Under Compression," *J. Am. Ceram. Soc.*, 60 [3-4], 150-155 (1977).
34. I.A. Aksay, "Diffusion and Phase Relationship Studies in the Alumina Silica System," Ph.D. Thesis, University of California, Berkeley, April 1973.
35. P. Boch and T. Chartier, "High-Purity Mullite Ceramics by Reaction-Sintering," in *Ceramic Transactions, Vol. 6: Mullite and Mullite Composites*, 353-374 (1990).
36. S. Yangyun and R.J. Brook, "Preparation of Zirconia-toughened Ceramics by Reaction-Sintering," *Sci. Sint.*, 17 [1] 35-47 (1985).
37. H.J. Frost and R. Raj, "Limiting Densities for Dense Random Packing of Spheres," *J. Am. Ceram. Soc.*, 65[2], C19-C21 (1982).
38. R. Liniger and R. Raj, "Packing and Sintering of Two-Dimensional Structure Made from Bimodel Particle Size Distribution," *J. Am. Ceram. Soc.*, 70 [11], 843-849 (1987).
39. F. Zok and F.F. Lange, "Packing Density of Composite Powder Mixtures," *J. Am. Ceram. Soc.*, 74 [8], 1880-1885 (1991).
40. W.D. Kingery and B. Francois, "Sintering of Crystalline Oxides, I. Interactions Between Grain Boundaries and Pores," in *Sintering and Related Phenomena*, 471-498 (1967).
41. W.D. Kingery, H.K. Bowen and D.R. Uhlmann, in *Introduction to Ceramics*, Chap. 10, 2nd edition, John Wiley & Sons, Inc., New York, 1976.
42. F.F. Lange, "Contributions of Sintering and Coarsening to Densification: A Thermodynamic Approach,'" in *Advanced Ceramics III*, 57-70 (1990).
43. J. Zhao and M. P. Harmer, "Effect of Pore Distribution on Microstructure Development: II, First- and Second- Generation Pores," *J. Am. Ceram. Soc.*,

71 [7], 530-539 (1988).

44. D.M. Mattox and S.R. Gurkovich, "Low Dielectric Constant , Alumina-Compatible, Co-Fired Multilayer Substrate," *Ceram. Eng. Sci. Proc.*, 9 [11-12] 1567-1578 (1988).
45. R. Gerhardt, "Composites for Electronic Substrate Applications," *Mat. Res. Soc. Symp. Proc.*, Vol. 108 101-107 (1988).
46. R.W. Rice, "Microstructure Dependence of Mechanical Behavior of Ceramics." in *Treatise on Materials Science and Technology, Vol. 11: Properties and Microstructure*, 199-381 (1977).
47. O. Vardar, I. Finnie, D.R. Biswas and R.M. Fulrath, "Effect of Spherical Pores on the Strength of a Polycrystalline Ceramic," *Int. J. of Fracture*, 13 [2], 215-223 (1977).
48. A.G. Evans and G. Tappin, "Effects of Microstructure on the Stress to Propagate Inherent Flaws," *Proc. Brit. Ceram. Soc.*, 20, 275-297 (1972).
49. R.W. Rice, "Pores as Fracture Origins in Ceramics," *J. Mat. Sci.* 19, 895-914 (1984).

Chapter 5

Conclusions

The dielectric constant, which determines the signal propagation speed, is an important property of microelectronic substrate. Currently, alumina is the most widely used substrate material due to its good combination of the necessary properties. However, the dielectric constant of alumina (k = 10) is too high for application in advanced computer systems. There is, therefore, an urgent need to reduce the dielectric constant of the substrate to a much smaller value ($k \rightarrow 5$). Various mixing rules indicated that by adding a second phase with low k value, the total dielectric constant of composites can be reduced significantly. The most effective method is to introduce free space, i.e. pores with $k = 1$, into bulk ceramics. However pores cuase severe degradation on both mechanical and hermetic properties. To minimize the degradation, adding porosity in a controlled manner is critical. Controlled porosity should have the following pore characteristics: spherical shape, small size, uniform spatial distribution and isolated porosity. The matrix itself should also be dense with small grain sizes.

Glass hollow spheres were chosen to be the porosity-adding agents and were added to the alumina matrix. However, due to the low softening point of the glass (900°C), which was well below the densification temperature of the alumina matrix (1400°C), glass spheres were not suitable for high temperature applications. One corrective method was to coat a thin layer of high temperature material on the surface of each hollow sphere. In the current study a controlled precipitation in aqueous solution method was used and demonstrated to be an effective method for this purpose. With good control of experimental parameters, a thin layer of alumina precursor was heterogeneously

precipitated on the surface of the glass hollow spheres. A minimum amount of free particles coming from homogeneous nucleation was observed. Coated spheres were then calcined at 1150°C to convert the alumina precursor into α-alumina. Subsequent studies proved that this alumina coating layer helped to maintain the integrity of glass hollow spheres at high temperature and ensure the isolation of pores after densification of the alumina matrix.

In preparing green samples of composite materials, a uniform distribution of different phases was required for a homogeneous microstructure. In the present investigation, slip casting was found to be a good sample consolidation method for the mixing of coated spheres in the alumina matrix. After sintering at 1400°C, spherical pores were uniformly distributed in the fully dense alumina matrix. Only negligible amounts of matrix defects could be seen. All pores were isolated from each other; no connected porosity could be observed. Detailed analysis of the chemical composition found that sintered samples consisted of α-alumina, mullite and residual glass. Mullite was the chemical reaction product of alumina and glass wall and was in the form of needle-like grains. Residual glass also existed because current firing conditions were not high enough to complete the mullitization reaction.

The dielectric constant of the sintered samples was measured and was compared with predicted values using Maxwell's mixing model. Maxwell's model was used because it best described the microstructure of the final products in this study. Good matching was observed, indicating that the designed microstructure with controlled porosity had been achieved in the final products. Mechanical strength was evaluated by four-point bending test. Although the flexural strength decreased exponentially with porosity, samples with

34% porosity ($k \approx 5.0$) still maintain adequate mechanical strength for the proper operation of an microelectronic substrate.

Table 3-1

Typical Properties of SDT60 Glass Hollow Spheres

(* indicated data obtained in current research)

PHYSICAL :

Density (g/cc)	0.5
Softening Point (°C)	900
Wall Thickness (μm)*	0.8-1.2
Average Diameter (μm)*	21
Standard Deviation (μm)*	10
Strength - % Collapse	
@ 500 psi	1%
@ 1000 psi	2%
@ 2000 psi	4%
@ 4000 psi	7%

CHEMICAL : (wt%)

SiO_2	93%
B_2O_3	3%
Na_2O	2%
BaO	1%

ELECTRICAL :

Dielectric Constant (1-8.6 GHz)	1.430
Dissipation Factor (1-8.6 GHz)	0.003

Table 4-1

Calculated *k* Values of Sintered Samples Using Maxwell's Equation

Porosity (%)	Approach (1) (second phase : air) (matrix : multiphase)	Approach (2) (second phase : mullite/glass hollow spheres) (matrix : single phase)
0	10	10
9.8	8.57	8.37
15.0	7.67	7.60
20.4	6.83	6.89
22.4	6.24	6.18
33.9	5.09	5.16

Table 4-2

Flexural Strength of Sintered Samples

by Four-point Testing Mode

Porosity (%)	Flexural Strength (MPa)	b in $\sigma = \sigma_0 \exp(-bp)$
0	470	
9.8	317	4.0
15.0	250	4.2
20.4	200	4.2
22.4	185	4.2
33.9	104	4.4

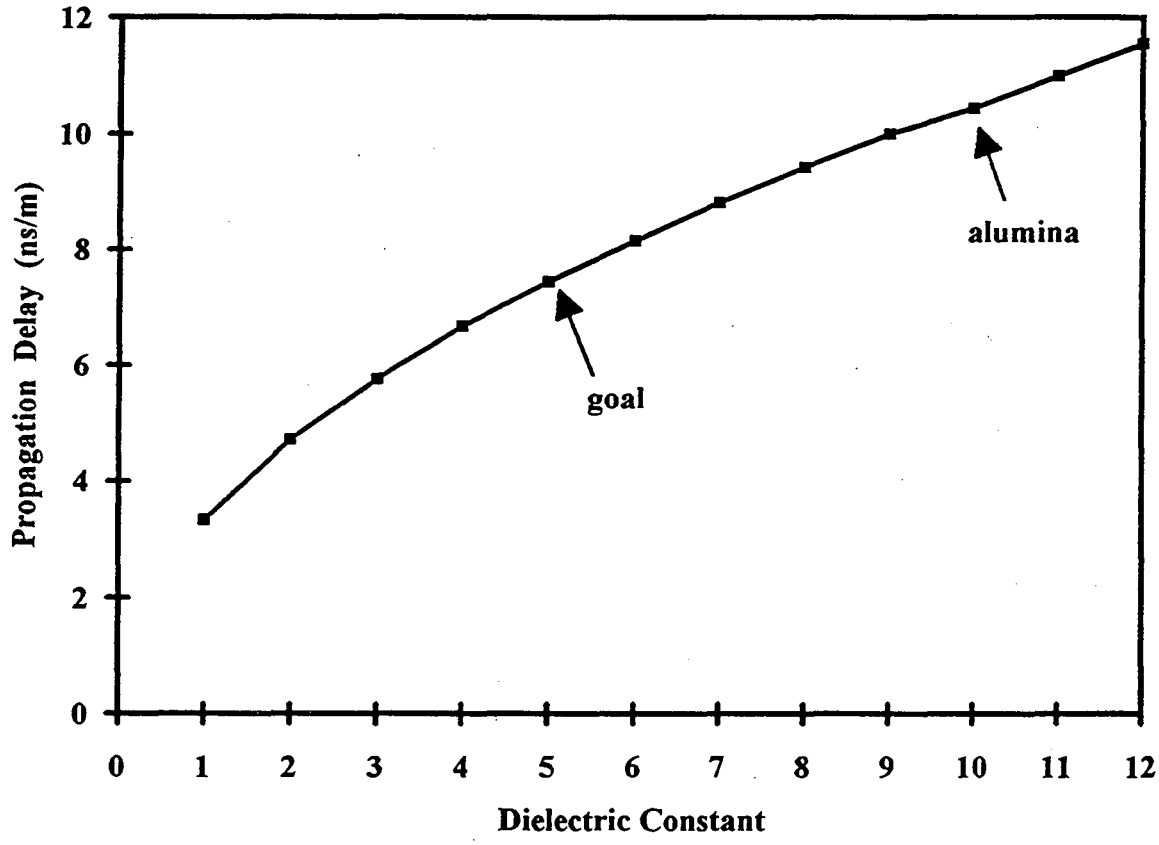

Figure 1-1. The signal propagation delay (ns/m) as a function of the dielectric constant (*k*) of the surrounding substrate material.

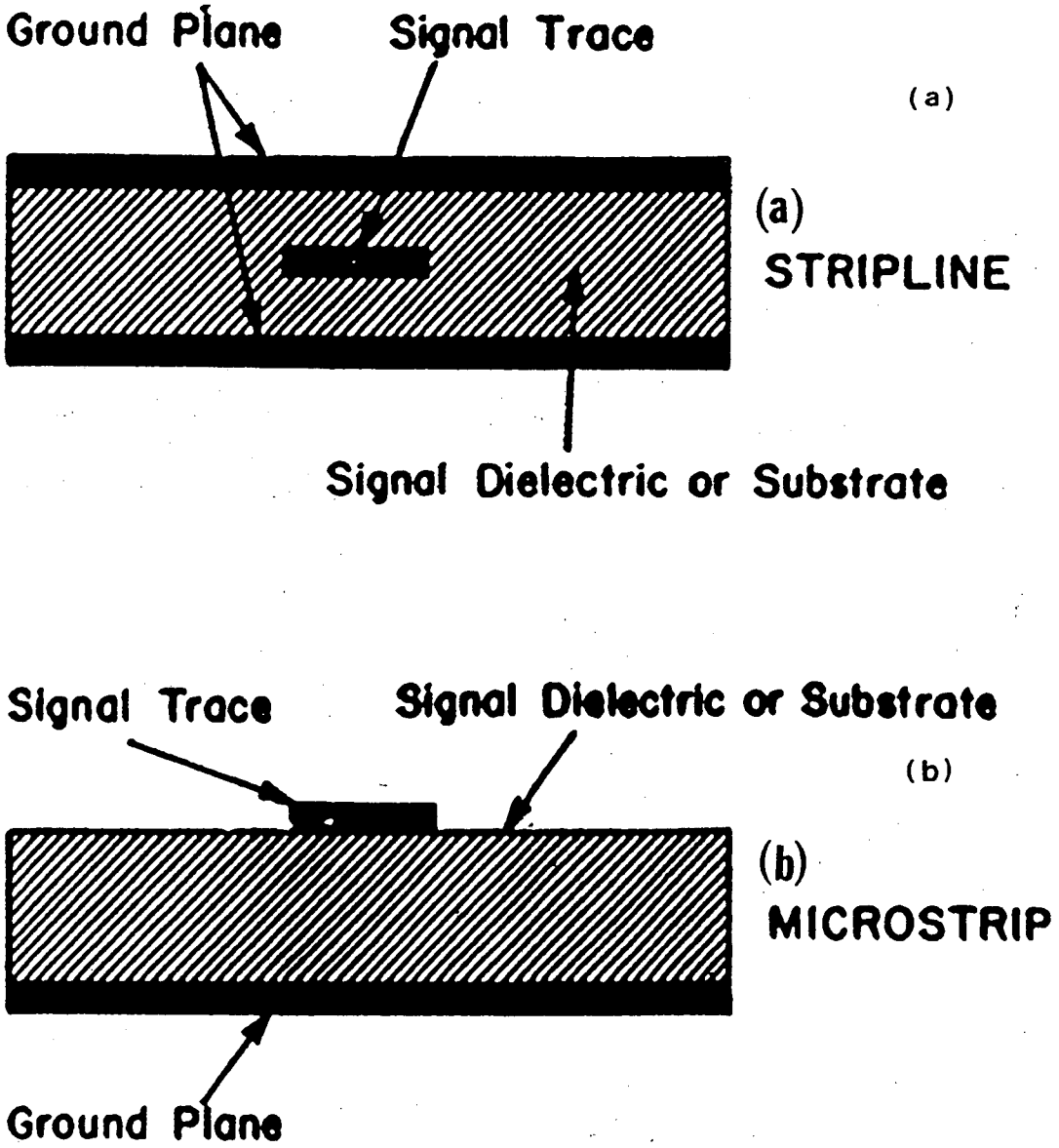

Figure 1-2. Two types of metal trace configurations in the microelectronic substrate: (a) stripline and (b) microstrip.

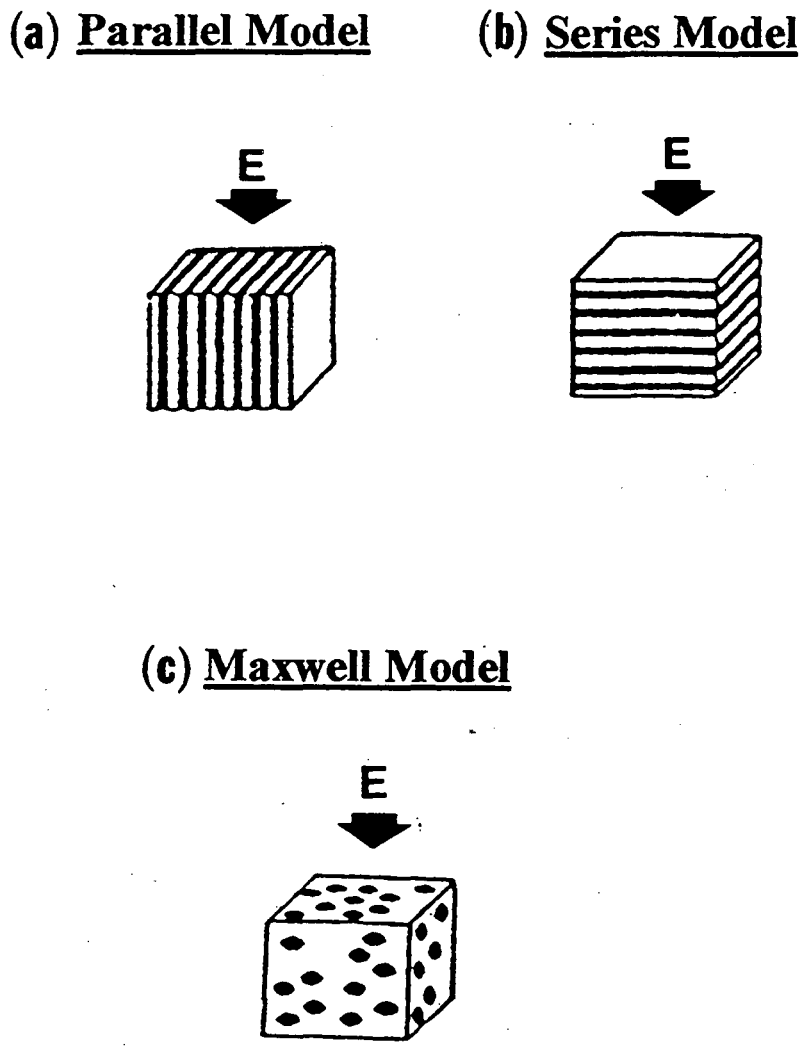

Figure 2-1. The geometry of three basic arrangements of two-phase composites. (a) parallel mixing model, (b) series mixing model, and (c) Maxwell's mixing model.

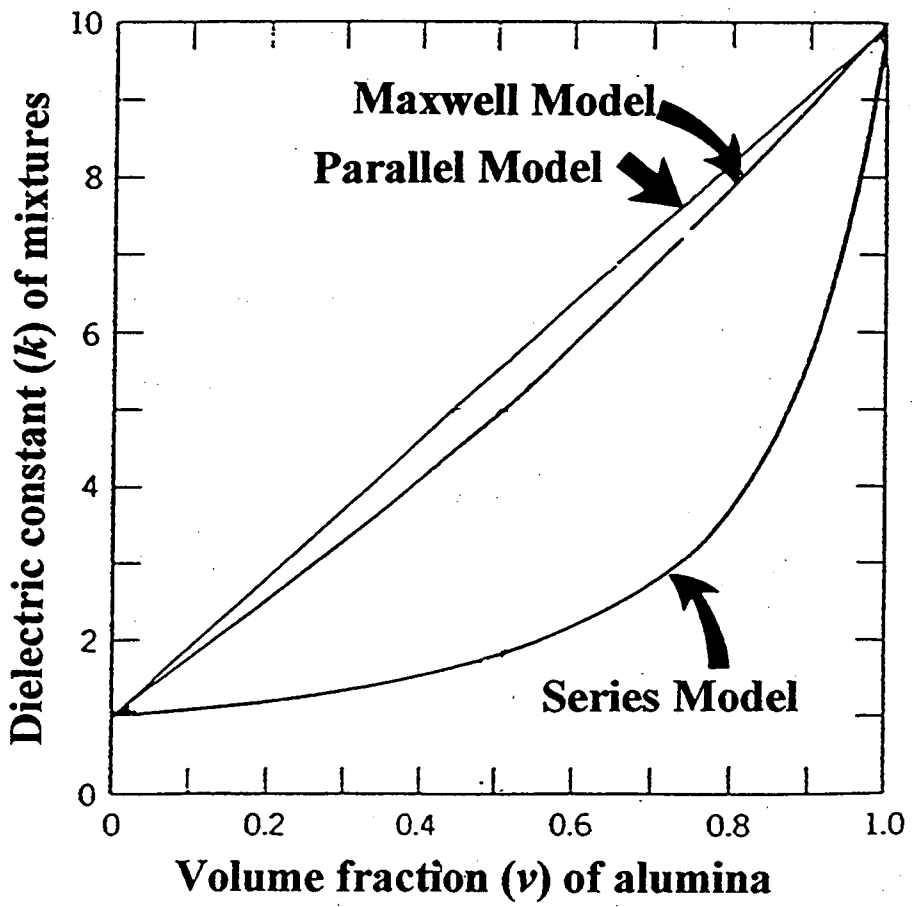

Figure 2-2. The dielectric constant of mixtures (alumina + porosity) as a function of volume fraction alumina for different mixing models.

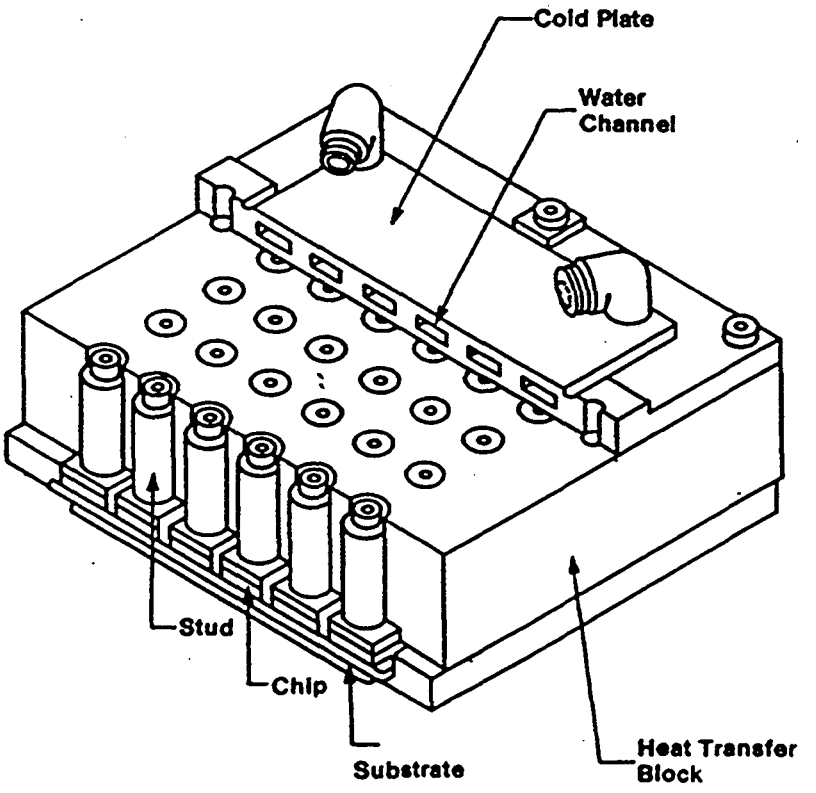

Figure 2-3. The schematic of a Thermal Conduction Module (TCM) with heat sink connected to IC chips the to dissipate heat. (from reference 2-11)

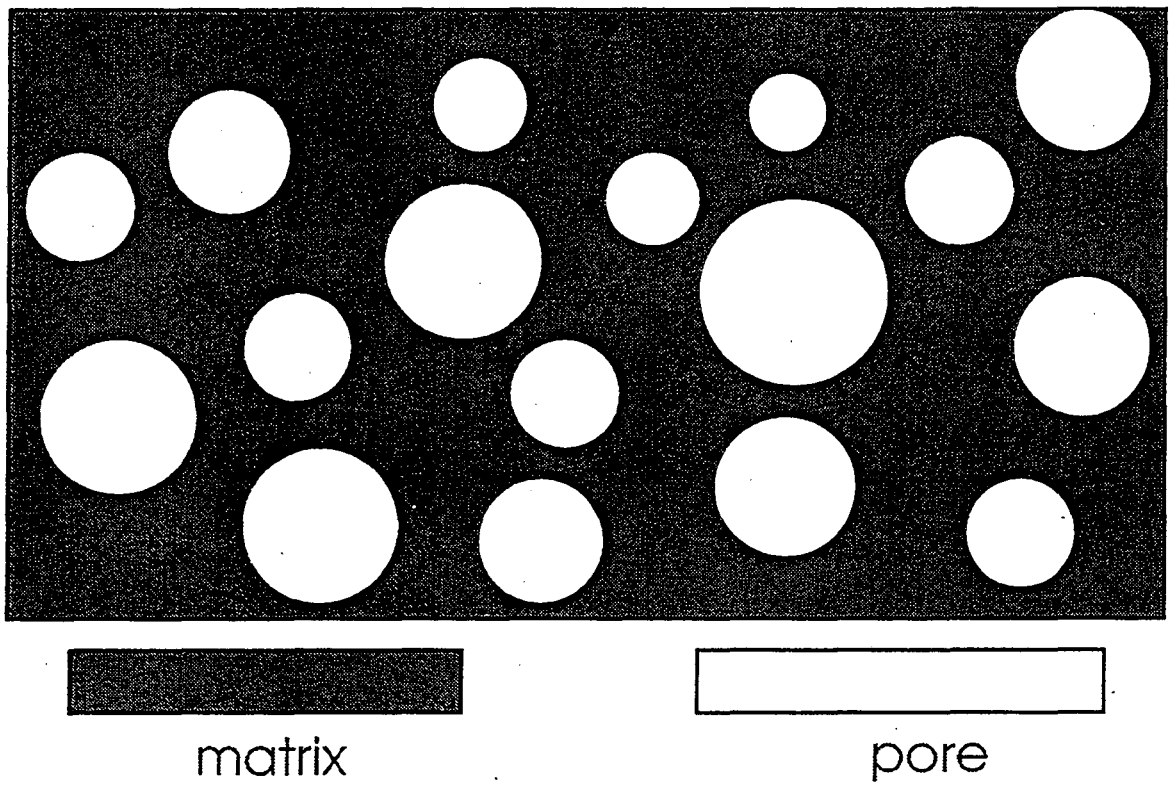

Figure 2-4. A schematic drawing of desired microstructure of final products in this study, showing dense matrix with controlled porosity.

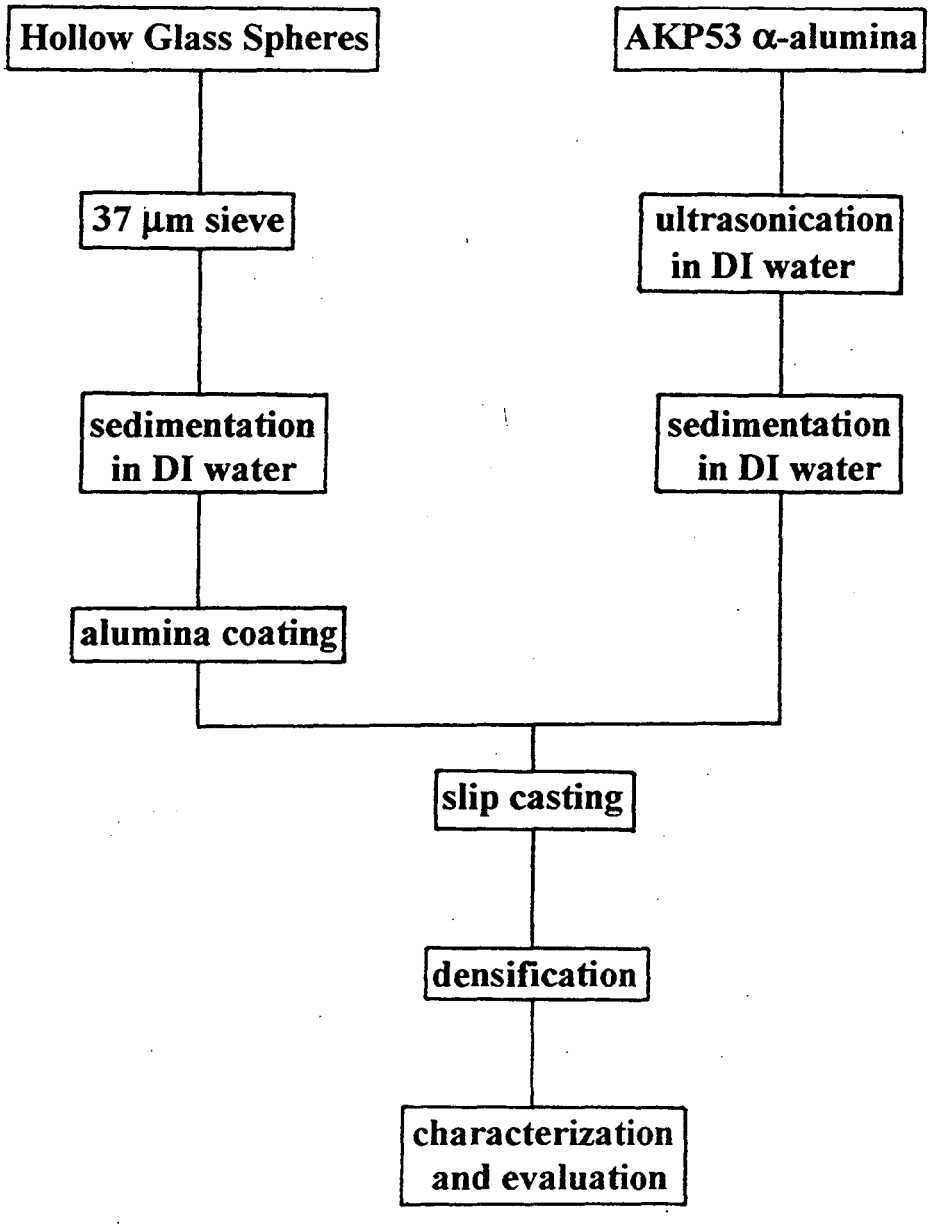

Figure 3-1. The experimental flowchart to prepare composite samples with alumina as the continuous phase and coated hollow spheres as the dispersed phase.

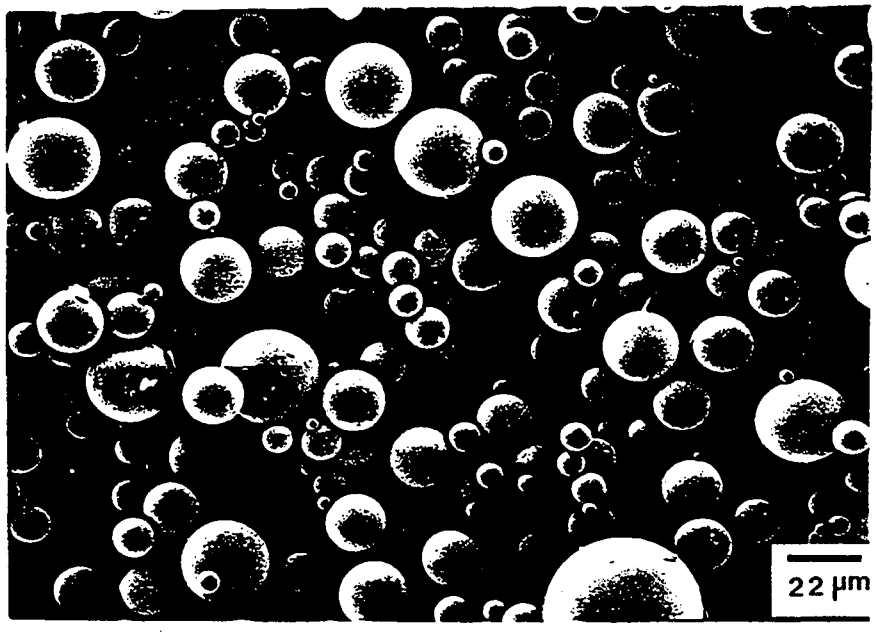

Figure 3-2. SEM micrograph of as-received SDT 60 glass hollow spheres from Grace Syntactis, showing good spherical shapes with a large size distribution.

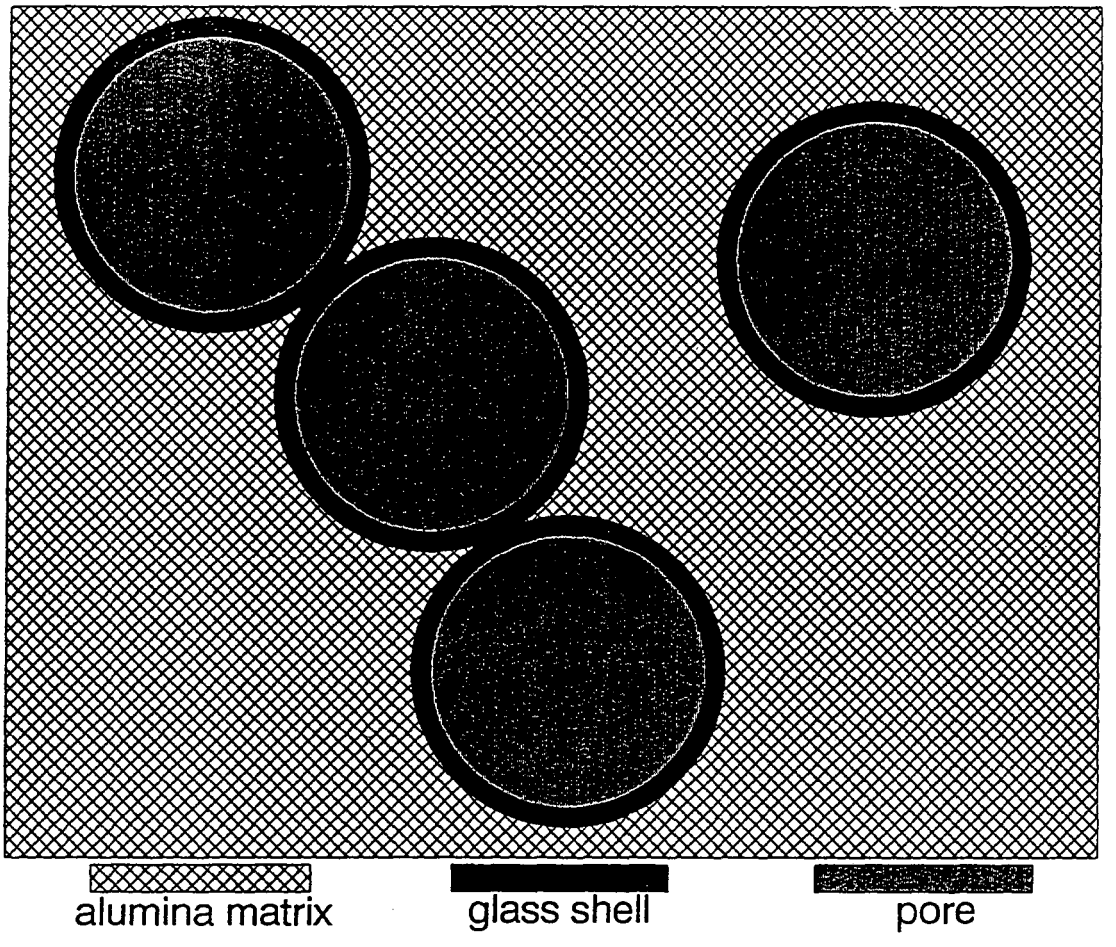

Figure 3-3. A schematic drawing of touching glass hollow spheres in the alumina matrix after green compacts formation, but before sintering.

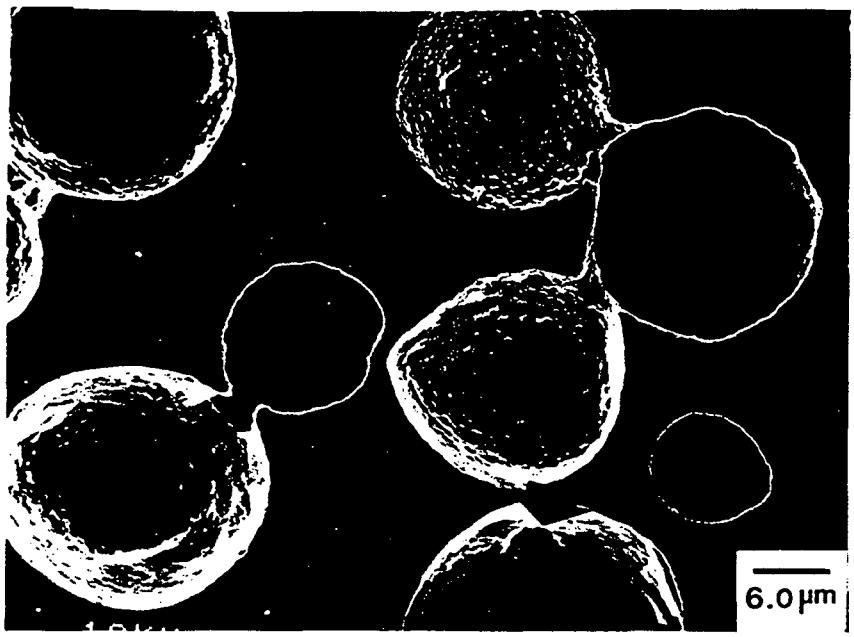

Figure 3-4. SEM micrograph of polished surface of sample containing 80 vol% alumina and 20 vol% as-received glass hollow spheres. Sintering was conducted at 1400°C in air (no soaking). The arrow indicates an early stage of interconnection between neighboring pores.

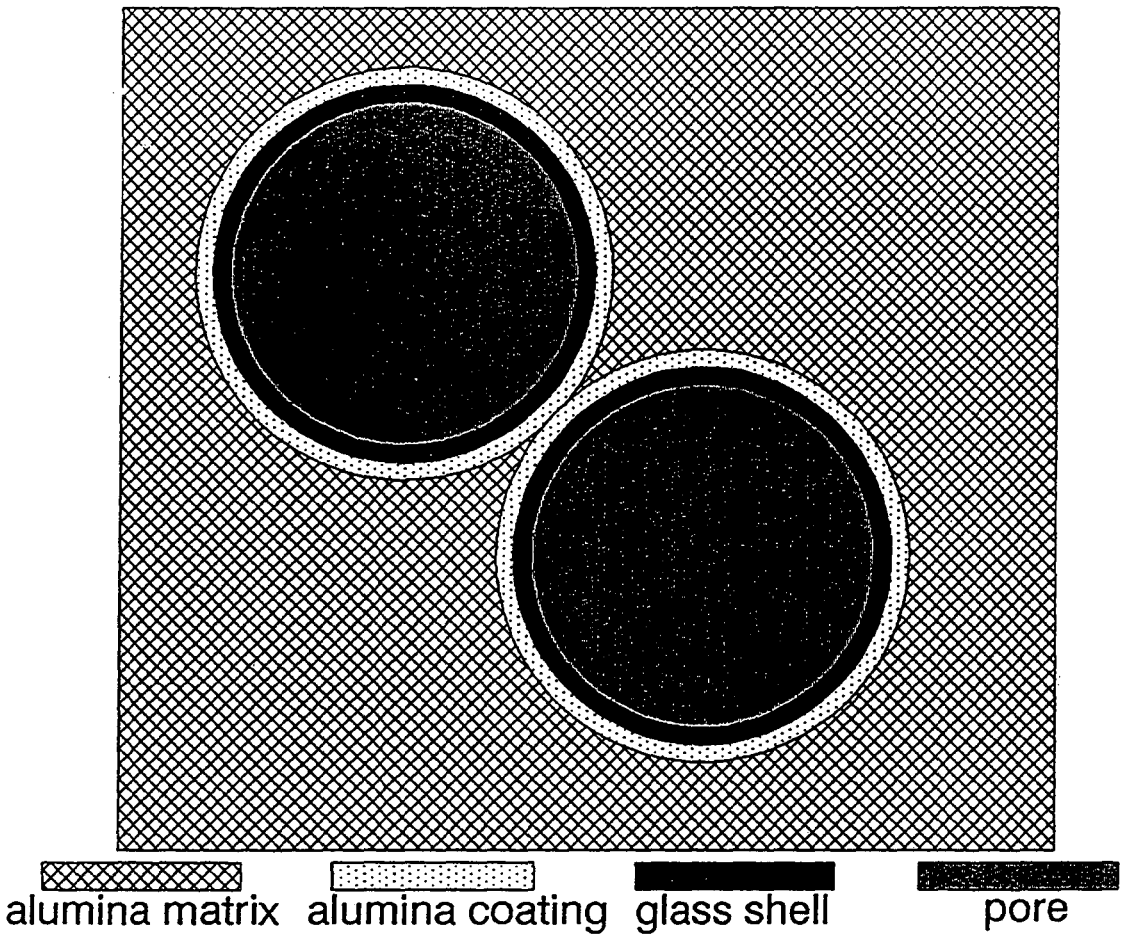

Figure 3-5. A schematic drawing of touching glass hollow spheres which are coated with a thin layer of alumina to preserve their integrity during the subsequent high temperature processes.

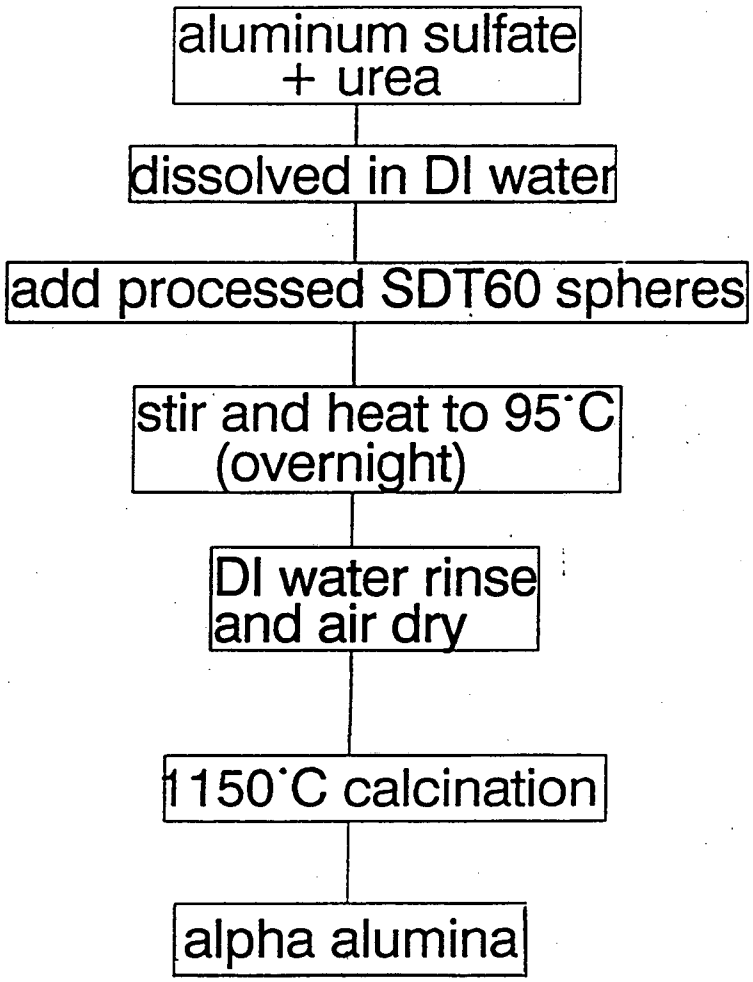

Figure 3-6. Flowchart of surface coating process via controlled heterogeneous nucleation in aqueous solution.

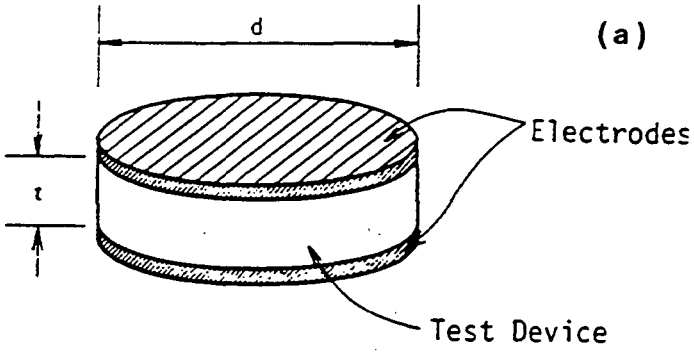

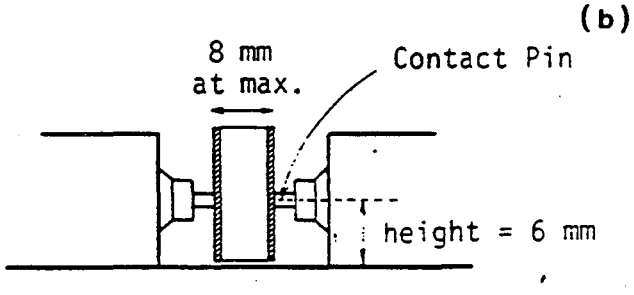

Figure 3-7. (a) Dielectric constant testing sample with electrode plating; (b) Testing ample setup on the test fixture.

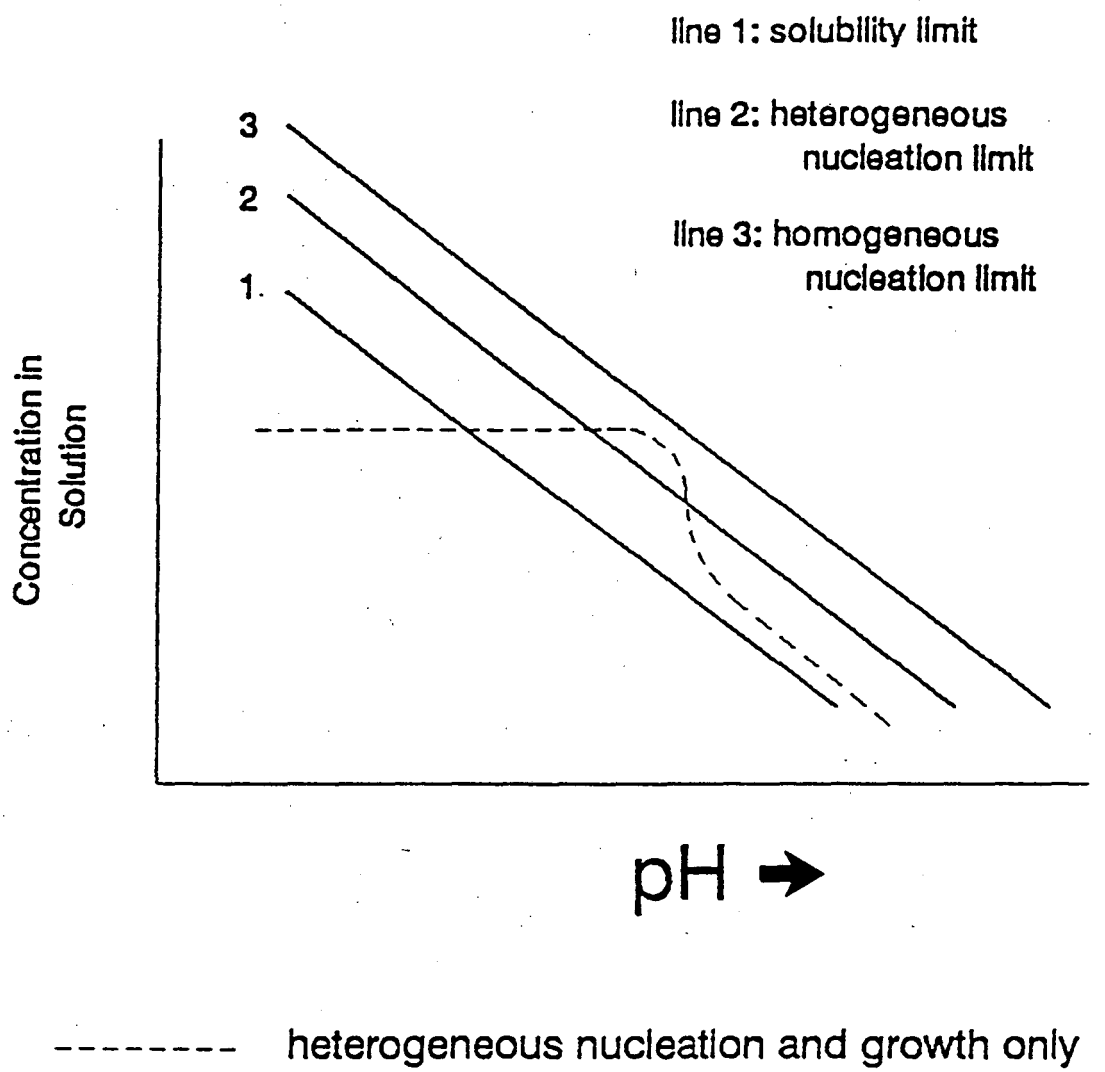

Figure 4-1. Modified LaMer Diagram showing nucleation and growth behavior of precipitation from solution with increasing pH value. (from reference 4-1).

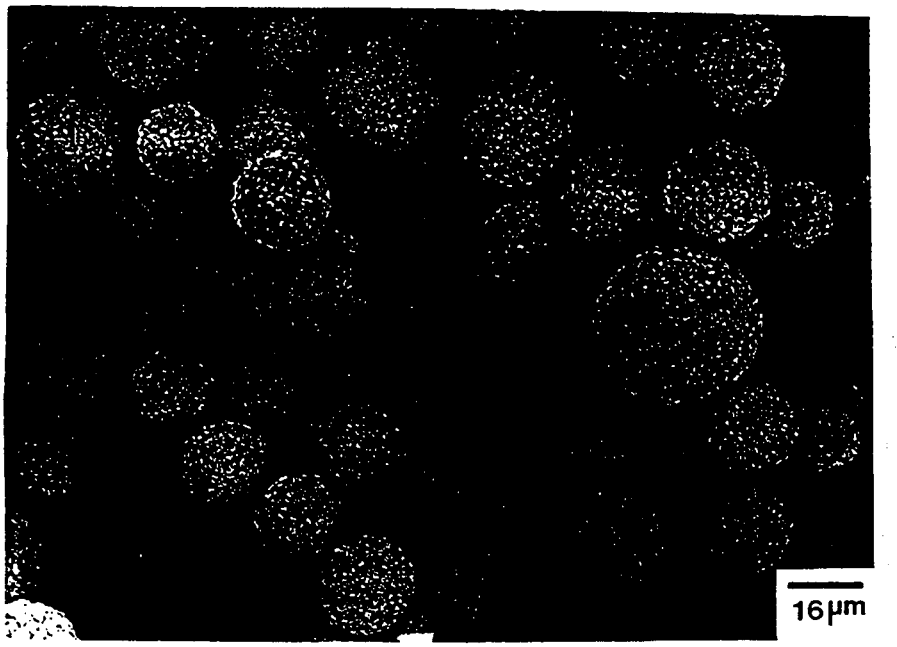

Figure 4-2. SEM micrograph of coated glass hollow spheres after drying. The amount of free alumina precursor (indicated by the arrow) is negligible.

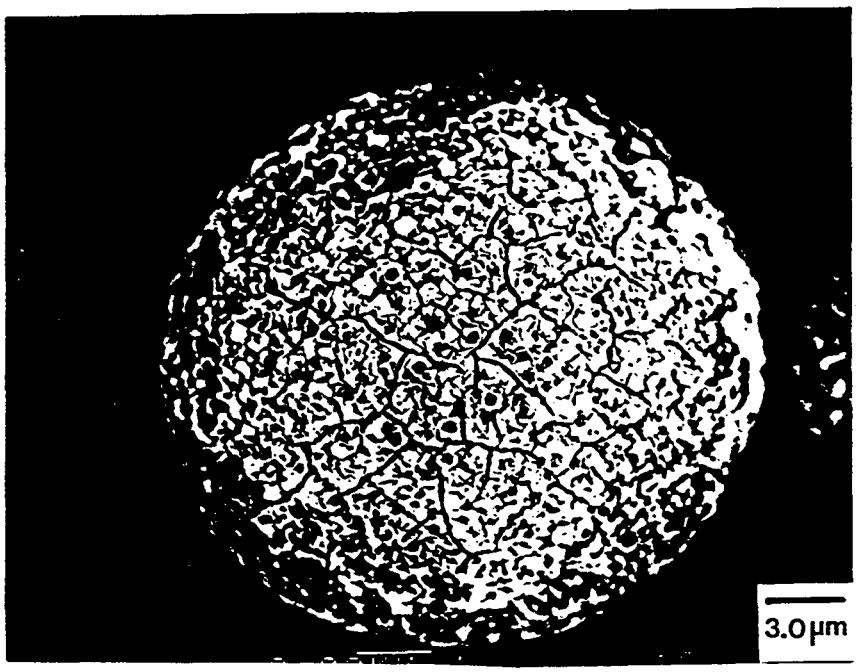

Figure 4-3. High magnification SEM micrograph of a coated glass hollow sphere after drying. Surface cracks are believed to be caused by the water loss during drying.

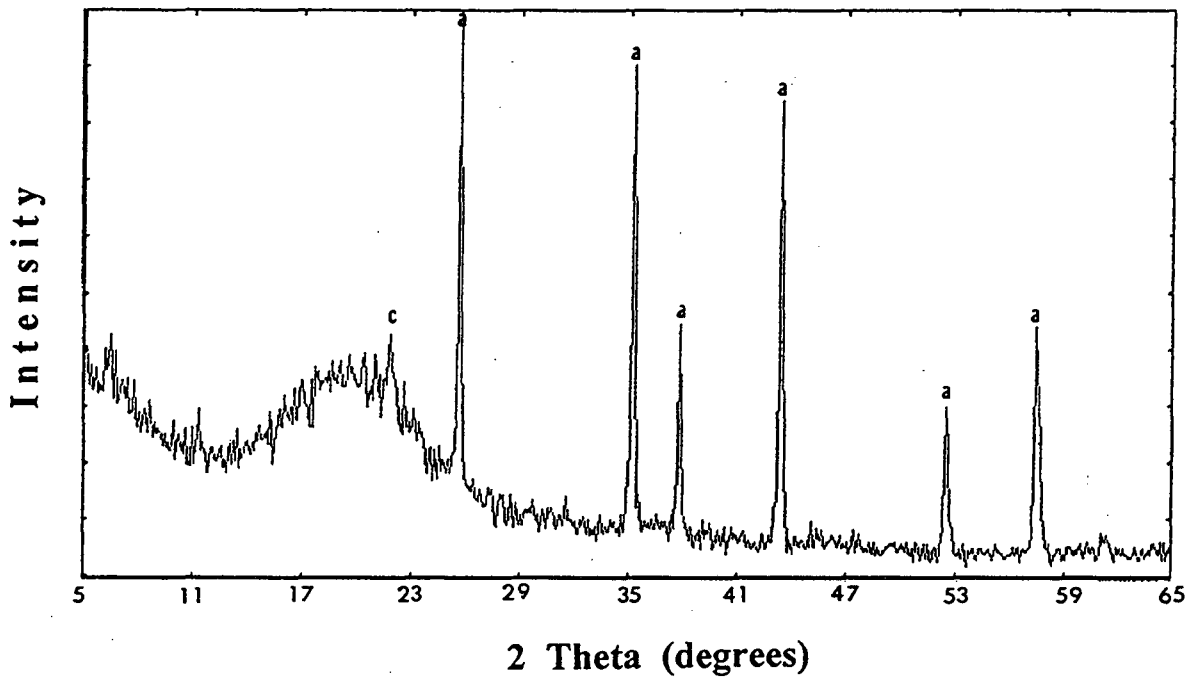

Figure 4-4. X-ray diffraction patterns of coated spheres after calcination at 1150°C in air for 2 hours. **a** : α-alumina, **c** : α-cristobalite.

(a)

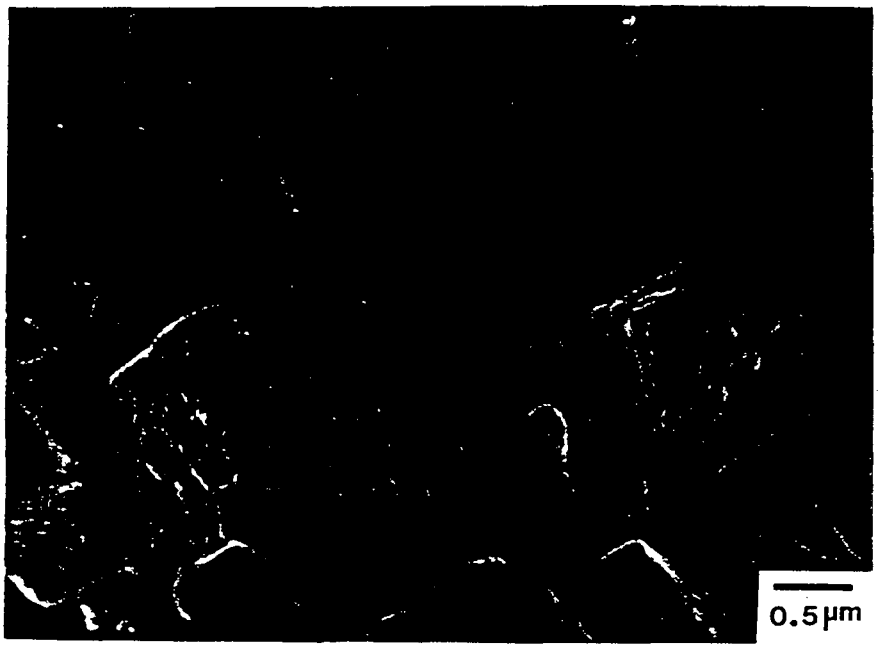

(b)

Figure 4-5. SEM micrographs of coated grains (a) before calcination and (b) after calcination at 1150°C for 2 hours in air. Note that α-alumina grains retained the original precursor shapes after calcination.

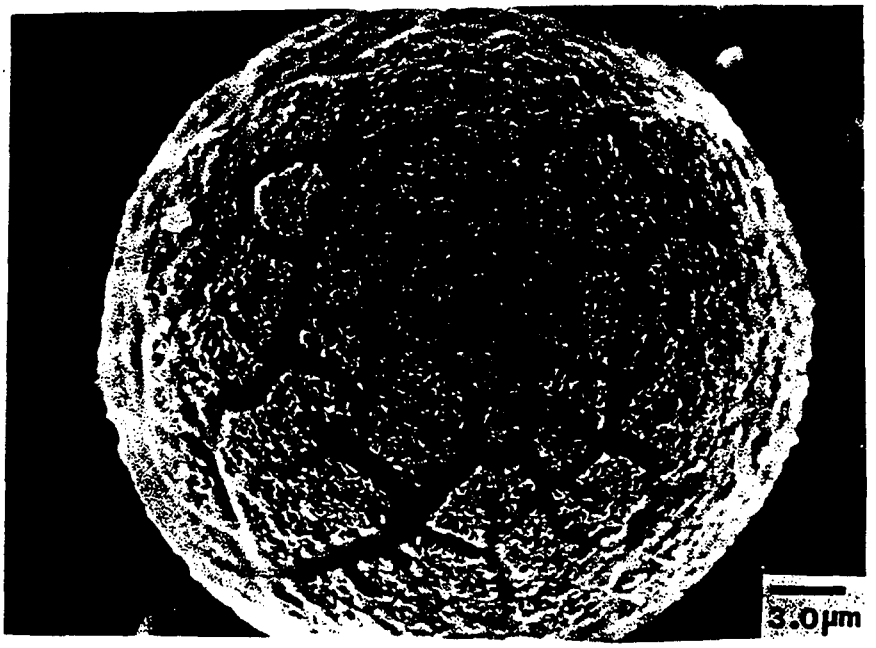

(a)

(b)

Figure 4-6. SEM micrographs of (a) an intact sphere after calcination and (b) a broken sphere (total amount < 1%). Note the lack of viscous flow of glass in (b).

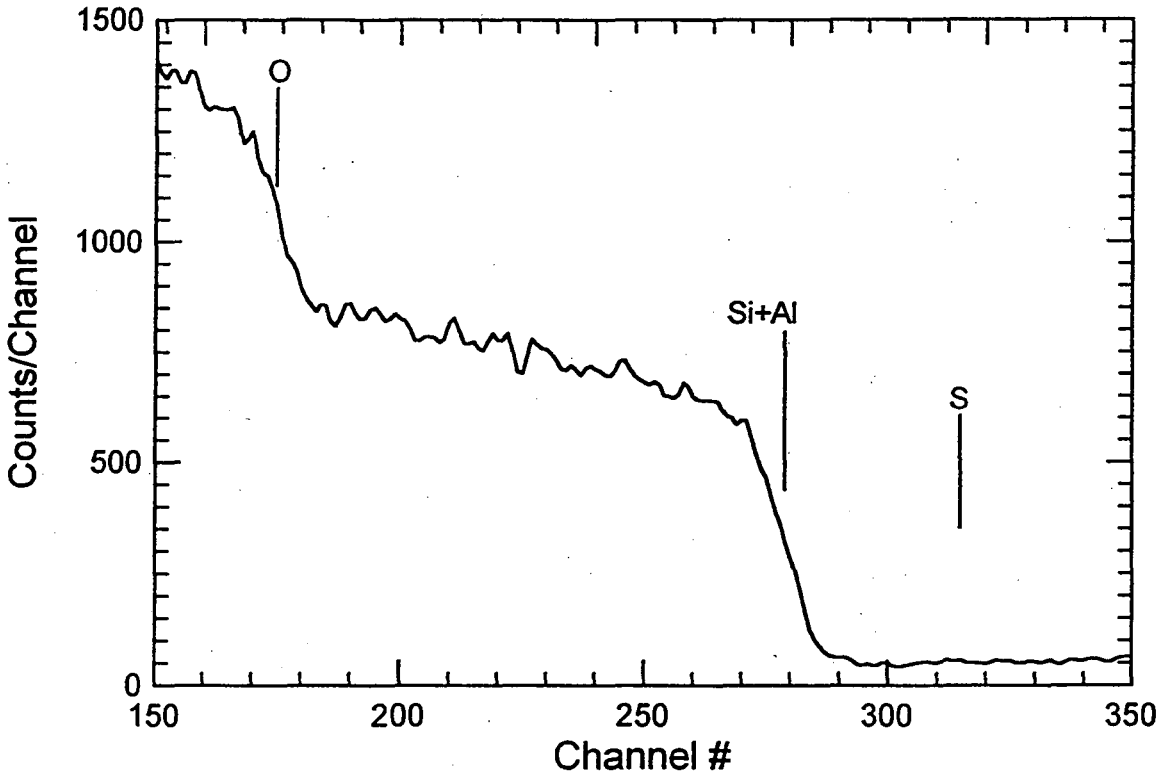

Figure 4-7. RBS results from coated spheres after calcination. No sulfur can be detected by this technique, meaning that its concentration is less than 100 ppm.

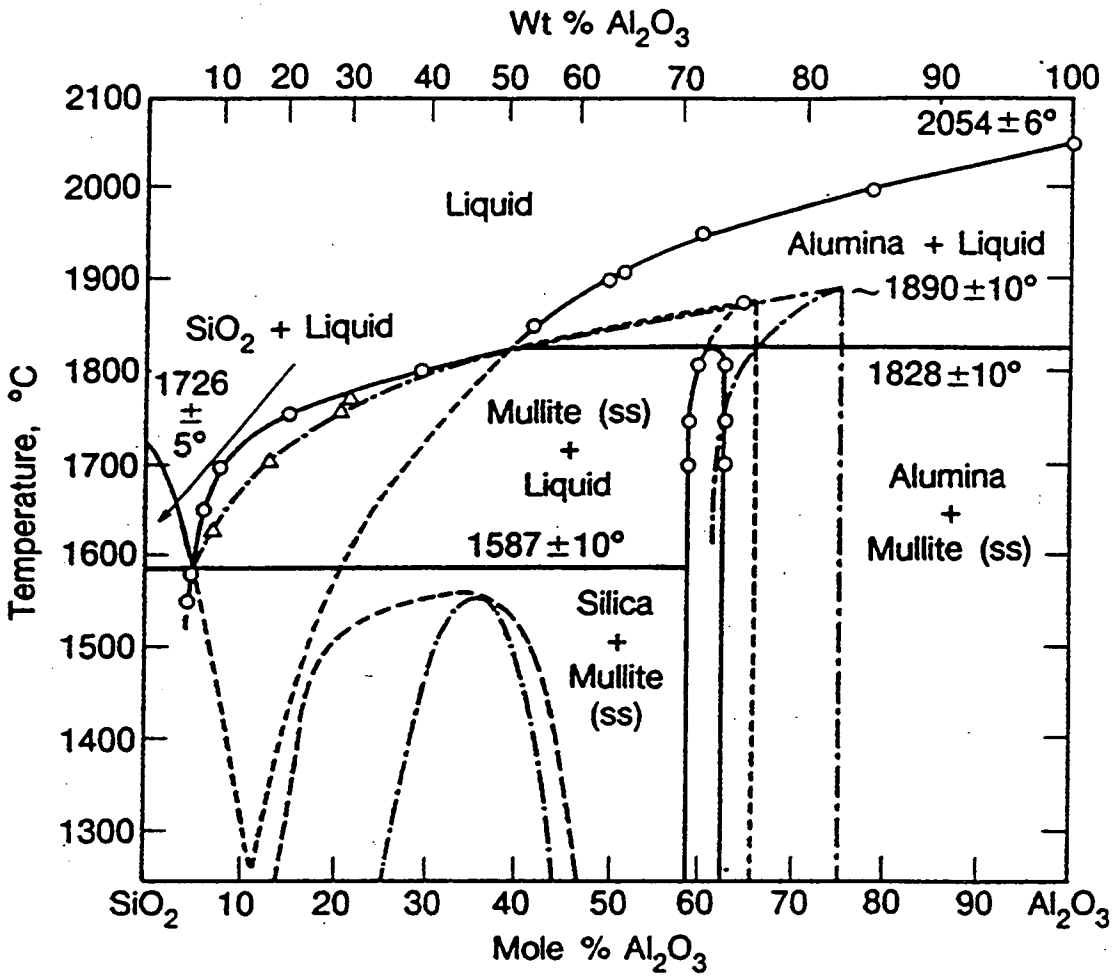

Figure 4-8. Stable and metastable equilibrium phase diagrams of the Al_2O_3-SiO_2 system. (from reference 4-13)

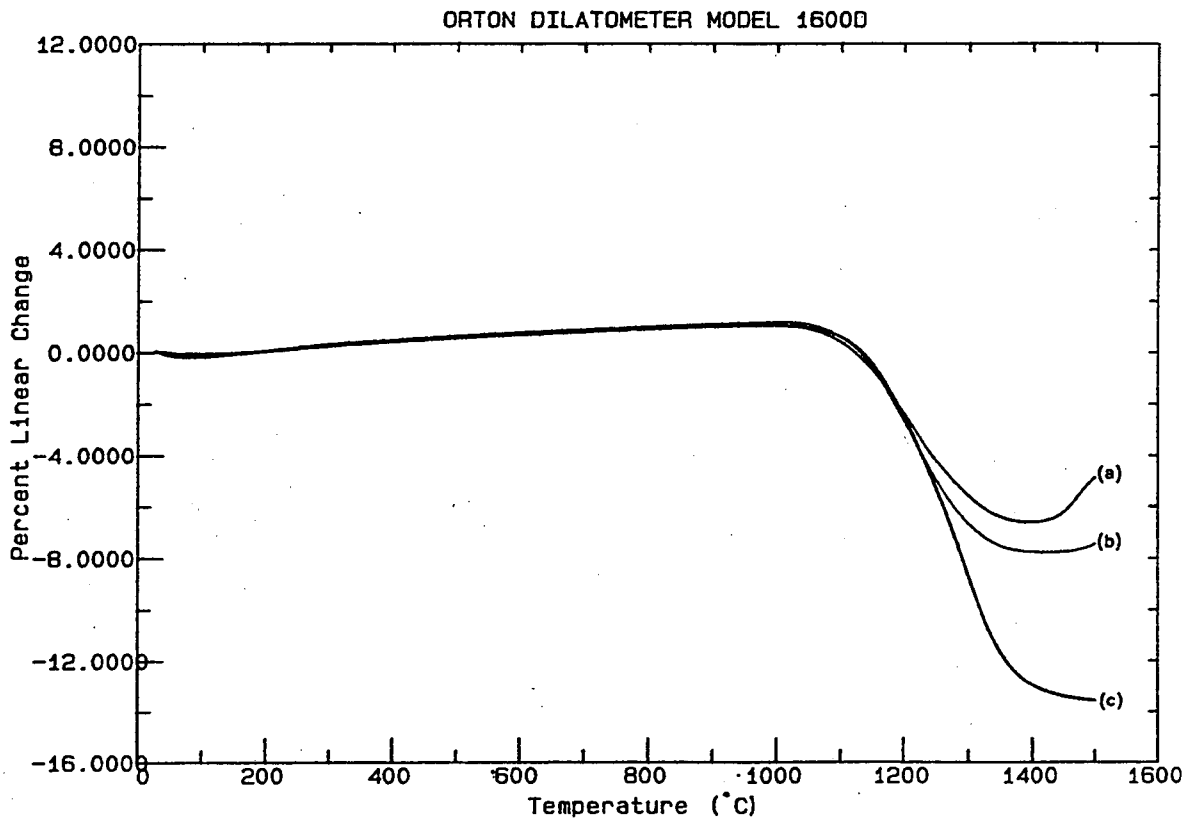

Figure 4-9. Shrinkage curves for composite samples with various loading of coated spheres: (a) 16.7 wt% (20.4% final porosity), (b) 7.4 wt% (9.8% final porosity) and (c) pure alumina.

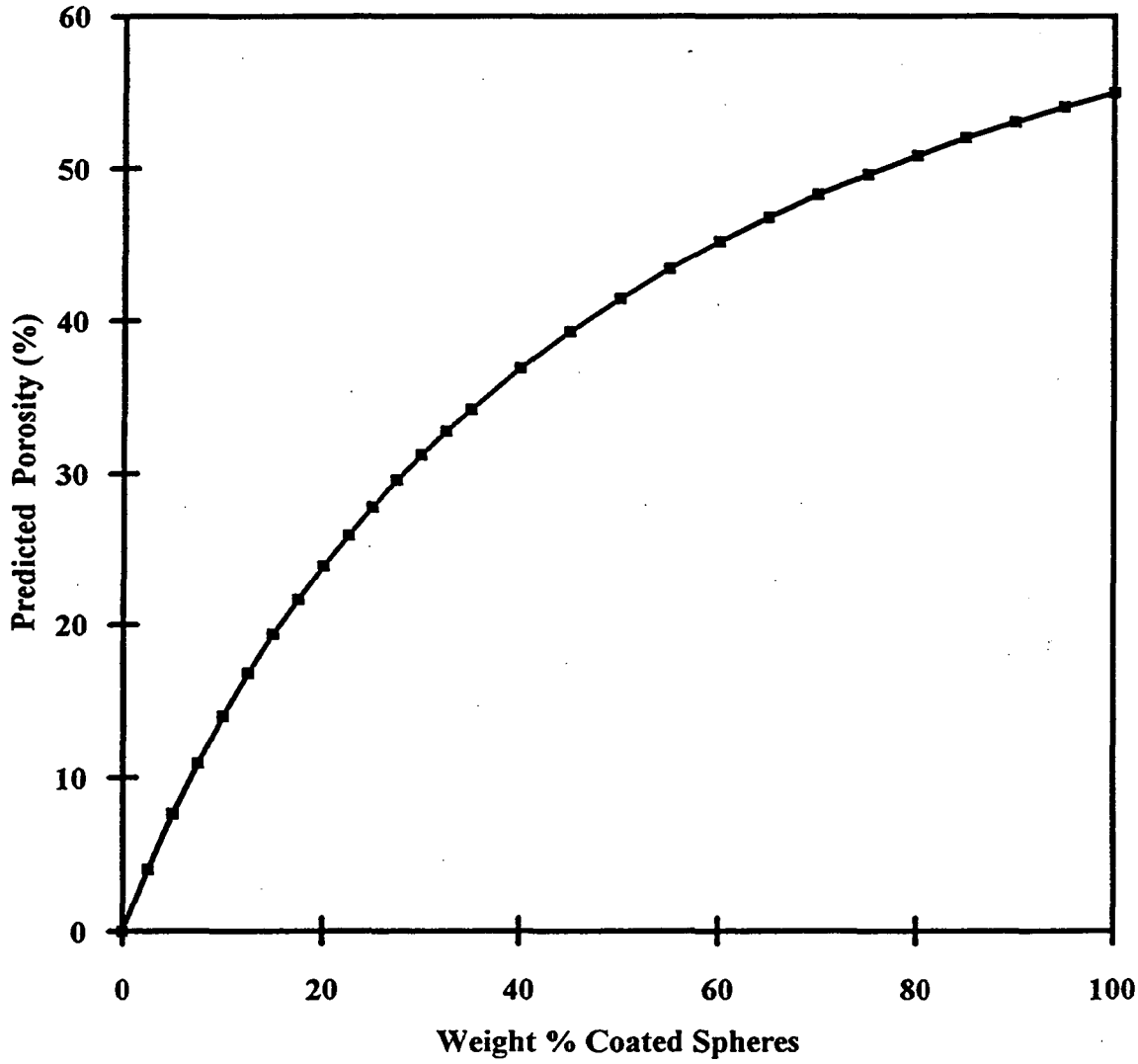

Figure 4-10. Estimated porosity in the sintered composite samples as a function of weight fraction of coated glass hollow spheres.

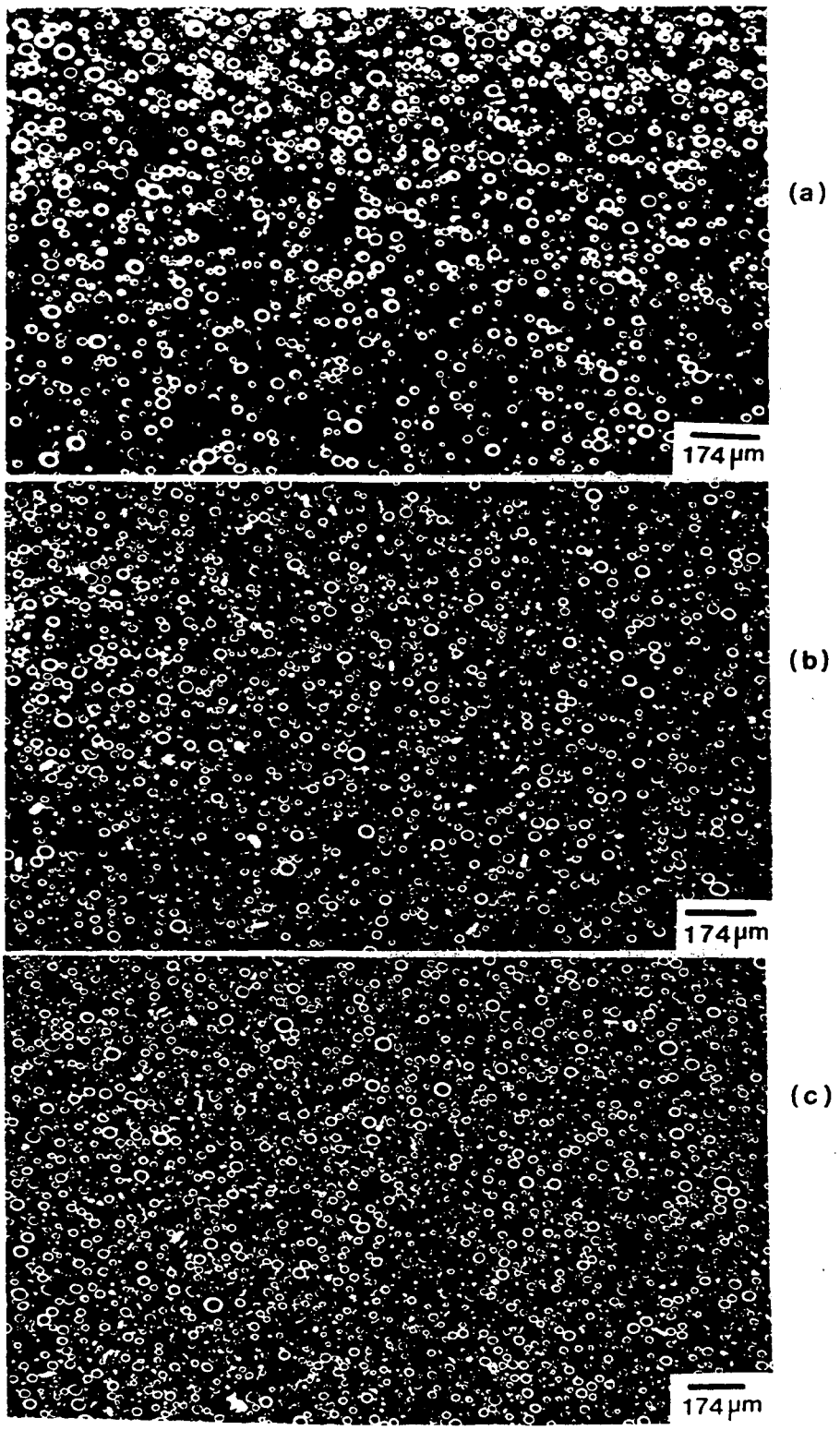

Figure 4-11. SEM micrographs of polished samples after sintering in air at 1400°C (no soaking) with various porosities: (a) 9.8%, (b) 22.4% and (c) 33.9%.

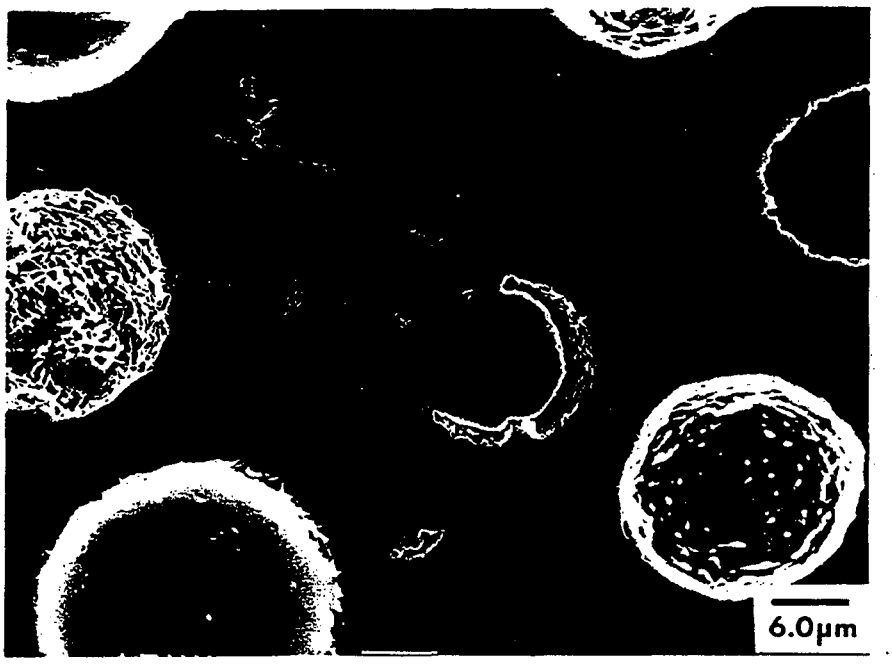

Figure 4-12. High magnification SEM micrograph of polished sample after sintering at 1400°C (no soaking) in air. (a), (b), (c) and (d) : pores with different morphologies, (e) : voids caused by broken spheres during calcination, and (f) matrix sintering defect.

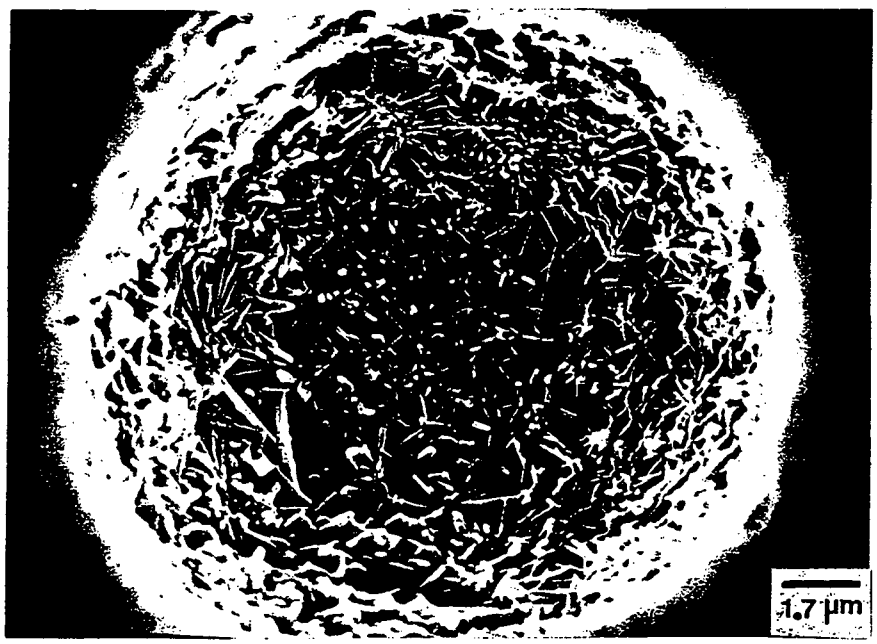

Figure 4-13. SEM micrograph of a pore surface after sintering at 1400°C (no soaking) in air, showing residual glass amid elongated mullite grains.

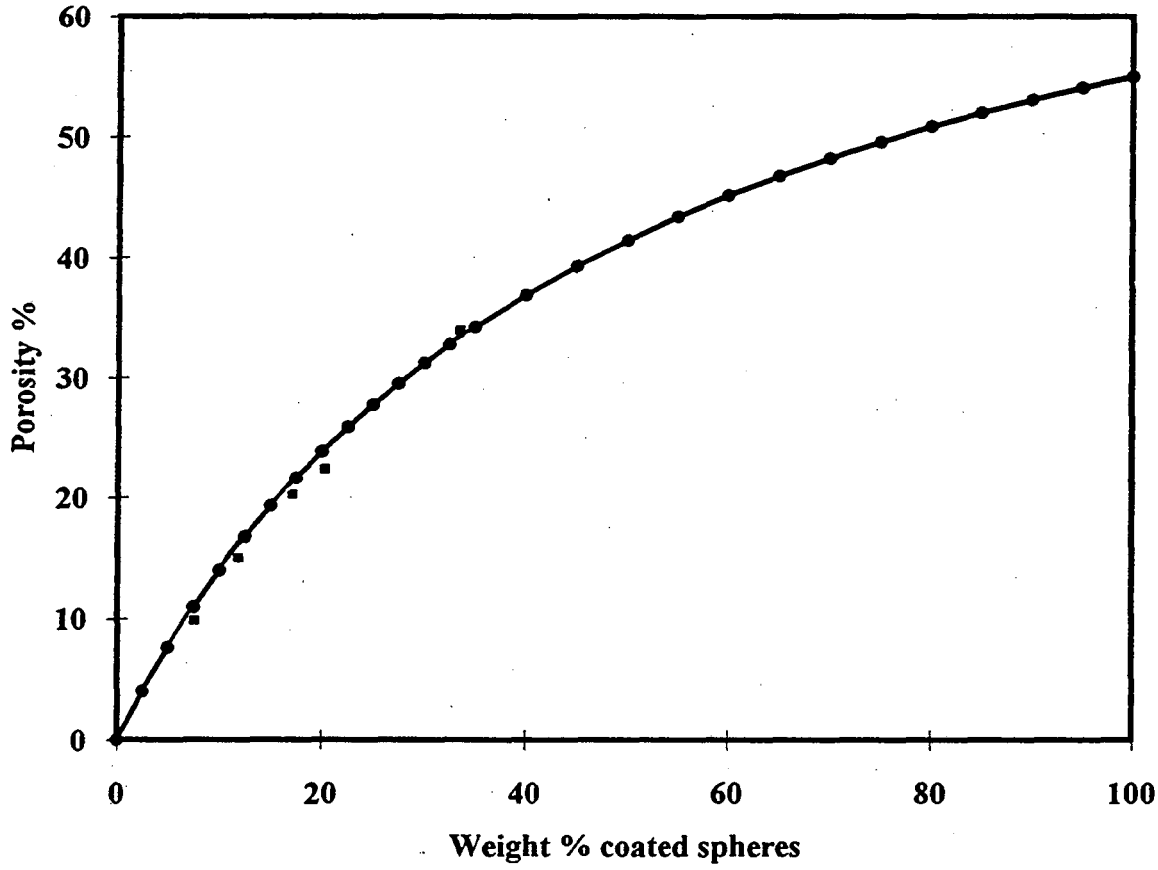

Figure 4-14. A comparison of predicted porosity and measured porosity of sintered samples as a function of weight fraction of coated spheres.

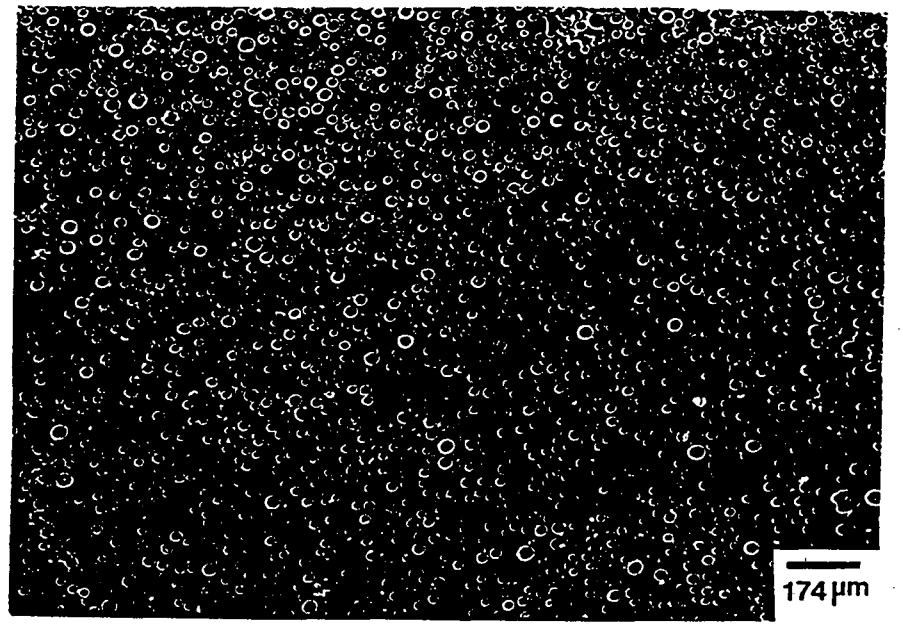

(a)

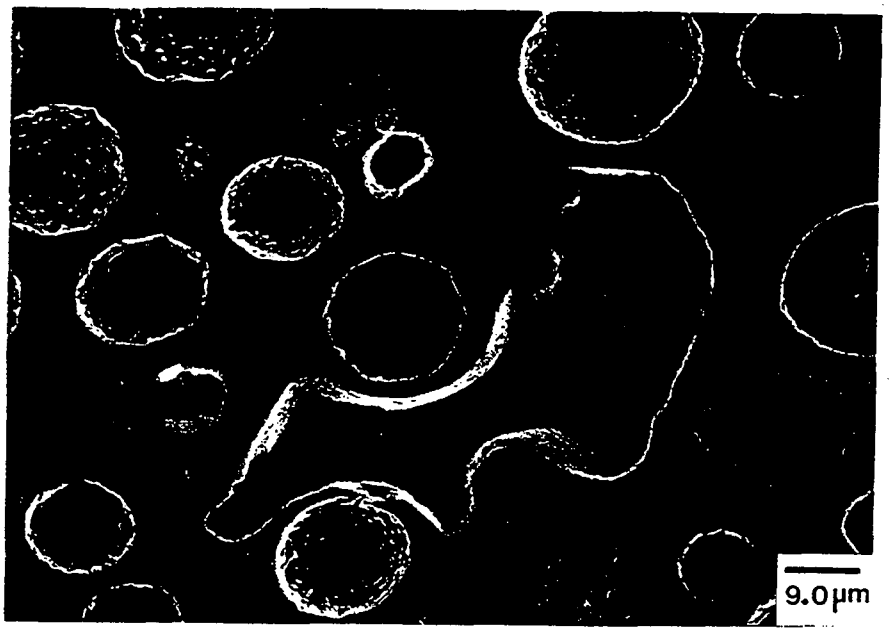

(b)

Figure 4-15. SEM micrographs of a polished sample (66 vol% spheres) after sintering at 1400°C (no soaking) in air. (a) low magnification, (b) a matrix void as indicated by the arrow in (a).

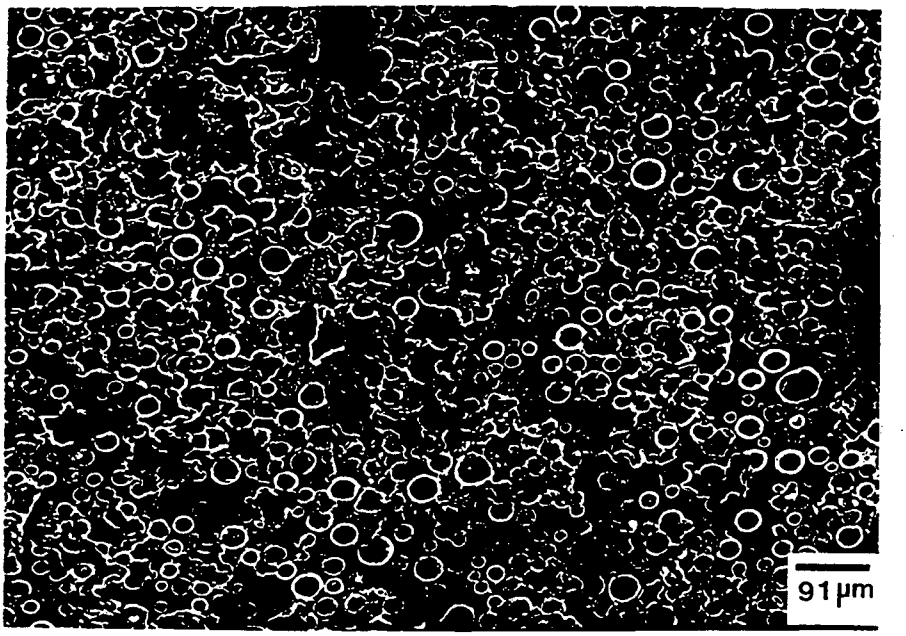

Figure 4-16. SEM micrograph of a polished sample after sintering containing large amounts of connected porosity due to too high loading (80 vol%) of coated glass hollow spheres.

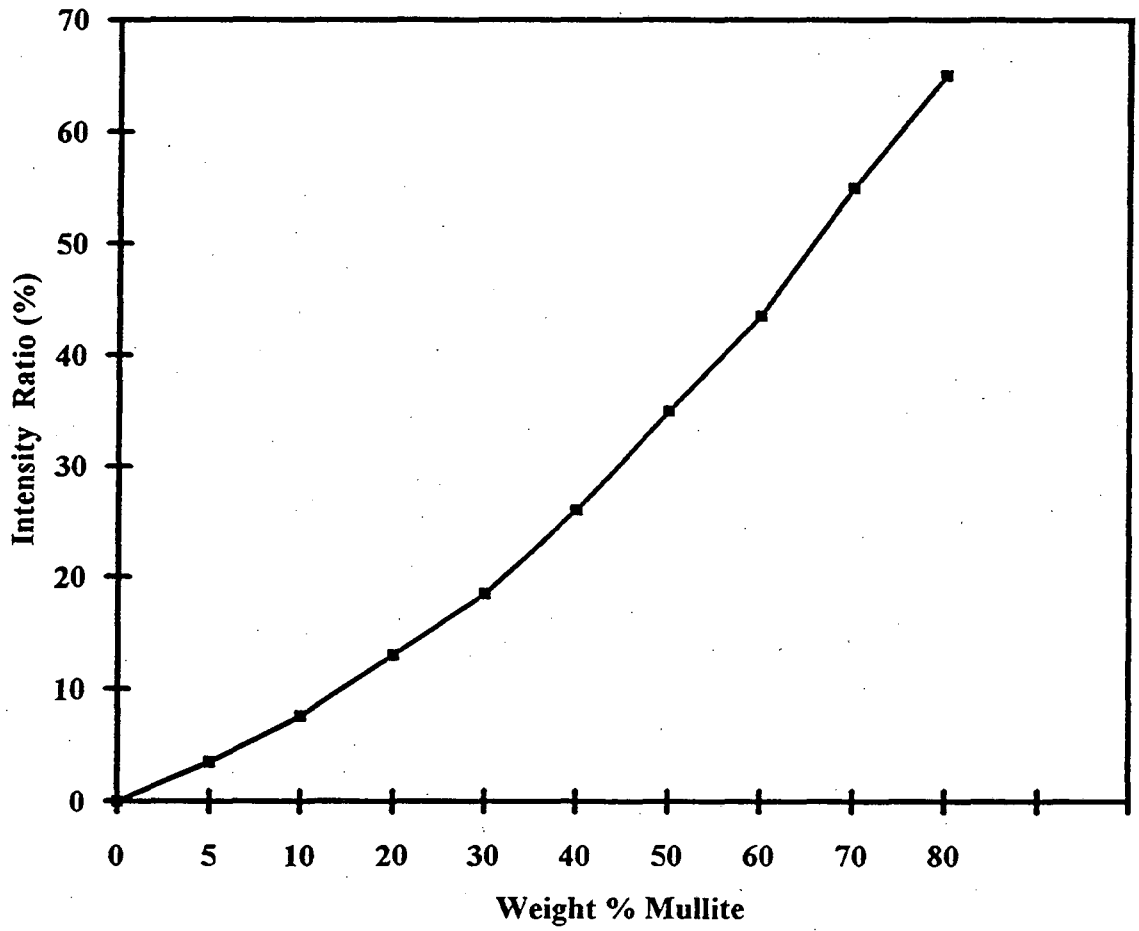

Figure 4-17. The calibration curve to determine the relative amounts of phases in the alumina/mullite mixtures. Intensity ratio = $I_M / (I_A + I_M)$, where I_A and I_M were areas under the α-alumina (113) peak and mullite (121, 211) peaks, respectively.

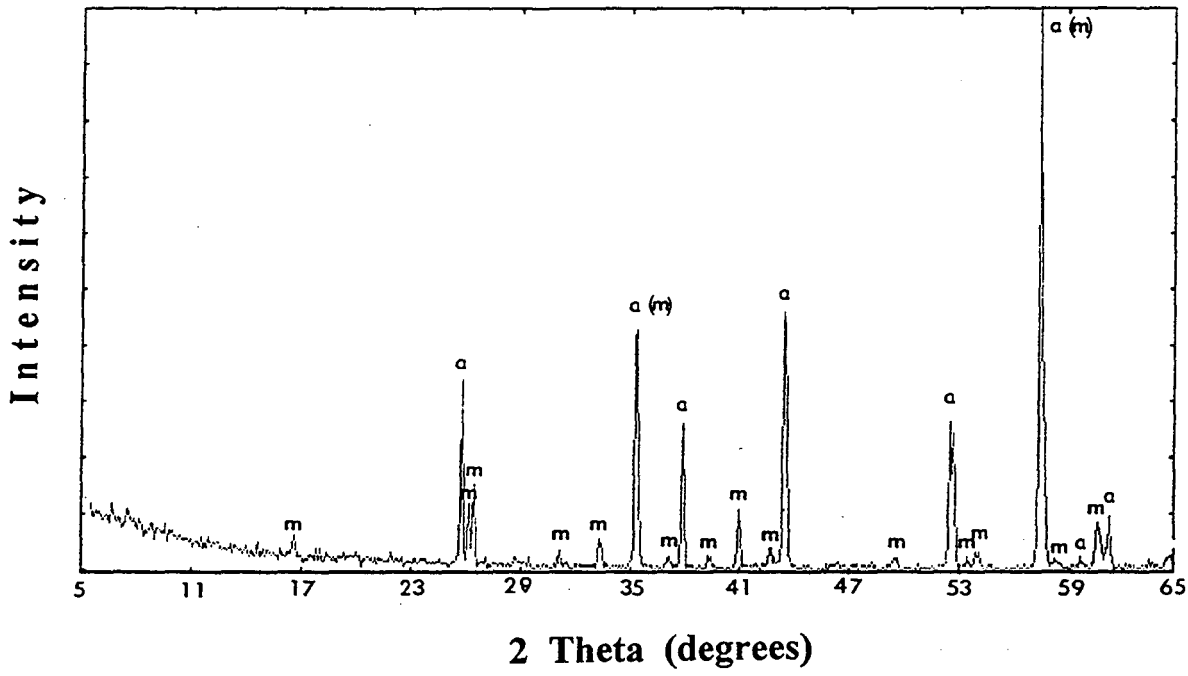

Figure 4-18. X-ray diffraction pattern of sample (80 wt% alumina / 20 wt% coated spheres) after sintering in air at 1400°C (no soaking). a: α-alumina, m: mullite.

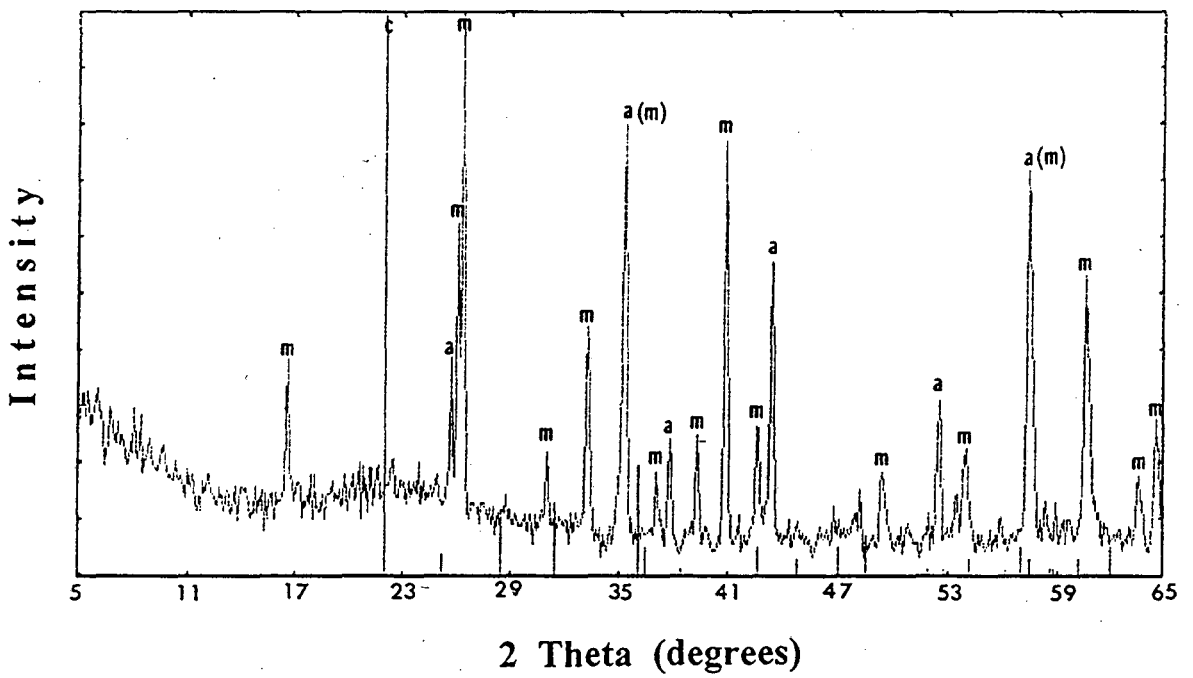

Figure 4-19. X-ray diffraction pattern of pure coated sphere sample after sintering in air at 1400°C (no soaking). Note there are no cristobalite peaks in the spectrum. a : α-alumina, m : mullite and c : cristobalite.

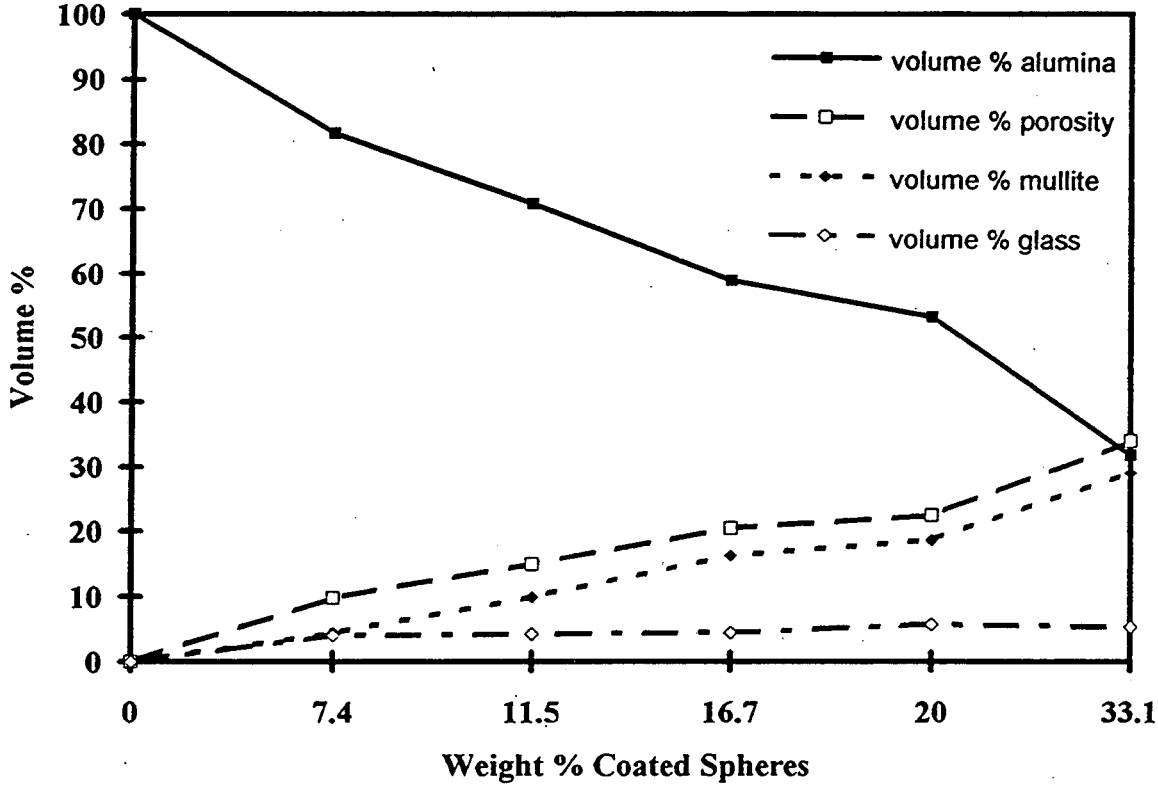

Figure 4-20. Volume fraction of different phases in sintered samples as a function of wt% of coated spheres.

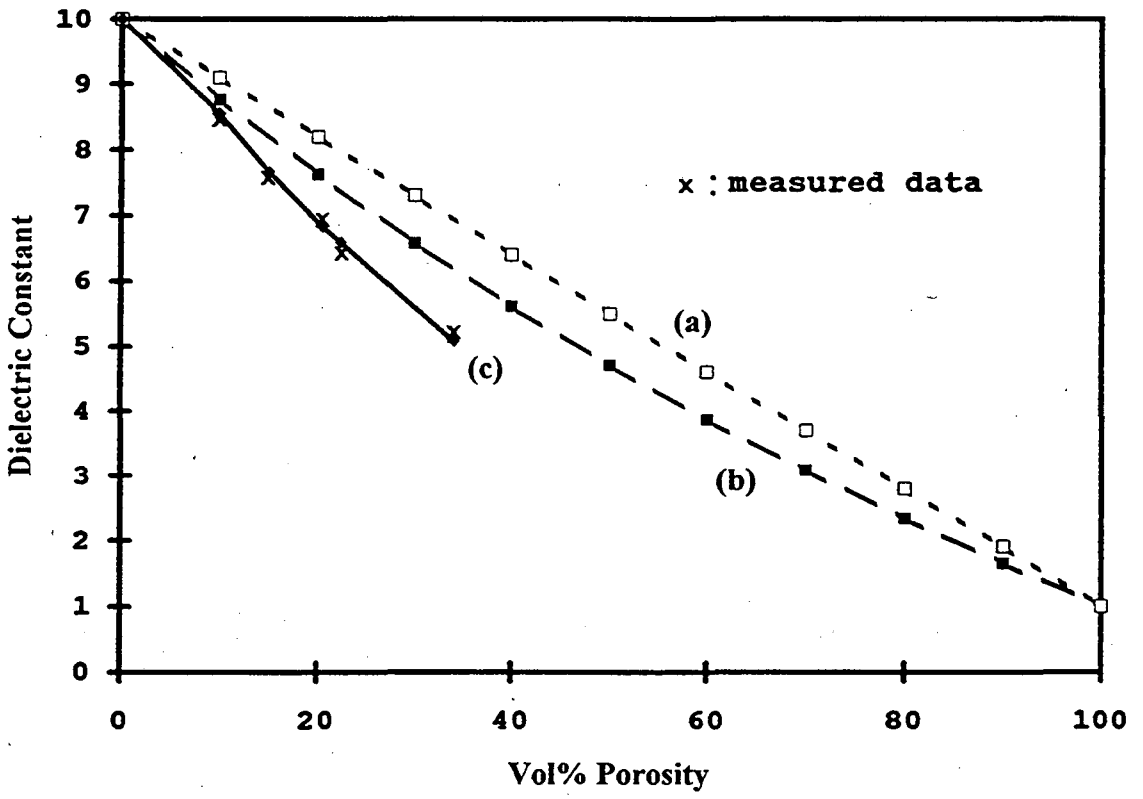

Figure 4-21. Measured dielectric constant of sintered samples as a function of volume fraction porosity. (a) simple mixing rule, (b) Maxwell's model based on alumina only matrix, (c) Maxwell's model based on multiphase matrix in this study.

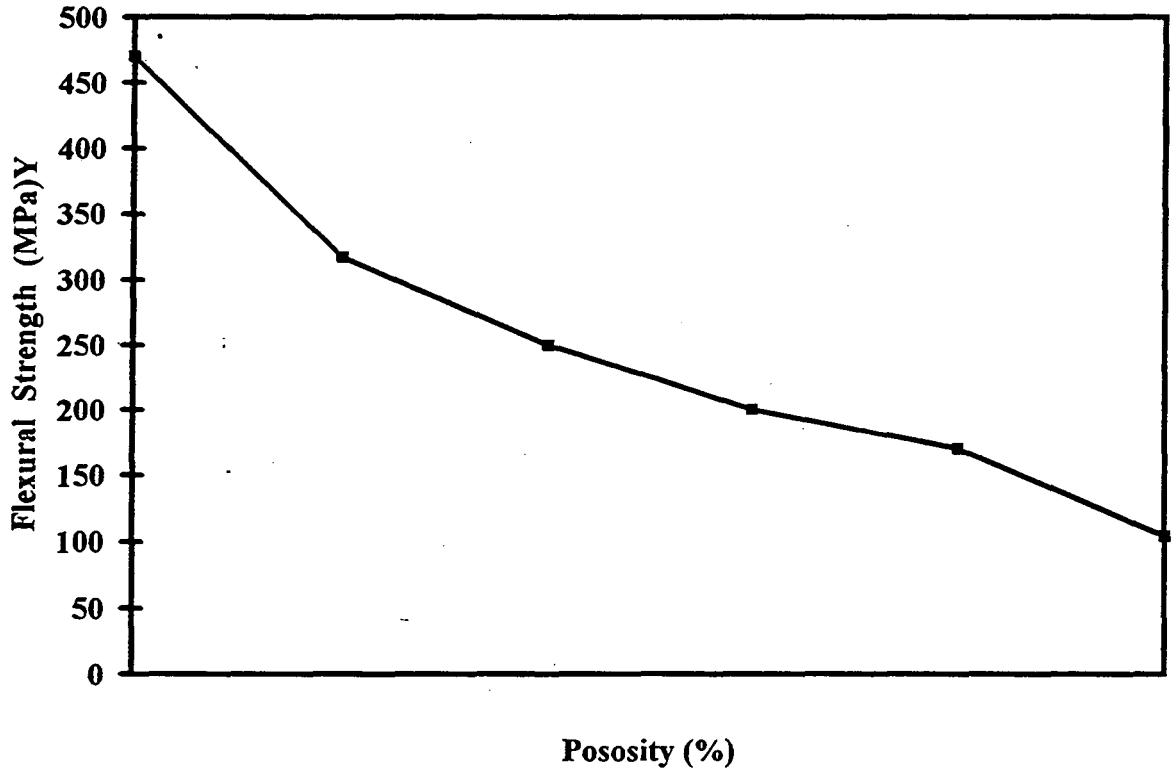

Figure 4-22. Flexural strength of sintered samples as a function of volume fraction porosity.

LAWRENCE BERKELEY LABORATORY
UNIVERSITY OF CALIFORNIA
TECHNICAL INFORMATION DEPARTMENT
BERKELEY, CALIFORNIA 94720